An investigation of computational fluid dynamics simulation for estimation of turbine remaining useful life

by

Charl Francois Maré

Submitted in partial fulfillment of the requirements for the degree

Master of Engineering
(Mechanical Engineering)

in the Faculty of

Engineering, Built Environment and Information Technology

at the

University of Pretoria

2018

Supervisor: Prof. P.S. Heyns
Co-supervisor: Dr. D. Dunn

Abstract

Turbines encounter blade failures due to fatigue and creep. It has been shown in the literature that the primary cause of steam turbine blade failures worldwide can be ascribed to fatigue in low pressure (LP) turbine blades. The failure and damage to these blades can lead to catastrophic consequences. Some utilities use empirical methods to determine the forces experienced by turbine blades, but desire more accurate methods. The inaccurate prediction of high-cycle fatigue (HCF), thermal durability and stage performance is introduced when one does not consider blade row interaction. Blade row interactions can however be accounted for by means of computational fluid dynamics (CFD). Furthermore, modern high-fidelity CFD tools would be able to contribute greatly in predicting the forces experienced by turbine blades.

Numerical tools such as CFD and finite element analysis (FEA) can greatly contribute in the estimation of the remaining useful life (RUL) of turbine blades. However, in this estimation process there are various uncertainties and aspects that affect the estimated RUL. Understanding the sensitivity of the estimated RUL to these various uncertainties and aspects is of great importance, if RUL is to be estimated as accurately as possible.

In this dissertation, a sensitivity analysis is performed with the purpose of establishing the sensitivity of the estimated RUL of the last stage rotor of a LP steam turbine, to the number of harmonics used in a nonlinear harmonic (NLH) CFD simulation. The sensitivity of the estimated RUL is evaluated in the HCF regime, where the cyclic stresses occur below the yield strength of the turbine blade. A CFD model, FE model, and fatigue model were therefore developed in such a manner that would suffice, regarding the purpose of the sensitivity analysis. The CFD model is validated by comparing the predicted CFD power to that of actual generated power of a dual 100MW LP steam turbine. The sensitivity analysis is performed for 3 operation conditions, and for each operational condition the aerodynamic forces were computed using 1, 2, and 3 harmonics in a NLH simulation.

The estimation process considers a weak coupling between the CFD model and FE model. NLH simulations are firstly performed to calculate the unsteady static surface pressure distributions on the last stage rotor. This is followed by the mapping thereof to the FE model, for which a transient structural analysis is performed. Finally, the RUL is estimated by performing a fatigue analysis on the stress history obtained from the transient structural analysis.

Based on the results of the sensitivity analysis, the following recommendations were made, from a conservative point of view. Firstly, in general if the RUL is to be estimated with reasonable accuracy, just using 1 harmonic in a NLH simulation will not be sufficient and 2 harmonics should be used. Secondly, if the RUL has to be estimated with high accuracy, 3 harmonics should be used.

Key terms: Steam turbine, low-pressure, high cycle fatigue, remaining useful life, computational fluid dynamics, nonlinear harmonic, harmonics, aerodynamic forces, finite element analysis, transient structural analysis, fatigue analysis.

Acknowledgement

I would like to give thanks to:

1. My supervisor Prof. P.S. Heyns for his guidance.

2. My co-supervisor Dr. Dwain Dunn from the CSIR for sharing his knowledge in the field of computational fluid dynamics (CFD). I would also like to thank him for his guidance and assistance with the CFD software package, which was used for the numerical investigation.

3. The CSIR for allowing me to use their computer and for their kindness and hospitality.

4. Eskom Power Plant Engineering Institute (EPPEI) and Mr. Noel Lecordier.

5. My parents, Manie and Gerda, for all their support.

6. My wife, Abbi Maré, who supported me throughout my dissertation.

7. God and the Lord Jesus Christ for giving me the wisdom, insight, knowledge, and understanding to complete this dissertation to the best of my abilities. Glory to Him forever and ever.

Contents

Nomenclature

Abbreviation or Acronym	Description / Definition
CAD	computer-aided design
CFD	computational fluid dynamics
DV	downstream vane
EOM	equation of motion
EPRI	Electric Power Research Institute
FE	finite element
FEA	finite element analysis
FEM	finite element method
HCF	high-cycle fatigue
HP	high pressure
IP	intermediate pressure
LP	low pressure
NDT	non-destructive testing
NLH	nonlinear harmonic
RAM	Random Access Memory
RUL	remaining useful life
SST	shear stress transport

Symbols	Description / Definition	Units
σ_a	amplitude of von Mises stress blade passing period	[Pa]
σ_{eff}	effective von Mises stress amplitude	[Pa]
σ_f'	tensile fatigue strength coefficient	[Pa]
σ_m	mean von Mises stress of blade passing period	[Pa]
σ_y	yield strength of material	[Pa]
b	tensile fatigue strength exponent	[-]
N_f	remaining useful life w.r.t HCF	[hours]

Chapter 1

Introduction

1.1 Problem statement

Turbines encounter blade failures due to fatigue and creep. According to Booysen (2014) the primary cause of steam turbine blade failures worldwide can be ascribed to fatigue in low pressure (LP) turbine blades. Transient blade operations which cause high cycle fatigue (HCF) damage, were identified to be a primary source of LP steam turbine blade failures. Booysen (2014) also mentions that failure of turbine blades and fatigue cracking is a predicament that a large number of power stations are facing.

HCF damage occurs in turbine blades when they vibrate during their varying operational conditions (Booysen, 2014). The fatigue can primarily be ascribed to the inherently unsteady aerodynamic flow through turbines (Ning et al., 2003). Jöcker (2002) explains that this unsteadiness is caused by the relative motion of non-rotating and rotating parts in the turbines. According to Lakshminarayana et al. (2000) these interactions substantially alter the mechanical life, reliability and the cycle performance.

Turbine blade resonance causes substantial HCF damage and Ning et al. (2003) explain that even though this blade resonance could be identified using traditional approaches like the Campbell diagram, this unfortunately does not provide any information on the amplitude of the vibration, which is required in the remaining useful life (RUL) estimation process. One could measure these amplitudes using strain gauges, but this approach can be very time consuming for turbine manufacturers and have large financial implications.

Utilities need to perform maintenance and inspections periodically, in an effort to prevent turbine blade failures. In cases where assets are used beyond their original design lives, which is increasingly the case in the power generation industry, additional effort is required to estimate RUL as accurately as possible. Remaining useful life is defined as the life of a component or machine from its current state until it is no longer considered useful (Mishra et al., 2014).

Some utilities use empirical methods to determine the forces experienced by turbine blades, but desire more accurate methods. According to Miller, Moss, Ainsworth and Horwood (2003), the inaccurate prediction of high-cycle fatigue, thermal durability and stage performance is introduced when one does not consider blade row interaction. Blade row interactions can however be accounted for by means of computational fluid dynamics

(CFD) and Mayorca (2011) concluded that modern high-fidelity CFD tools would be able to contribute greatly in predicting forces which turbine blades are experiencing.

Numerical tools such as CFD and finite element analysis (FEA) can greatly contribute in the estimation of the RUL. However, in this estimation process there are various uncertainties and aspects that affect the estimated RUL. Understanding the sensitivity of the estimated RUL to various uncertainties and aspects is very important if RUL is to be estimated as accurately as possible. The aim with this work is to determine the sensitivity of the estimate RUL of a last stage rotor blade of a LP steam turbine to number of harmonics used in a nonlinear harmonic (NLH) CFD simulation. The sensitivity of the estimated RUL is to be evaluated in the HCF regime, where the cyclic stresses in the blade occur below the yield strength of the turbine blade.

1.2 Literature review

1.2.1 The necessity of estimating RUL

According to Brits et al. (2016) steam turbines in South Africa are often used beyond their original design life. Therefore, periodic inspections are performed to determine the damage to the various turbine parts. These inspections comprise of locating and sizing the damage by means of non-destructive testing (NDT). Finally, the damage is recorded and evaluated, but due to the high costs associated with replacing every damaged part, only critically damaged parts are replaced, while less critically damaged parts are monitored. However, if no replacement parts are available, more downtime could be expected which in turn could result in unforeseen expenses.

Failure and damage in turbomachinery can primarily be ascribed to fatigue and can lead to catastrophic consequences (Branco et al., 2015). According to Mohan et al. (2014) steam turbine blade failures are a common incident and blade failures during operation poses a safety risk and results in non-operational revenue and repair costs. Hou et al. (2014) explained that damage to mechanical structures are unavoidable, especially when the structures are used beyond their design life.

According to Latcovich et al. (2005) a turbine undergoes a service every 25 000 hours or every 3 years. If damaged turbines are left for 3 years, fatigue failure could occur which could lead to financial losses due to downtimes, and the probability for fatigue failure increases when turbines are used beyond their original design life.

Fatigue is responsible for more than 90% of all the mechanical service failures of machine components (Mestanek, 2008). Booysen (2014) states that this is particularly the case in machinery containing rotating components. Blade failure in HP and IP stages due to fatigue are not as significant and problematic compared to low pressure stage's longer blades (McCloskey et al., 1999). According to Rieger (1988) and Mccloskey (2002) the primary cause of steam turbine blade failures worldwide can be ascribed to fatigue in low pressure turbine blades.

Estimating the RUL for the above-mentioned cases can help to prevent blade failures and therefore minimize or prevent downtime, non-operational revenue and repair costs.

As explained by Hou et al. (2014) damage is unavoidable when structures are used beyond their design life, thus emphasizes the necessity for estimating the RUL.

1.2.2   Turbine blade failure and fatigue cracking

Xu et al. (2007) inspected a first stage blade found in a certain type of low pressure steam turbine. Cracking occurred at a number of these first stage blades' fork-type roots. The results of the inspection showed that the crack initiated due to surface defects caused by rough machining. The crack propagated due to HCF loading which resulted from the second type axial vibratory mode being excited at the nozzle passing frequency.

Mazur et al. (2008) gave an overview regarding an investigation of the HCF failure of a number of last stage steam turbine blades in two 660MW units. The LP steam turbines operated under low load/poor vacuum conditions which result in flow recirculation and pressure instabilities. The LP steam turbines also experienced sudden load changes resulting in the blades resonating as they passed through 2 of their natural frequencies. Evaluation of the cracks, which formed in the blade roots, revealed that the blade failures occurred due to HCF.

Cracks were found on the suction side, in the quenched region, of the final stage blades of a low pressure steam turbine (Wang et al., 2007). Cracks of various lengths formed only after the blades have been in operation for about 13 200 hours. A crack micrograph and composition on the cracked surface as well as a fractography analysis indicated that these cracks formed due to corrosive fatigue.

In 1985 a survey of steam turbine blade failures was conducted by Electric Power Research Institute (EPRI). The survey revealed that 75% of all reported blade failures were found to occur in low-pressure turbines, of which three quarters were located in the last two stages of the LP turbines (Dewey et al., 1985).

HCF damage has been found to occur anywhere along the length of a

Figure 1.1: Common fatigue damage locations (McCloskey et al., 1999).

LP turbine blade (McCloskey et al., 1999). Figure 1.1 shows the most common locations for HCF (H) and LCF (L) damages on a LP blade.
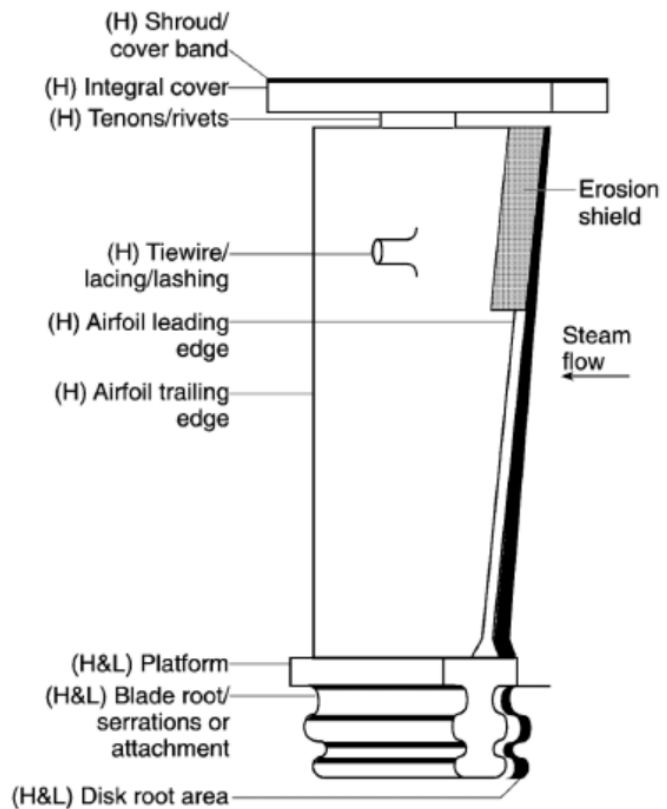
1.2.3 Turbine blade vibration

Fatigue cracking and blade failure of a turbine blade due to HCF occurs as the blade responds to a periodic loading and vibrates, producing cyclic stresses below the yield strength of the turbine blade. The periodic loading results from the inherently unsteady aerodynamic flow through turbines (Ning et al., 2003). The manner in which the turbine blade vibrations depends on the characteristics of the unsteady aerodynamic flow and the turbine blade structure as discussed later in Sections 1.2.4 and 1.2.5, respectively. The turbine blade vibrations can mainly be categorized into forced vibrations and self-excitation vibrations.

Forced vibrations

Turbine blade experiences forced vibration (forced response) when the vibrations of the blade are caused by external excitation sources such as aerodynamic flow through turbines. These aerodynamic excitation sources are flow disturbances that originate from either downstream and/or upstream obstacles, and act periodically on the turbine blades. An example in steam turbines are the periodic interactions of the unsteady flow between the rotating blades (rotors) and non-rotating blades (stators or vanes), called blade-row interaction (Jöcker, 2002).

In all of these above-mentioned cases, the time-periodic excitations are due to the relative rotational motion of the turbine blades and the excitation sources. This then results in excitation frequencies that are multiples of the rotation frequency (Jöcker, 2002). In the case of blade-row interaction these excitation frequencies can mainly be ascribed to the flow mechanisms found in the unsteady flow of a turbine. These flow mechanisms are wakes, vortex shedding, potential interaction and shock waves (Mayorca, 2011).

According to Miller, Moss, Ainsworth and Harvey (2003b) resonance can occur when the excitation frequencies experienced by the turbine blade are close to one of its natural frequencies, resulting in significant vibration. Due to all the vibrations experienced by the turbine blades, their blade life is reduced. Over time these vibration also cause HCF, which eventually can, if not identified, lead to catastrophic blade failures (Miller, Moss, Ainsworth and Harvey, 2003b).

Self-excitation vibrations (Flutter)

In the event of self-excited vibrations (flutter), the turbine blade vibrates due to a positive feedback between the interacting unsteady aerodynamic and structural-dynamic forces (RPMturbo, 2016). It is important to note that the different flow mechanisms are most likely present during flutter. Flutter occurs close to the blade's natural frequencies. However, it should be noted that during flutter the blade vibration frequency will most probably not coincide with the frequency content of the aerodynamic excitation source, as in the case of forced vibration.

Flutter leads to the dynamic instability of the elastic structure and can cause HCF in the long-term and dramatic blade losses in the short-term (RPMturbo, 2016). According to Jöcker (2002) flutter is usually initiated by small mechanical or aerodynamic disturbances above the rotating speed (see Figure 1.2). The author further mentions that this

can then result in blade failure, if the mechanical damping of the blade is not sufficient to dissipate the aerodynamic energy put into it.
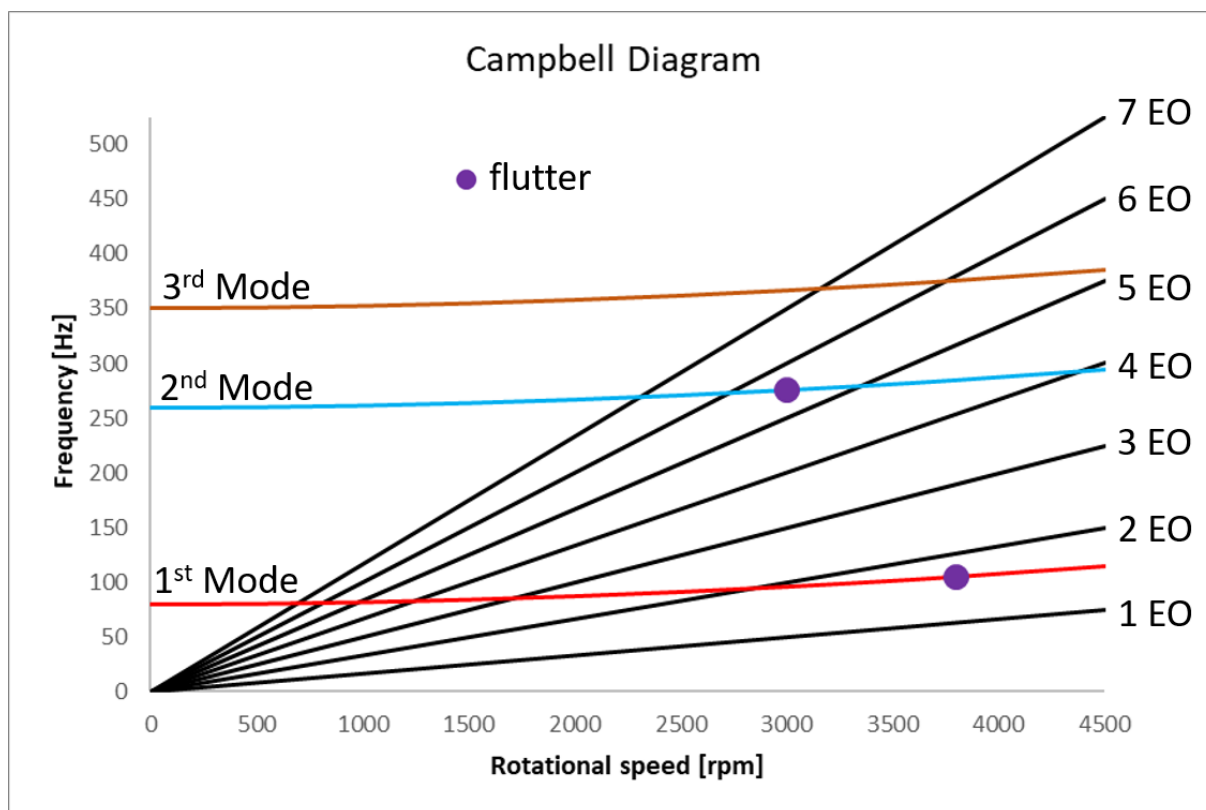

Figure 1.2: A schematic of a Campbell diagram

1.2.4 Unsteady aerodynamic flow

The periodic loading results from the inherently unsteady aerodynamic flow flowing through turbines (Ning et al., 2003). Jöcker (2002) explains that this unsteadiness is caused mainly by the relative motion of non-rotating and rotating parts in the turbines. The main flow mechanisms that characterize and make up the unsteady aerodynamic flow in turbines are wakes, vortex shedding, potential interaction, shock waves and secondary flow.

Shock waves

Shock waves occur due to the presence of strong pressure gradients (Jöcker, 2002), and are found at the trailing edges of blades (see Figure 1.3). In a transonic turbine stage the trailing edge shock from an upstream stator, excites the unsteady surface pressure of the rotor suction surface periodically (Laumert et al., 2002). The trailing edge shocks of the stators/vanes which impinge on the rotor suction surfaces close to its leading edge, are also reflected. These reflected shocks contribute to the unsteady surface pressures on the rotors' pressure surface and on the stators'/vanes' suction surface (Laumert et al., 2002). The shock wave excitation found in transonic turbine stages are most likely the primary flow mechanism which contributes to the blade vibration excitations (Chiang and Kielb, 1993; Kachel and Denton, 2006).

Potential field

The downstream and upstream static pressure field of a blade row, varies in the radial and circumferential directions due to blade load (Jöcker, 2002). The downstream vane (DV) static pressure field or potential field (the dashed line) for a 1.5 stage turbine is shown in Figure 1.3. Kachel and Denton (2006) explain from a theoretical analysis point of view, that for a steady flow field one would find the potential field is frozen to a blade row. The other blade rows will experience, due to their relative motion, this potential field periodically at the blade passing frequency. In transonic turbine stages, potential field interaction has the second largest contribution, amplitude wise, on the rotor's unsteady surface pressure (Miller, Moss, Ainsworth and Harvey, 2003a). In a subsonic turbine stage, potential field interactions are primarily responsible for the large unsteady surface pressure (Laumert et al., 2002).
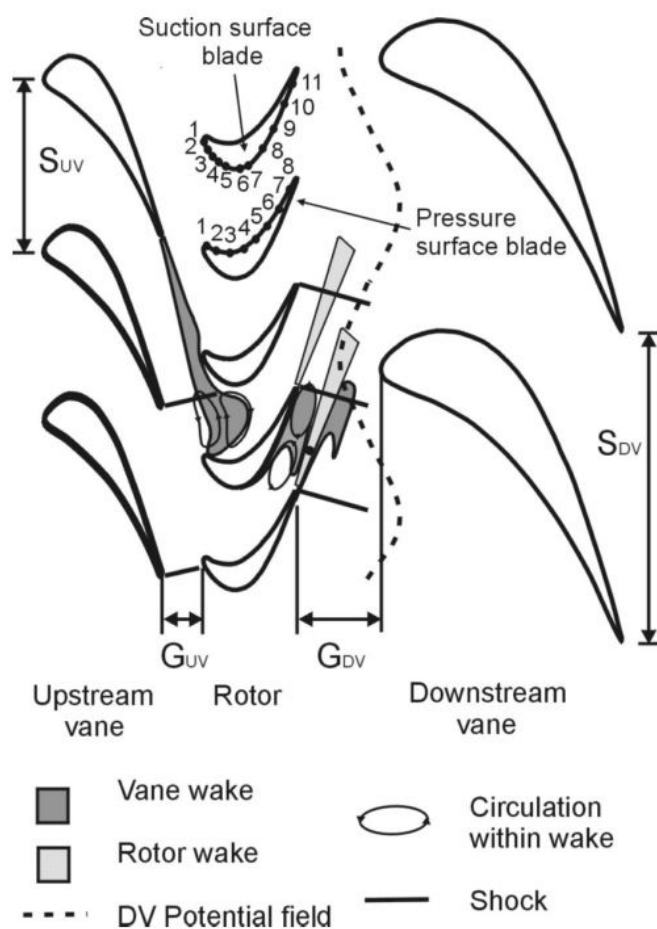

Figure 1.3: Wake, Shock, and Potential field (Miller, Moss, Ainsworth and Harvey, 2003b)

Wakes

Wakes are formed due to the development of a boundary layer on the surface of a blade (rotor and stator), which detaches from the surfaces at the blade's trialing edge (Jöcker, 2002). When the stator's wake is cut by the leading edge of the rotor, segments form and convect through the rotor passage at the free stream velocity, Figure 1.3 shows a schematic of this wake interaction (Miller, Moss, Ainsworth and Harvey, 2003b).

Now as these wake segments flow through the rotor passage, they are also rotating clockwise and anti-clockwise, see Figure 1.3. These rotating segments will either increase or decrease the fluid velocity at the suction surface or pressure surface of the rotor. This will then either result in a static pressure decrease (when the rotational direction is the same as the flow direction) or increase (when the rotational direction is opposite to the flow direction) (Hodson et al., 1996).

In the investigation by Miller, Moss, Ainsworth and Harvey (2003a) it was shown for a transonic high pressure turbine stage, that a wake has a negligible effect on the unsteady surface pressure of the rotor blade. However the study by Lakshminarayana et al. (2000) on a subsonic turbine stage, showed that the blades were also excited due to wakes. This excitation occurs at the wake passing frequency. Also according to Miller, Moss, Ainsworth and Horwood (2003) the dominant interaction mechanism in the high-aspect ratio subsonic blades is caused by the blade wake.

Vortex shedding

Just as the wakes, vortex shedding also occurs due to the boundary layer that separates at the trailing edge of the rotor and stator, see Figure 1.4. The vortices rotate clockwise and anti-clockwise and shed at a Reynolds number dependent frequency. This frequency is in most cases much higher than that of the wake passing frequencies (Jöcker, 2002). Due to the small variation in velocity and high frequencies associated with vortex shedding, the excitation caused by vortex shedding is not usually regarded as a source which causes forced vibrations (Hummel, 2002). Although the impact vortex shedding has on the performance of a turbine is quite significant.
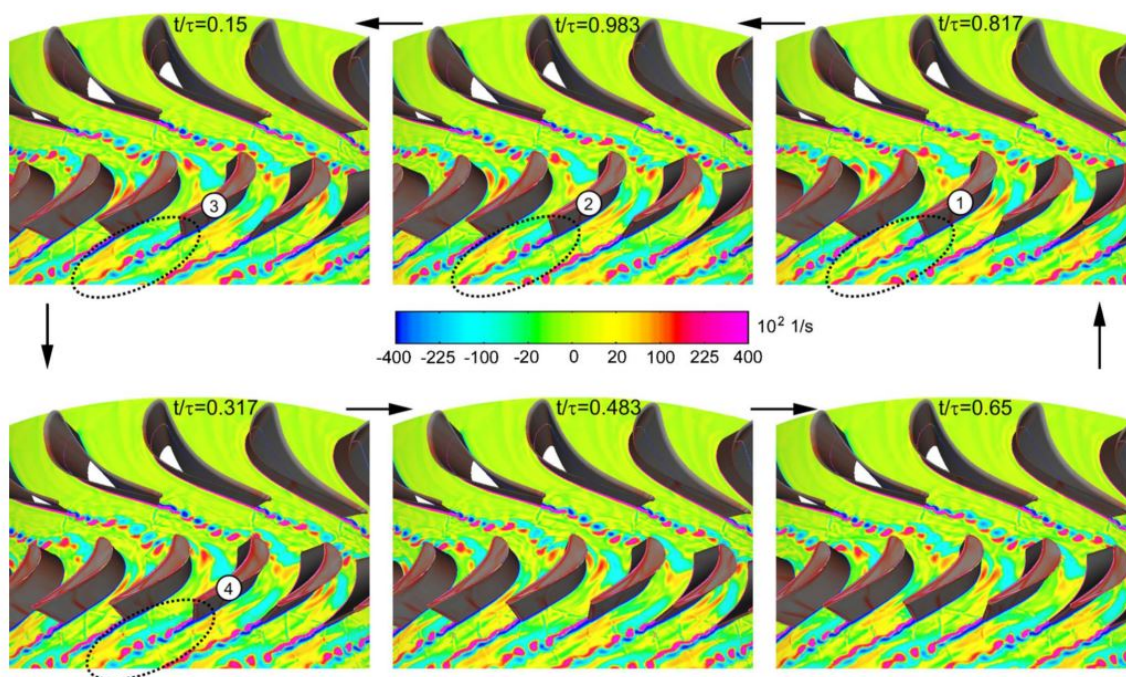

Figure 1.4: Vortex shedding from stator and rotor from an unsteady CFD simulation (Gottlich et al., 2006)

Secondary flow

Secondary flow can be described as any flow whose flow direction is not in the ideal or primary flow direction (Wissenschaften, 2003). Secondary flows are the resultant flow generated by local pressure gradients within the passages and are inherently three dimensional (Jöcker, 2002).

There are a various kinds of flow features that makes up secondary flow. Some of these common flow features, depicted in Figure 1.5, are: horse-shoe vortices (pressure side H_p and suction side H_s), passage vortex and corner vortex (Wissenschaften, 2003). From the investigation conducted by Fan and Lakshminarayana (1995), on an axial turbine stage, it was found that the nozzle's secondary flow had a significant contribution towards the unsteady surface pressure of the rotor blade.
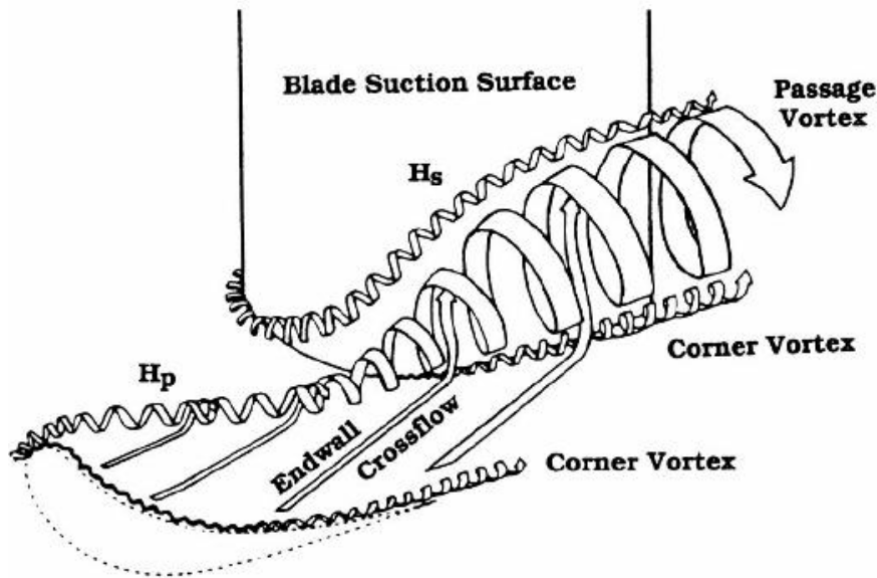

Figure 1.5: Secondary flow - common features (Moon and Koh, 2001)

1.2.5   Structural response

There are various aspects regarding the structural side that impact the RUL of a turbine blade. The response of a mechanical structure, such as a turbine blade, is described by the equation of motion (EOM). The cyclic stress history of the turbine blade is related to how the turbine blade responds to the various loadings (centrifugal, aerodynamic, etc.). The aspects that influence the response of the turbine blade can be categorized into three categories, evident from the EOM, namely the mass, damping and stiffness of the turbine blade.

The mass of a turbine blade is a function of geometrical shape as well as material properties such as density. A heavier turbine blade will result in higher mean stresses for a given rotational speed which reduces the RUL of a turbine blade. Also the natural frequencies of a turbine blade is a function of mass, thus certain masses will help avoid resonance. The stresses induced on a turbine blade due to resonance could result in heavy damage and reduce the RUL of a turbine blade (Prabakaran and Pradeep, 2015).

The damping experienced by a turbine blade consists of the material damping, which is small and negligible, aerodynamic damping, and frictional dissipation (Szwedowicz, 2008). Frictional dissipation/damping is obtained by using for example friction bolts, lacing wires or damping pins (Szwedowicz et al., 2008; Drozdowski et al., 2015). Damping reduces the response of the turbine blade as it is being excited by periodic aerodynamic forces and as a result reduces the amplitudes of the cyclic stresses, therefore extending the RUL of a turbine blade.

The stiffness of a turbine blade is a function of material properties (Young's Modulus, Poisson ratio), geometrical shape and features, rotational speed (centrifugal loading), pre-assembly forces, blade deformation resulting from external aerodynamic loading, and friction shear coupled forces (Szwedowicz, 2008). Over the years, turbine designers introduced additional geometrical features such as lacing wires to increase the blade stiffness (Drozdowski et al., 2015). As mentioned before resonance could result in heavy damage and reduce the RUL of a turbine blade. The natural frequencies of a turbine blade and its disk assembly is also a function of stiffness; therefore it is extremely important to obtain a blade stiffness that will prevent the occurrence of resonance.

1.2.6 Centrifugal forces and aerodynamic forces

According to Frey and Fleeter (1998) rotating blades are more likely to be receptive to HCF due to the large mean stresses induced by centrifugal forces. Ubulom et al. (2017) noted that the HCF was substantially effected by the mean stresses. According to Alwan et al. (2007) the stresses induced by the centrifugal forces contribute the most to the total stresses experienced by rotor blade. However, according to Patel and Palazotto (2004a) just considering the impact of the stresses resulting for the centrifugal forces on the HCF life is inadequate, and that it is important to account for the aerodynamic forces acting periodically on the turbine blade.

1.2.7 Preventing turbine blade failure

Steps need to be taken in order to prevent turbine blade failure due to fatigue. One such step is to make use of a Campbell diagram during the design phase of a turbine to ensure that under normal operational conditions resonance will not occur. The Campbell diagram can be created by means of an analytical approach where the turbine blade is represented by a simplified model. An alternative is to use a finite element method (FEM) model, which is able to predict natural frequencies and mode shapes more accurately, seeing that it uses a more representative geometry (Misek et al., 2007). Furthermore, the authors mention that even though the Campbell diagram provides an indication of where resonance could occur, it does not provide information regarding the amplitude of the resulting stresses. The cyclic loads result in alternating stresses in turbine blades which finally causes HCF. In order to predict the RUL due to HCF will require that the amplitudes of the stresses to be known.

According to Misek et al. (2007) unsteady aerodynamic forces experienced by turbine blades during operation, can be obtained using either time-resolved CFD or nonlinear harmonic CFD. CFD can be used to predict the aerodynamic forces experienced by the turbine blades, as well as the temperature distribution within the turbine blades. May-

orca (2011) concluded that modern high-fidelity CFD tools would be able to contribute greatly in predicting forces which turbine blades are experiencing. Aerodynamic forces consist of a shear and a pressure component. The aerodynamic forces experienced by the turbine blades are mostly due to pressure forces acting on the blade. Comparing the direct pressure measurements to the predicted CFD pressures showed that the unsteady forces that excite the turbine can be predicted quite accurately (Ning et al., 2003).

The unsteady surface pressures obtained using CFD are used to perform a forced response of the turbine blade (Misek et al., 2007). Advances in CFD and FEM software and computer hardware have allowed the computation of unsteady stresses which result from aerodynamic forces.

1.2.8 Aspects that affect blade surface pressures and temperatures

Estimating the RUL of a turbine blade will firstly require the prediction of the excitation forces consisting basically only of pressure forces and also the prediction of the temperature distribution in the blade. As mentioned before, CFD can determine the excitation forces (Misek et al., 2007) and temperature distributions within a turbine blade. When using CFD there are various aspects that will affect the predicted pressures and the temperatures. In the sections below aspects that affect the pressures and temperatures are discussed.

Geometry

Krishnababu et al. (2009) investigated the flow and heat transfer of a flat and two squealer type tip geometries in an unshrouded axial turbine using CFD. The area weighted heat transfer at the tip was found to be lower for the two squealer geometries compared to the flat tip. According to Lampart et al. (2005) it is important to model the effect of leakage flow and extractions in order to predict realistic flow patterns in multi-stage turbomachinery.

Rahman et al. (2013) performed a steady state CFD simulation of a single stage gas turbine to investigate the tip leakage and heat transfer in the vicinity of the rotor tip, for different rotational speeds and tip clearance heights. The investigation showed that the tip leakage and secondary flow interaction had a substantial impact on the heat transfer at the rotor tip. It was observed that the tip leakage flow was strongly dependent on the tip gap height clearance. The recirculation region size, resulting from tip leakage flow, was found to be proportional to the clearance height, the size increasing as the clearance height increased.

Andreini et al. (2012) performed steady state CFD simulations of a gas turbine blade to study the effect of de-featuring. CFD simulations were performed of a full-featured geometry and a simplified geometry of a gas turbine blade. The effect that the de-featuring had on heat transfer and surface temperature was clearly evident, see Figure 1.6 and Figure 1.7. The authors concluded that modifying the end wall and hub regions subsequently altered both the wall temperature and heat transfer coefficient distributions.
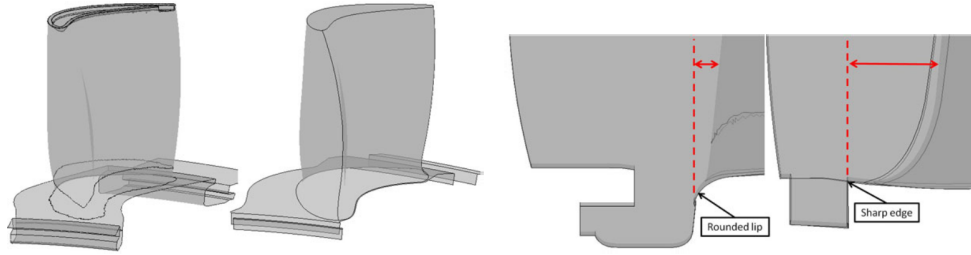
Figure 1.6: Full-featured geometry and simplified geometry (Andreini et al., 2012)
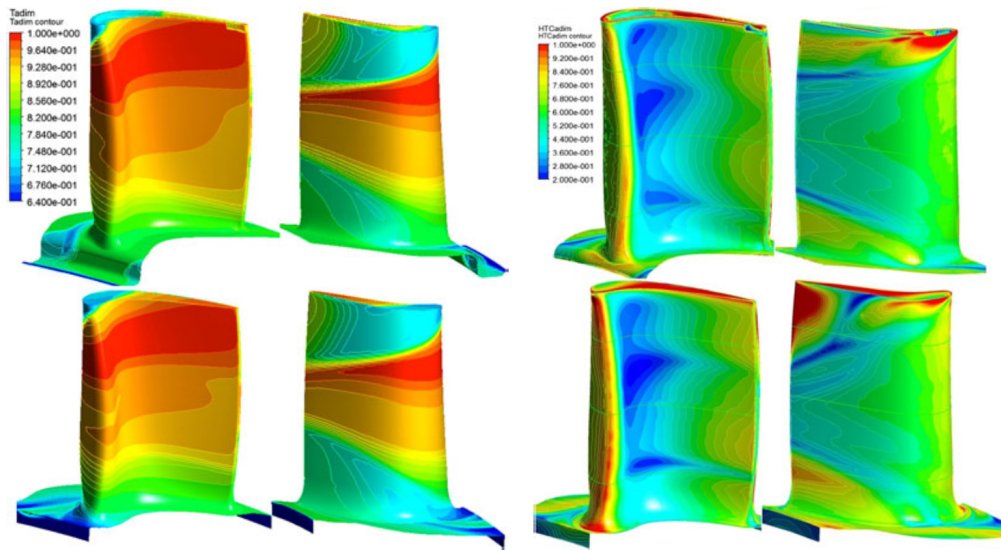

Figure 1.7: Adiabatic wall temperature (Left) and heat transfer coefficient (Right) (Andreini et al., 2012)

Numerical grid

According to Montomoli et al. (2015), it is of fundamental importance to perform a mesh independence study. The authors are of the opinion that poorly predicted flow structures as well as integral parameters can result from improper grid spacings. Therefore, when performing hi-fidelity CFD the effect of the numerical grid must be accounted for by means of mesh independence.

Boundary conditions (Turbulence intensity and length scale)

Choi et al. (2004) investigated the effect that free-stream turbulence has on a turbine blade's heat transfer and pressure coefficient for Reynolds numbers ranging from 15 700 to 105 000. An experiment was conducted in a wind tunnel using a linear test cascade consisting of 5 turbine blades. The turbulence intensity was varied from 0.68% to 15.31%, using a fine and course turbulence grid. The local pressure coefficient on the suction side of the blade was found to increase as the turbulence intensity increases, the opposite was found to be true for the blade's pressure side. The local Nusselt number was found to increase as the turbulence intensity increased.

Butler et al. (2001) also conducted an experiment using a linear cascade of turbine blades. The authors also investigated the effect of turbulence intensity at low Reynolds numbers, but for low-pressure turbine blades. Their findings were in many respects the same as that of Choi et al. (2004), such as it was also found that the heat transfer at the stagnation region increased as the turbulence intensity increased. However, Butler et al. (2001) noted that at 10% turbulence intensity no flow separation was evident, while at low turbulence intensity (0.4-0.8%) the flow still separated.

Time and frequency domain

Asghar et al. (2018) performed steady state, time-marching and nonlinear harmonic (NLH) CFD simulations of a transonic high pressure turbine. Comparison showed that the main unsteady flow interactions were resolved and captured sufficiently when 3 harmonics were solved for in the NLH simulation. According to the authors the first and second harmonics mainly contribute to the pressure amplitude.

Green et al. (2013) simulated a single-stage high-pressure transonic turbine using the NLH method and the time-marching method. The NLH simulation was solved for 3 harmonics. The unsteady pressure results for both methods were in good agreement with experimental data. However, the phase-lag approach did overpredict the time dependent experimental pressure data for multiple measurement locations. The NLH method however predicted the time dependent experimental pressure data much better from a magnitude point of view.

Green et al. (2013) mentioned that the time-marching method with phase-lag require significantly more iterations and took about 10 times longer to converge. The only down side to the NLH method was that it required 5 times more RAM to solve. Asghar et al. (2018) found that the time-marching method took about 7 times longer when they simulated a transonic high pressure turbine.

Turbulence modelling

As mentioned earlier, Krishnababu et al. (2009) investigated the flow and heat transfer of a flat and two squealer type tip geometries in an unshrouded axial turbine using CFD. The authors also simulated the flat tip geometry using SST k-ω, standard k-ω and standard k-ϵ turbulence models and compared the predicted heat transfer coefficient with experimental results (Figure 1.8). Comparing the average heat transfer coefficient at the tip revealed that the SST k-ω and standard k-ω underpredicted by nearly 10% and 20%, respectively, whereas the standard k-ϵ overpredicted by nearly 50%.

Dunn et al. (2011) performed 2D CFD simulations of a turbine blade in order to study the external surface heat transfer predictions for four different turbulence models and a boundary layer solver. The boundary layer solver consistently predicted the pressure and suction surface heat transfer well. The Yang-Shih k-ϵ and Spalart-Allmaras turbulence models both overpredicted the suction surface heat transfer. The Spalart-Allmaras with AGS (Abu-Ghannam and Shaw) and intermittency underpredicted the heat transfer on the suction surface, whereas without intermittency only a fairly accurate prediction could be obtained. Reasonably good pressure surface heat transfer predictions were obtained by all four of the turbulence models.
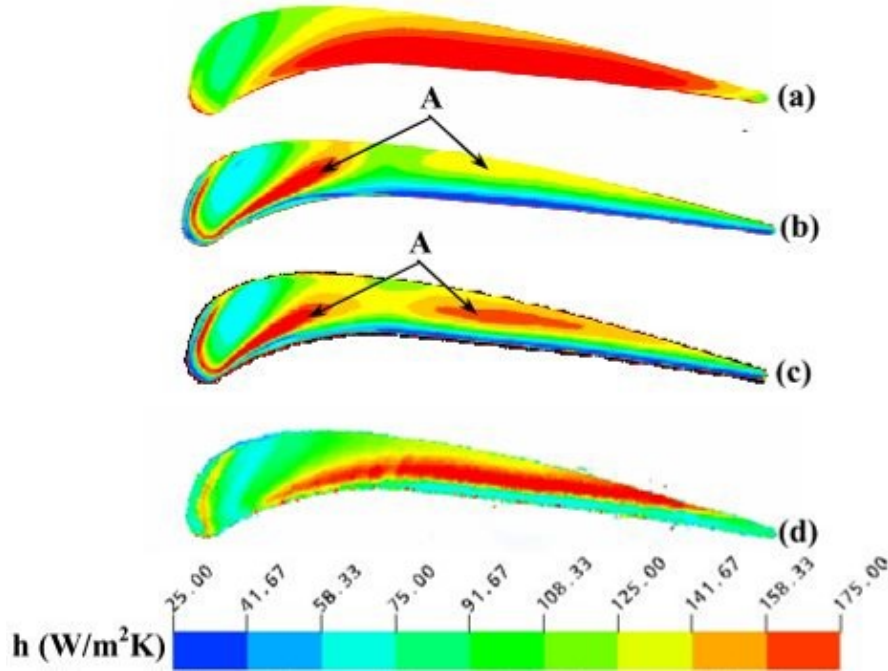
Figure 1.8: Heat transfer coefficient comparison (a) k-ϵ, (b) k-ω, (c) SST k-ω models and (d) experimental (Krishnababu et al., 2009)

According to Laumert (2002) the Spalart-Allmaras, k-ϵ and k-ω turbulence models have been shown to predict the unsteady pressure perturbations in turbines with reasonably good accuracy.

1.2.9 RUL estimation and sensitivity

Ubulom et al. (2017) investigated the effect of the chosen fluid-structure approach on the high-cycle fatigue life estimation of a turbine blade. The authors used a fully coupled and decoupled method to estimate the stress histories used for the fatigue life estimation. The effect of the two methods on the estimated high-cycle fatigue life were evaluated using both a frequency and time domain method. It was shown for both the frequency and time domain fatigue life estimation methods, that the decoupled method estimated a shorter high-cycle fatigue life, thus providing a more conservative estimation. Both fully and decoupled methods had a mean stress equivalent of 200 MPa, but the former method resulted in a stress ratio of 0.77 and the latter of 0.3.

Patel and Palazotto (2004b) recognized the need for high-cycle fatigue prediction of turbine blades, and developed a method which uses finite-element evaluations. The authors mention that by following this method, crack-growth can be studied within the HCF environment.

Misek et al. (2007) performed a high-cycle fatigue analysis of a high pressure steam turbine with shrouded blade rows. The fatigue life prediction was performed using CFD and FEM in a decoupled manner. The fatigue life prediction was used to evaluate an existing and a new design of the stator. The newly designed stator resulted in unsteady stresses which were below the actual fatigue limit.

18

1.3 Scope of research

From the Problem statement and Literature review, it is clear that high-cycle fatigue (HCF) is the primary cause for turbine blade failure and with steam turbines being used beyond their original design life, there exist a need to estimate the remaining useful life (RUL) as accurately as possible. Section 1.2.1 clearly state the necessity for RUL estimation.

According to Frey and Fleeter (1998) rotating blades are more likely to be receptive to HCF due to the large mean stresses induced by centrifugal forces. According to Alwan et al. (2007) the centrifugal forces mainly contribute to the overall mean stresses experienced by a turbine blade. Consequently, the overall contribution of the aerodynamic forces to the magnitude of a turbine blade's stress field is very small compared to that of the centrifugal forces.

However, even though the centrifugal forces mainly contribute to the overall stresses that impact the RUL of a turbine blade due to HCF, the contribution of the aerodynamic forces cannot be neglected. According to Patel and Palazotto (2004a) just considering the impact of the steady stresses resulting from the centrifugal forces on the HCF life is inadequate, and that it is important to account for the aerodynamic forces acting periodically over the turbine blade.

In order to estimate the RUL of a turbine due to HCF, the unsteady pressure and temperature fields need to be known so that the cyclic stresses can be computed. Then using the computed cyclic stresses, the RUL can be estimated by performing a fatigue analysis. Some utilities use empirical methods to determine the excitation forces, but require more accurate methods. According to Miller, Moss, Ainsworth and Horwood (2003), the inaccurate prediction of high-cycle fatigue, thermal durability and stage performance is introduced when one does not consider blade row interaction.

Computational fluid dynamics (CFD) can however account for blade row interactions and determine the excitation forces (Misek et al., 2007), and temperature distributions within a turbine blade. Mayorca (2011) concluded that modern high-fidelity CFD tools would be able to contribute greatly in predicting the excitation forces, and the work of (Ning et al., 2003) demonstrated that these predictions can be quite accurate.

From Section 1.2.8 it is clear that there are aspects that affect the temperature and pressure distributions on a turbine blade surface. Section 1.2.5 discusses some aspects' that affect the response of a turbine blade to excitation forces. If RUL is to be estimated as accurately as possible, the sensitivity of the estimated RUL to these aspects needs be known. Ubulom et al. (2017) investigated the sensitivity of the HCF life estimation of a turbine blade to the chosen fluid-structure approach. The decoupled approach estimated the high-cycle fatigue life more conservatively, than the coupled approach.

When estimating the RUL of a turbine blade the unsteady pressures and temperatures need to be predicted. These unsteady predictions can be obtained using CFD, by either solving the unsteady flow in the time domain (time-marching method) or in the frequency domain (Harmonic balance or nonlinear harmonic (NLH) method). It has been seen in

the literature that the NLH method predicts the unsteady pressures more accurately and faster compared to the time-marching method. Therefore, understanding the sensitivity of the estimated RUL to the NLH setup in a CFD simulation, would greatly contribute to the RUL estimation process.

The purpose of this work is to conduct a sensitivity analysis in order to establish the sensitivity of the estimated RUL of a turbine blade, to the number of harmonics used in an NLH CFD simulation. The work of Asghar et al. (2018) and Green et al. (2013) showed that the number of harmonics used in a NLH simulations affect the predicted pressures on a turbine blade surface. Furthermore, based on the work of Asghar et al. (2018) it was decided to consider 1, 2, and 3 harmonics for the sensitivity analysis, seeing that it was found that the first and second harmonics mainly contribute to the pressure amplitude.

From the literature review in Section 1.1 and Section 1.2.2, it was decided to perform the sensitivity analysis on a LP steam turbine's last stage rotor blade. The sensitivity analysis considered 3 operational conditions, in order to be able to draw more meaningful conclusions regarding the sensitivity of the estimated RUL to the number of harmonics used in an NLH simulation. The sensitivity of the RUL to the number of harmonics will be evaluated in the HCF regime in the sense that the predicted stress histories will be below the yield strength of the material, but not necessarily of such nature that HCF failure will occur. For a given operational condition and number of harmonics used in a NLH simulation, the RUL was estimated as follows:

1. Solve for the unsteady flow by performing an NLH CFD simulation.

2. Performing the needed FEM analyses of a turbine blade, in order to compute the time dependent stress field, resulting from the unsteady flow computed in step 1.

3. Lastly, perform a fatigue analysis to estimate the remaining useful life (RUL) of the turbine blade using the time dependent cyclic stress computed in step 2.

1.4   Document overview

This dissertation consists of four chapters. The first chapter starts by giving some background and describing the problem which is to be addressed. This is followed by a literature review which discusses the necessity of estimating the RUL and turbine blade failure and fatigue cracking occurrences. Further the unsteady aerodynamic flow inside a turbine and the response of turbine blade to this unsteady flow are discussed. Lastly, aspects that affect the surface pressures and temperatures of turbine blade are reviewed and some work conducted on RUL estimation and the sensitivity thereof are reported. The scope of research is defined, describing the main outcome of this work.

Chapter 2 covers the development of the numerical model, which is used to establish the sensitivity of the estimated RUL to the number of harmonics used in an NLH simulation. The assumptions and simplifications made are discussed and explained for both the CFD model and FE model. Finally, the fatigue analysis approach, followed to estimate the RUL, is described.

Chapter 3 contains the results of the sensitivity analysis. The aerodynamic forces predicted by the NLH simulations utilizing 1, 2, and 3 harmonics for the 3 load conditions are presented and discussed. The stress histories computed by performing a transient structural analysis are also presented and discussed, followed by the fatigue analysis results where the RUL was estimated.

Lastly, the fourth chapter gives the conclusions to the sensitivity analysis and the work performed as well as the recommendations regarding future work.

Chapter 2

Numerical Model

2.1 Introduction

This chapter describes the numerical model used to estimate the RUL of a LP steam turbine's last stage rotor. The numerical model consists of a CFD, FE and fatigue model. The numerical model was set up in such a manner that would be sufficient for the purpose of the sensitivity analysis, the purpose being to establish the sensitivity of the estimated RUL to the number of harmonics used in a nonlinear harmonic (NLH) CFD simulation. For example, all assumptions and simplification made in the CFD model will still ensure that the predicted unsteady flow field of the LP steam turbine is representative of what one would find in a LP steam turbine.

2.2 Turbine configuration

The LP steam turbine modelled is a dual flow turbine capable of producing around 100MW at 3000 rpm, when operating at 100% load. The two halves of the turbine each consists of 5 stages, but only one half was modelled. The RUL was estimated for the last stage rotor, approximately 1.02m in height (measured from root to tip), made of 12% Chromium steel, see Figure 2.1. The RUL of the last stage rotor was estimated for when the LP steam turbine operates at 100%, 79%, and 44% load.
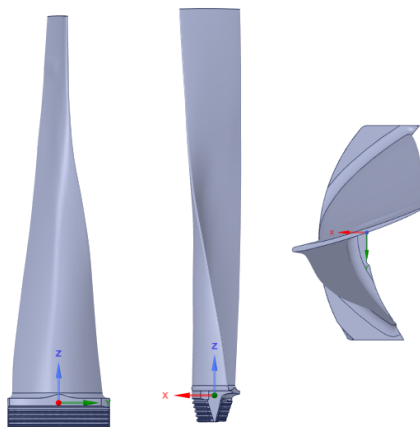

Figure 2.1: Last stage rotor - axial, tangential and radial view

2.3 Methodology

The diagram in Figure 2.2 demonstrates the systematic procedure followed to estimate the RUL of the last stage rotor. The estimation process considers a weak coupling between the CFD model and FE model, seeing that it results in the more conservative RUL estimations (Ubulom et al., 2017). An NLH simulation was performed to firstly calculate the unsteady static surface pressure distributions on the last stage rotor, followed by the mapping thereof to the FE model, for which a transient structural analysis was performed. Finally, the RUL was estimated by performing a fatigue analysis on the stress history obtained from the transient structural analysis. The effect of temperature on the estimated RUL was not accounted for, due to the limited computational resources available.
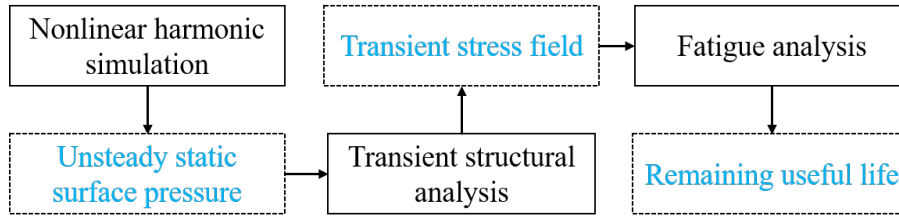
Figure 2.2: Remaining useful life (RUL) estimation methodology

The CFD model was developed and solved using NUMECA FINE^{TM}/Turbo 11.2rc. ANSYS 19.1 was used to develop a FE model and to perform all the required structural analyses of the last stage rotor. Quick Fatigue Tool from Matlab was used to perform the fatigue analysis required to estimate the RUL of the last stage rotor.

2.4 CFD model

2.4.1 Geometry

A CAD assembly drawing of the LP steam turbine was available and imported as a parasolid into NUMECA's AutoGrid5^{TM} 11.2rc for further modelling. The hub and shroud were simplified, but were still representative of the actual LP steam turbine's hub and shroud. The simplified hub and shroud can be seen in Figure 2.3. The diffuser outlet was also simplified, but the outlet area of the original diffuser and simplified diffuser outlet was kept the same.

Due to limited computational resources of 32GB RAM and the high computational cost associated with NLH simulations, it was not possible to include all geometrical features, therefore some geometrical features such as seals, were excluded. Fillets were also excluded, primarily due to the information of fillets radii not being available at the beginning of this study. This information only became available closer to the end the study, which at that stage could not be included any more, due to time constraints.

Furthermore, according to Ning et al. (2003) the fatigue in turbines can be primarily ascribed to the inherently unsteady aerodynamic flow through turbines. This unsteady aerodynamic flow in turbines is characterized by flow features such as vortex shedding,

wakes, shocks, potential fields and secondary flow. Excluding the fillets will not result in the absence of any of these characteristic flow features, therefore the predicted unsteady flow field will still be representative of what one would find in a LP steam turbine.

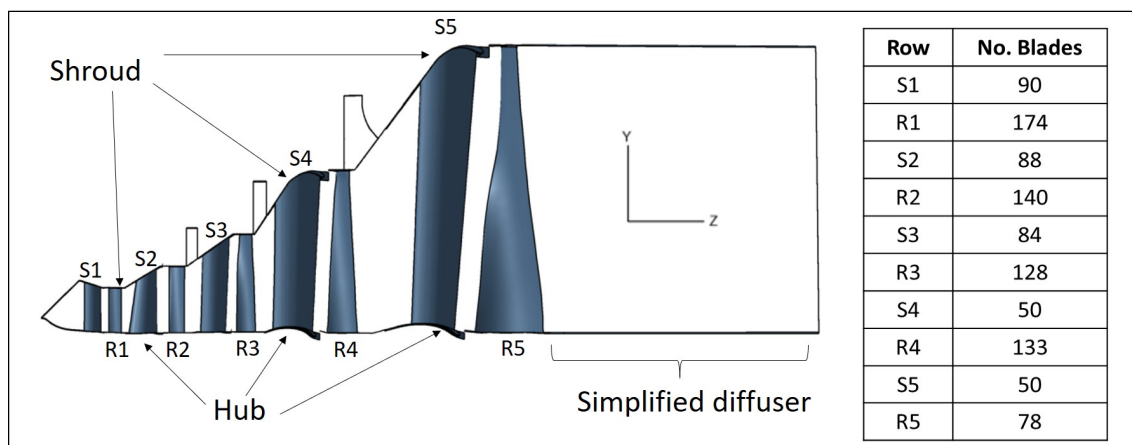| Row	No. Blades
S1	90
R1	174
S2	88
R2	140
S3	84
R3	128
S4	50
R4	133
S5	50
R5	78

Figure 2.3: Simplified hud, shroud, and diffuser

Furthermore, considering a long slender body or cantilever beam, the contribution of the distributed forces close to the fixed end to the high resulting stresses at the fixed end, are negligible. The last stage rotor can be thought of as a long slender beam fixed at the hub. Considering that the region of interest for the RUL estimation is located in the hub region, the contribution of accurate static surface pressure (distributed forces) predictions within the region, will be negligible.

When the rotor blades of the LP turbine rotate at 3000rpm, centrifugal forces deform the blades. Figure 2.4 shows the total deformation of the last stage rotor blade due to the centrifugal forces. The largest total deformation is 10.397mm. The geometrical differences between a last stage rotor blade that rotates at 3000rpm and at 0 rpm, were considered to be negligible for the purpose of the sensitivity analysis. Therefore, the geometry of the rotor blades used in the CFD model were that of the non-rotating rotor blades, seeing that it was already available.
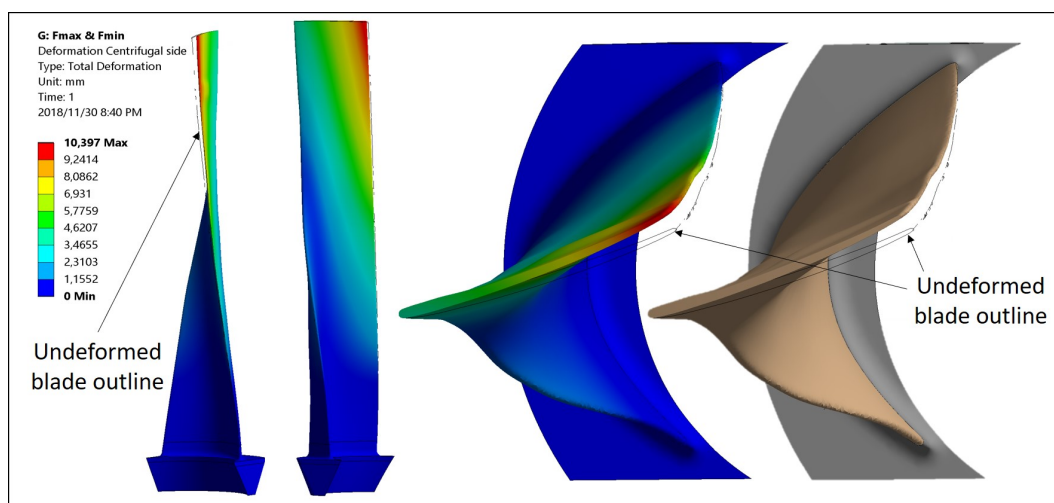

Figure 2.4: Deformation of last stage rotor due to centrifugal forces

2.4.2   Mesh

A high-quality structured mesh was generated utilizing NUMECA AutoGrid5^{TM} 11.2rc. A low y+ mesh was considered, seeing that the region of interest is the surface of the last stage rotor. Due to limited computational resources it was not possible to generate a very fine mesh. Consequently, the mesh size was limited to about ∼7.1 million cells.

A mesh independence study was performed by means of steady state simulations, to assess whether the solution would be mesh independent for the ∼7.1 million cell mesh. The mesh was refined in all directions, but the greatest amount of refinement was performed in the axial and tangential directions. The study was performed for the 100% load case and not for the 79% and 44% load case. The reason being that the velocity, pressure, and temperature distributions within the LP turbine were found to be, for all practical purposes, the same for all three load conditions, with the only difference in magnitude. Thus, if a mesh was found to be independent for the 100% load case, it would also be the mesh independent for the 79% and 44% load cases.

The parameters of interest for the mesh independence study were the power generated by the LP turbine and the aerodynamic forces exerted on the last stage rotor. Table 2.1 shows the results for the mesh independence study. The directions of the aerodynamic forces are depicted in Figure 2.5. It is evident that as the mesh size increase the relative error (relative to the finest mesh), decreases. All of the relative errors are less than 1%, and given these small relative errors, it can be concluded that the parameters of interest are mesh independent for the ∼7.1 million cell mesh. The mesh size of ∼7.1 million cells was also found to be acceptable seeing that for all three simulated loading conditions the power was predicted within 6%, see Section 2.4.5. Figure 2.6 shows the blade surface mesh for the ∼7.1 million cell mesh.

To ensure an accurate prediction of the static surface pressure distributions, the wall y+ values were kept below or close to one. Figure 2.7 and Figure 2.8 show the wall y+ values for the 100% load case. The 100% load case produced the highest wall y+ values of the three load cases, seeing that the greatest amount of steam entered the LP steam turbine at 100% load. The wall y+ values, for 79% and 44% load, were lower than the 100% load case, seeing that the mass flow into the LP steam turbine decreases as the load decreases.

Table 2.1: CFD mesh independence results

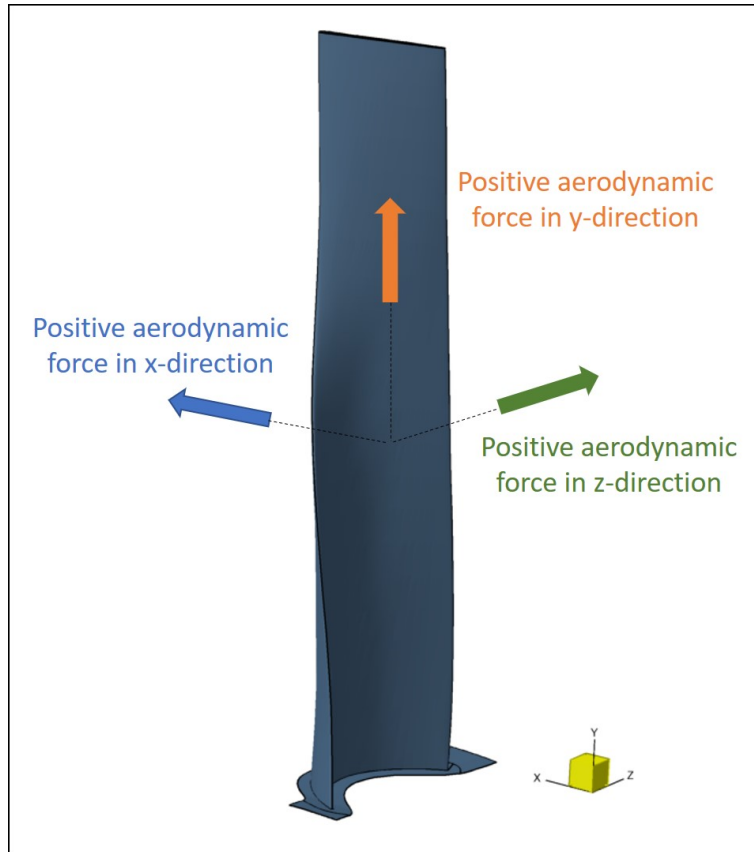| Mesh Size [No. Cells]	Power [MW]	Relative error	Force X [N]	Relative error	Force Y [N]	Relative error	Force Z [N]	Relative error
4 569 808	47.85	0.901%	310.70	0.703%	-25.13	0.653%	552.00	0.345%
7 064 276	48.14	0.293%	311.30	0.511%	-25.03	0.240%	551.40	0.236%
11 358 160	48.28	0%	312.90	0%	-24.97	0%	550.10	0%

Figure 2.5: Direction of aerodynamic forces
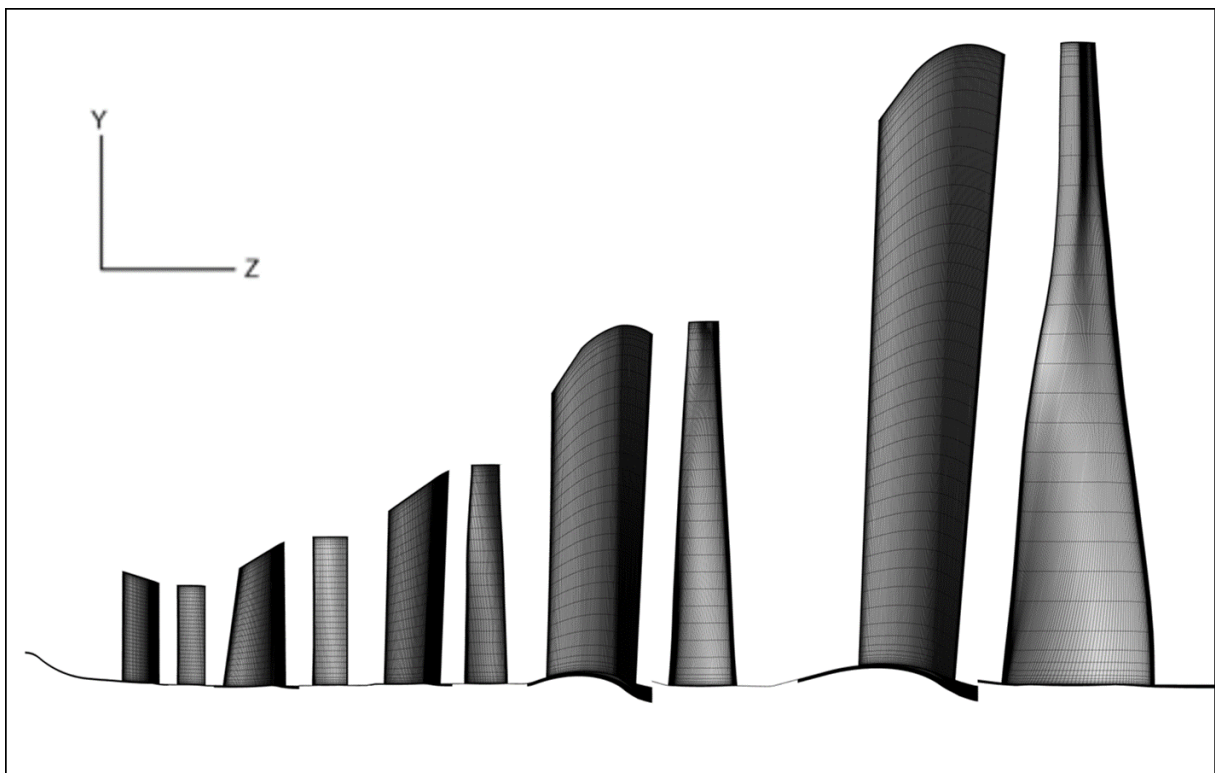

Figure 2.6: Blade surface mesh

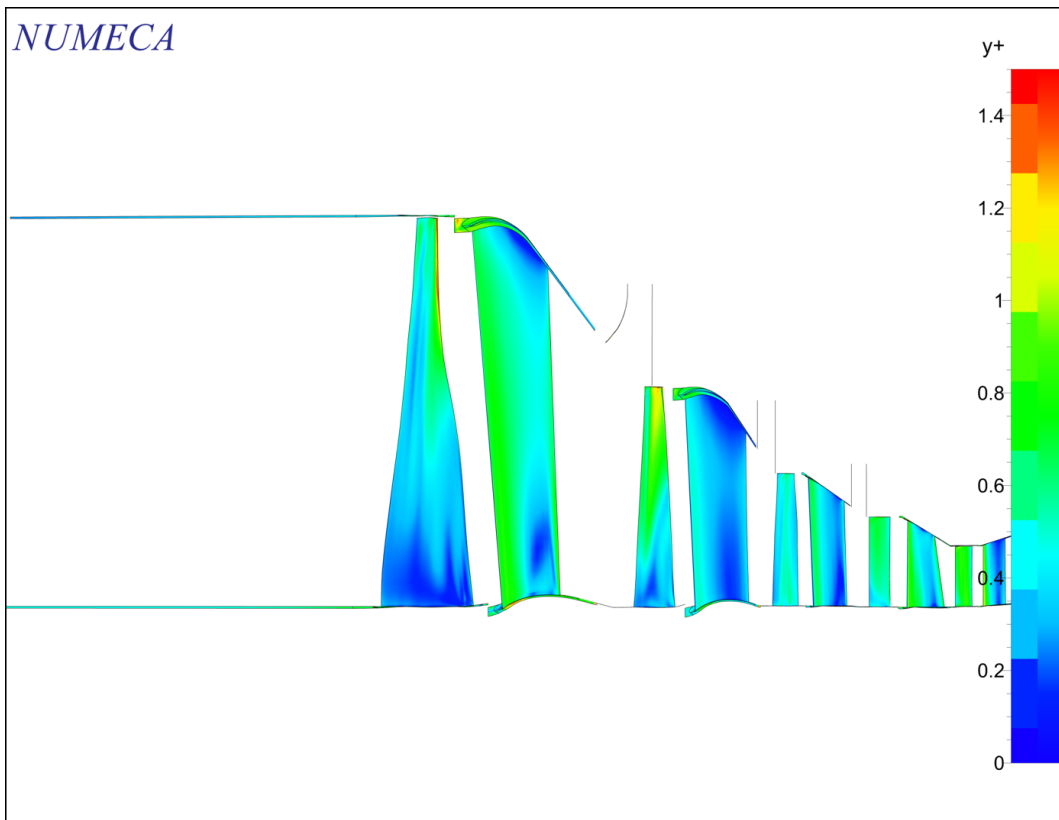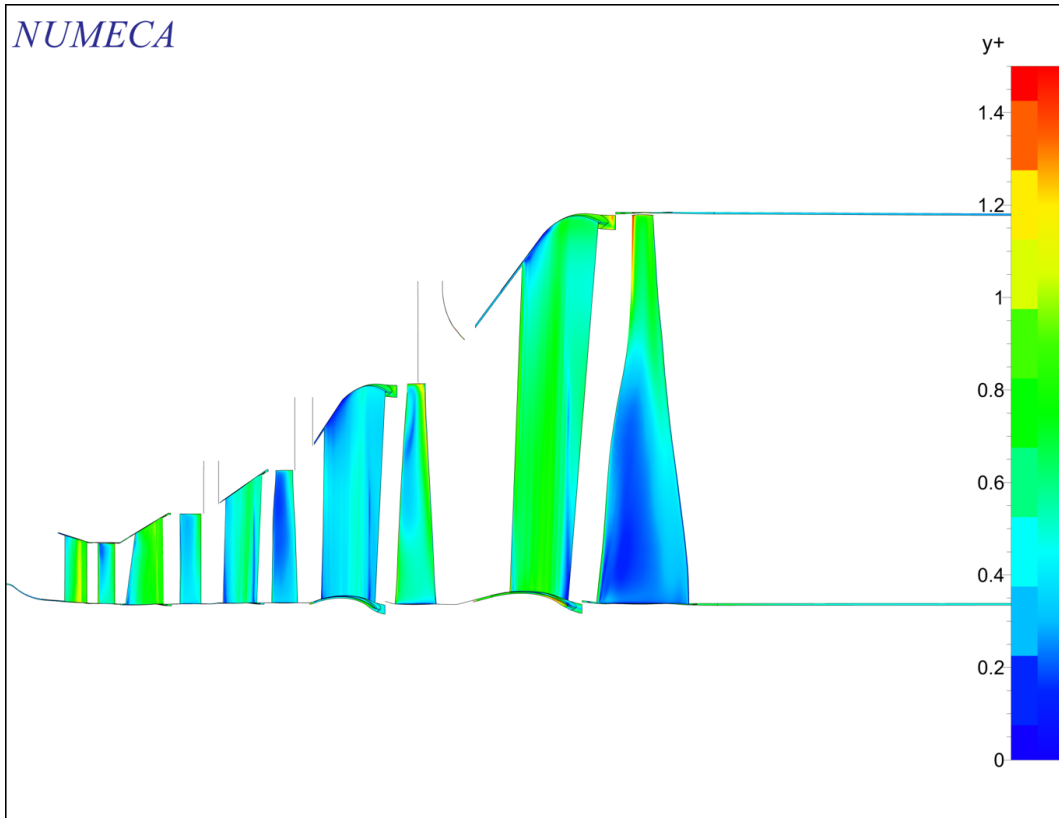Figure 2.7: Wall y+ (View 1)

Figure 2.8: Wall y+ (View 2)

2.4.3 Physics

The CFD model considered condensable steam operating in the turbulent flow regime. The effect of turbulence was modelled using the 1-equation Spalart-Allmaras turbulence model with a low Y+ treatment. There were three reasons why the Spalart-Allmaras was chosen. Firstly, the Spalart-Allmaras was the highest order turbulence model available, in FINE^{TM}/Turbo 11.2rc, that could be used in a NLH simulation that considered condensable steam as its working fluid. Secondly, according to Laumert (2002) the Spalart-Allmaras, k-ϵ and k-ω turbulence models have been shown to predicted the unsteady pressure perturbations in turbines with reasonably good accuracy.

Thirdly, the findings of Laumert (2002) were confirmed by performing a steady state simulation of the LP steam turbine, operating at 100% load, with the k-ω SST and Spalart-Allmaras turbulence models. The two turbulence models were only simulated for the 100% load case, seeing that the flow, pressure and temperature fields show the same distributions but just at different magnitudes.

Table 2.2 shows the predicted power and aerodynamic forces exerted on the last stage rotor, for the two turbulence models. Figure 2.9 shows the static surface pressure distributions on the last stage rotor predicted by the two turbulence models. From the tabulated values it is evident that the percentage error in the predicted power and aerodynamic forces are less than 1.108%. It can be seen from Figure 2.9, that the static surface pressure distribution for the Spalart-Allmaras and k-ω SST are practically the same. Based on these results, it was found acceptable to use the Spalart-Allmaras turbulence model, for the purposes of this work.

Table 2.2: Turbulence model comparison

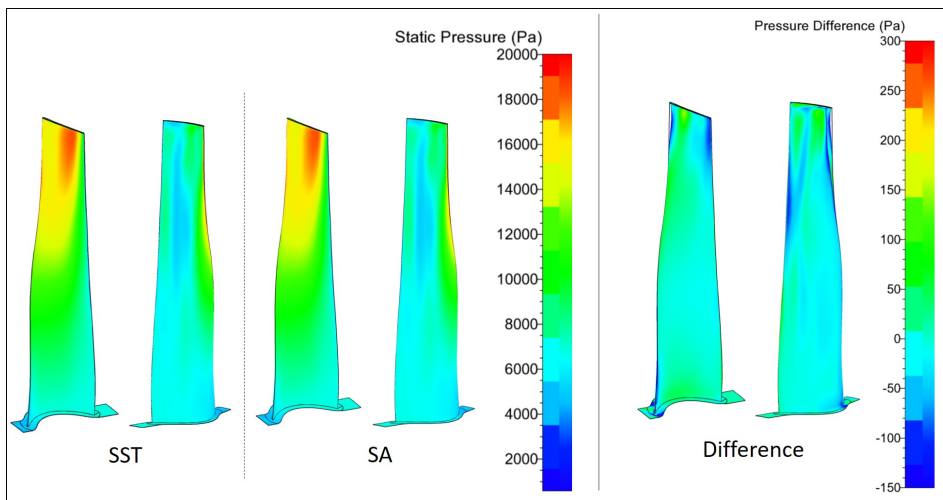| Turbulence model	Power [MW]	Last stage rotor		
		Force X [N]	Force Y [N]	Force Z [N]
Spalart-Allmaras	48.14	311.60	-25.01	551.90
k-omega SST	48.46	315.10	-24.92	551.30
Percentage error	0.6561%	1.1108%	0.3612%	0.1088%

Figure 2.9: Turbulence model comparison static surface pressure

The dominant frequencies present in the unsteady periodic flow of the LP steam turbine are equal to the blade passing frequencies and its harmonics (Laumert, 2002; Drozdowski et al., 2015). For the last stage rotor row the first, second, and third harmonic frequencies are 2500Hz, 5000Hz, and 7500Hz, respectively. The first harmonic was calculated by considering the rotational speed of 3000 rpm and the number of stators in the last stage. The NLH simulations were solved for 1 harmonic (2500Hz), 2 harmonics (2500Hz and 5000Hz) and lastly for 3 harmonics (2500Hz, 5000Hz, and 7500Hz). The basic harmonic method from NUMECA FINE^{TM}/Turbo 11.2rc was used in the NLH simulations, which deals with rotor/stator interaction of only the adjacent rows. Other higher order harmonic methods such as the Clocking harmonic method and Multi-rank harmonic method were not considered, due to their very high computational cost.

The flow domain of the CFD model is shown in Figure 2.10. The boundary condition values are tabulated in Table 2.3 and the boundary conditions specified were:

- **Inlet:** Constant inlet mass flow, static temperature and turbulent viscosity

- **Three steam extractions:** Constant mass flow outlet (pressure adaptation)

- **Diffuser outlet:** Average static pressure

- **Stator surfaces**: Adiabatic walls with no-slip condition, rotating at 0 rpm

- **Rotor surfaces:** Adiabatic walls with no-slip condition, rotating at 3000 rpm

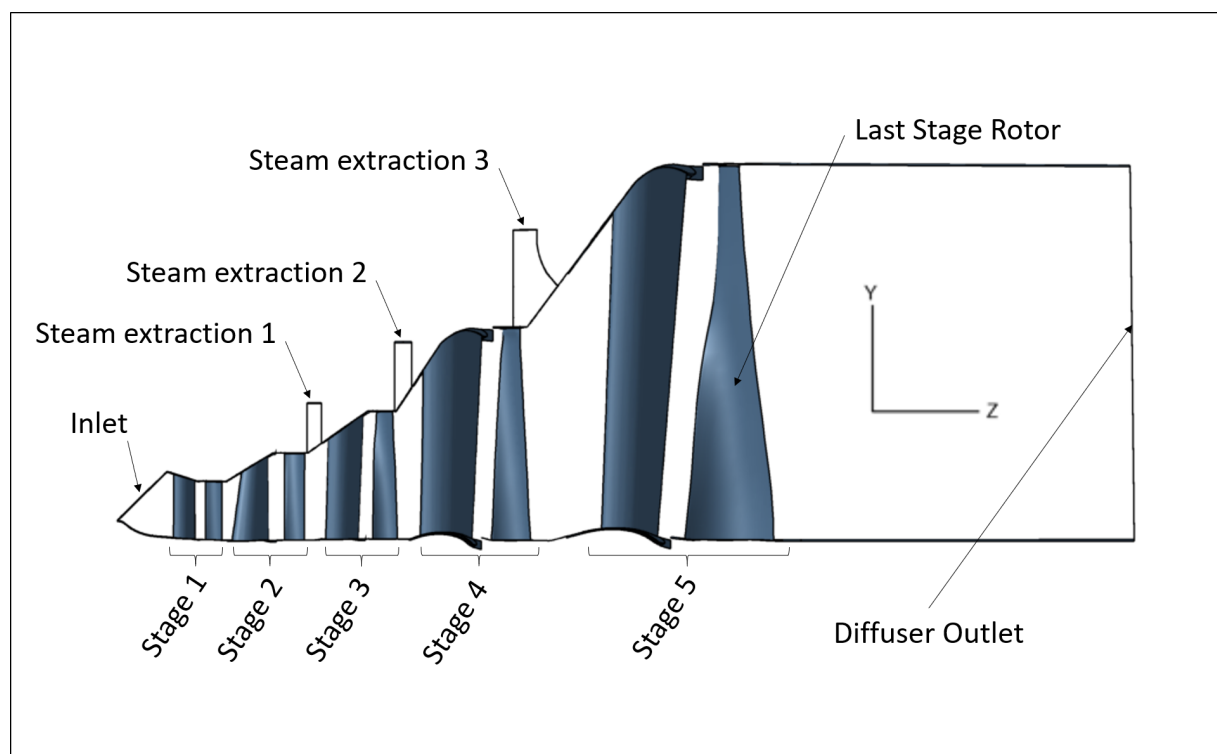- **Rotor/stator interface:** Full Non Matching (Non Reflecting)

Figure 2.10: Flow domain of CFD model

Table 2.3: Boundary conditions for 3 load conditions

Parameter		Units	Load		
			100%	**79%**	**44%**
Atmosphere	Static Pressure (absolute)	Pa	83226.0	83226.0	83226.0
Inlet	Mass flow rate	kg/s	90.44	73.07	42.96
	Static Temperature	K	514.85	512.85	505.15
	Turbulent viscosity	m^2/s	1.0E-05	1.0E-05	1.0E-05
Extraction 1	Mass flow rate	kg/s	3.30	2.55	1.35
Extraction 2	Mass flow rate	kg/s	3.15	3.01	1.59
Extraction 3	Mass flow rate	kg/s	3.29	2.49	1.05
Diffuser Outlet	Static Pressure (gauge)	Pa	6880.0	5410.0	4060.0

2.4.4 Convergence

The NLH simulations were considered to be converged when the mass imbalance was less than 0.1%, and the global residual, torque produced by the LP steam turbine, and the 3 aerodynamic force components exerted on the last stage rotor, had for all practical purposes, flat lined showing negligible changes as the simulations continued to iterate.

All of the 1 harmonic NLH simulations adhered to the above, however all the 2 and 3 harmonics NLH simulations after many thousands of iterations adhered to all of the above except that the mass imbalance continued to iterate around 2%. Seeing that all other parameters were converged and due to negligible change evident in the flow field as the simulations continued to iterate, all of the 2 and 3 harmonics NLH simulations were considered to be converged. The effect that the additional mass has on the aerodynamic forces experienced by the last stage rotor blade was eliminated in the appropriate manner, see Section 3.2.

2.4.5 Validation

Unfortunately, no pressure or force measurements for any of the stator or rotor stages were obtainable for the modelled LP steam turbine to be used as validation for the CFD model. Even though the parameters of interest were the aerodynamic forces, it was thought that using the power generated by the LP steam turbine, as the validating parameter, would be a good alternative. This was due to the fact that the generated power is a function of the rotational speed and torque, and the torque being a function of force and distance. It was reasoned that the only unknown to the predicted power was the force, seeing that rotational speed and distance were always constant and the same for both the actual and modelled LP steam turbine. Therefore, the accuracy of the CFD's predicted forces could, to a reasonable extent, be evaluated based on the percentage error between the predicted power and the power actually generated. Also, the LP turbine was known to produce a steam quality of less than 1 at the last stage outlet, for all the simulated operation conditions. Evaluation of the steam quality at the last stage outlet for all the NLH simulations revealed that the steam qualities were below 1.

Based on the above reasoning, the CFD model was validated for the three operational conditions by comparing the predicted turbine power output to the actual power output. Tabulated below are the predicted CFD and real-life measured power of the LP steam turbine, for the three operational conditions considering 1, 2, and 3 harmonics. The percentage difference between predicted and actual power ranges from 3.306% to 5.695%. This indicates that the CFD model predicts the power generated by the LP steam turbine with reasonably good accuracy. Thus, suggesting that the CFD model also predicts the aerodynamic forces exerted on the last stage rotor, with reasonably good accuracy.

Table 2.4: Predicted and actual LP steam turbine power - 100% load

Number of harmonics	Predicted Power [MW]	Actual Power [MW]	Percentage difference
1	48.120	50.600	4.902%
2	48.487	50.600	4.175%
3	48.580	50.600	3.993%

Table 2.5: Predicted and actual LP steam turbine power - 79% load

Number of harmonics	Predicted Power [MW]	Actual Power [MW]	Percentage difference
1	38.774	41.115	5.695%
2	38.880	41.115	5.435%
3	38.934	41.115	5.305%

Table 2.6: Predicted and actual LP steam turbine power - 44% load

Number of harmonics	Predicted Power [MW]	Actual Power [MW]	Percentage difference
1	21.322	22.350	4.600%
2	21.492	22.350	3.841%
3	21.611	22.350	3.306%

2.5 FE model

2.5.1 Geometry

A CAD assembly drawing of the LP steam turbine was available containing the last stage rotor. The rotor blade was imported into Space Claim 19.1 of ANSYS for further modelling.

The original last stage rotor geometry contained unrealistic stress concentrations in the fir-tree root, which could not be sufficiently removed without drastically altering the shape. Thus, it was decided to simplify only the root of the blade, see Figure 2.11. This

resulted in the HCF location to move to the hub fillet region. Even though HCF damage mostly occurs in the fir-tree root, the simplification was acceptable seeing that the actual HCF location was not of interest for the sensitivity analysis. Also, according to McCloskey et al. (1999) HCF damage has been found to occur anywhere along the length of a LP turbine blade. Due to the region of interest not being located in the root any more, there was no need to include the rotor disc in the FE model.

The simplified blade was sliced into three sections, to assist in the appropriate distribution of meshing elements, see Figure 2.12. Consequently, the highest density of elements could be allocated in the region of interest located in the sliced section numbered as 2 in Figure 2.12.
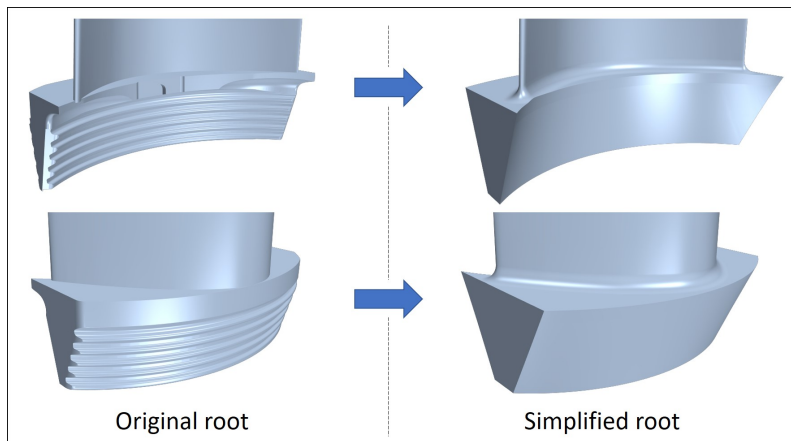

Figure 2.11: Last stage rotor (left) original root (right) simplified root
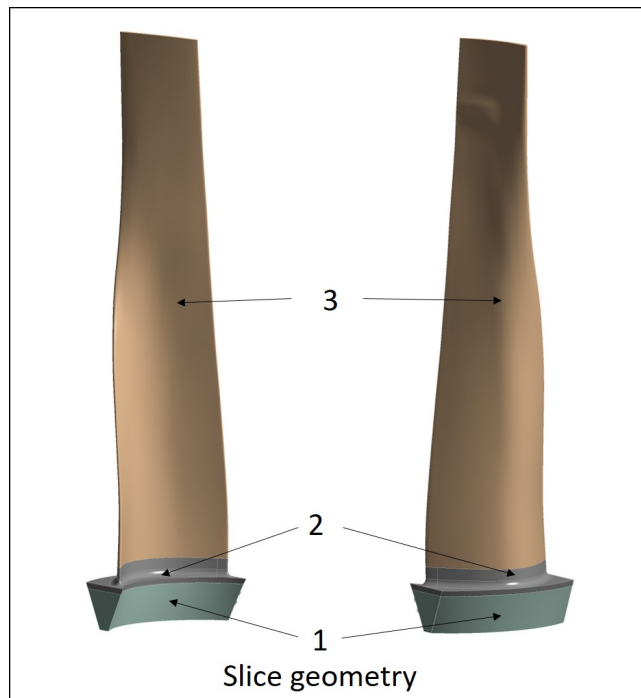

Figure 2.12: Last stage rotor sliced into three sections

2.5.2 Material properties

The homogeneous and isotropic material properties specified for the 12% Chromium steel in ANSYS, were the modulus of elasticity, density, Poisson ratio, and damping ratio. As mentioned in section 2.3, temperature was not accounted for in the RUL methodology. Therefore, all the material properties were specified as constant values. The density specified for the simplified blade ensured that the mass of the last stage rotor corresponded to the actual last stage rotor's mass of 23.75 kg.

The modulus of elasticity of the 12% Chromium steel was available and specified as 212.87GPa, whilst the damping ratio and Poisson ratio were unknown. Thus, alternative values which would adequately represent the last stage rotor's behaviour, had to be acquired. Alternative representative material properties were found to be acceptable for the purpose of the sensitivity analysis, as it will still result in realistic predictions. From the work conducted by Booysen (2014), a damping ratio of 0.003 was found to be representative. The best representative value for the Poisson ratio was that of martensitic steel Manet(1.4914 type), which has a very similar chemical composition to that of the 12% Chromium steel (FERP (2017)). The Poisson ratio was subsequently specified as 0.3.

2.5.3 Mesh

Static structural analysis

Static structural analyses were performed to evaluate mesh independence based on the max von Mises stress at the location on the rotor blade where the HCF damage was most likely be the greatest. The location was found to be where the trailing edge intersects the hub fillet, see Figure 2.13. This location was also the location of interest of the sensitivity analysis, seeing that this was the location where the HCF damage was mostly to be the greatest. The analyses considered the centrifugal forces induced by the 3000rpm rotation of the rotor blade as well as the aerodynamic forces of the 100% load of the 3 harmonics case, which resulted in the highest von Mises stress state.
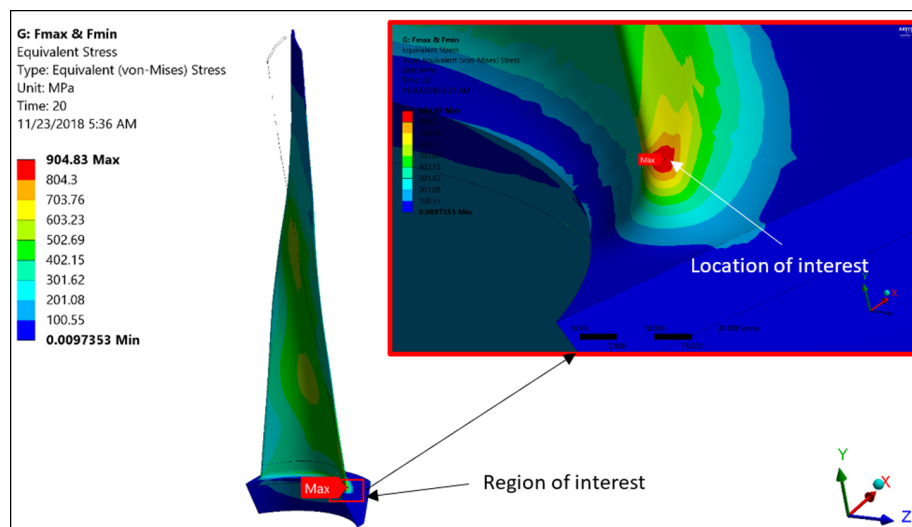

Figure 2.13: Location on the rotor blade for which the mesh independence study was performed.

Table 2.7 shows the mesh independence study results. It is evident that as the mesh size increases the relative error in the predicted maximum von Mises stress decreases. The relative error between the 214878 nodes and 108745 nodes was 0.059%. Considering the very small relative error, the maximum von Mises stress was found to be mesh independent for 108745 nodes. Figure 2.14 shows the 108745 nodal mesh used for the sensitivity analysis.

Table 2.7: FE model mesh independence results

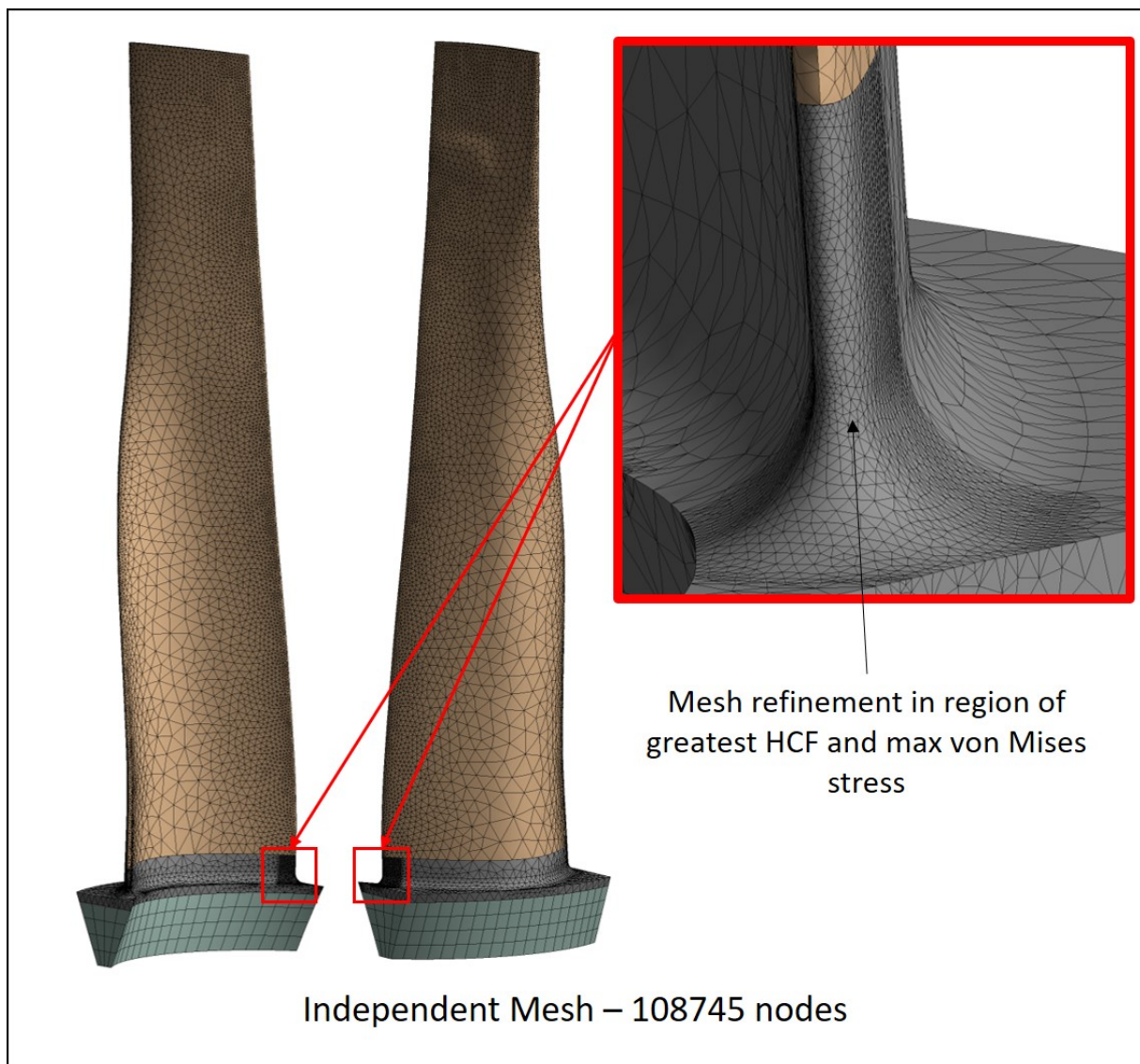| Node count	Max von Mises [MPa]	Relative Error
47424	890.39	1.928%
108745	907.35	0.059%
214878	907.89	0.000%

Figure 2.14: FE model independent mesh

Modal analysis

A modal analysis was performed to identify whether any of the last stage rotor's natural frequencies would coincide with the excitation frequencies of the unsteady aerodynamic forces. The two natural frequencies closest to each of the three excitation frequencies are shown in Table 2.8. From the modal analysis results it is evident that the last stage rotor blade will not resonate, seeing that the excitation frequencies do not coincide with the natural frequencies of the rotor.

The natural frequencies are however very close to the excitation frequencies, which seems unrealistic when considering that this is very unlikely to be the case for the actual last stage rotor blade. This phenomenon can be ascribed to the simplification made to the actual last stage rotor blade. However, in the end what mattered was that the simplified rotor blade should not have natural frequencies that coincide with the excitation frequencies, as would be the case with the actual last stage rotor blade.

Table 2.8: Natural frequencies of rotor, in vicinity of excitation frequencies

Excitation frequency [Hz]	Lower natural frequency [Hz]	Higher natural frequency [Hz]
2500 (Blade passing frequency, or 1st harmonic)	2434.8	2504.0
5000 (2nd harmonic)	4908.8	5040.4
7500 (3rd harmonic)	7498.1	7522.2

2.5.4 Transient structural analysis

Inherently a transient analysis requires a number of time steps (or certain time step size) to capture the transient nature of the problem being solved. It is recommended by the ANSYS user reference manuals that one period of a periodic excitation and subsequently a periodic response, should be represented by at least 20 time steps. However, due to limited computational resources as well as in an effort to obtain a converged stress history, the number of time steps were reduced. Consequently, the number of time steps per blade passing, was reduced to 10 for the all the 1 harmonic cases and to 15 for all the 2 and 3 harmonic cases.

An approach was followed in choosing the 10 and 15 time steps from the ideal number of time steps. The approach entailed that the reduced time steps must firstly capture the maxima and minima of the excitation forces, as the estimated RUL is based on maximum and minimum stress values. Secondly, as far as possible the time steps must capture the slopes as closely as possible. As an example, please consider Figure 2.15. Figure 2.15 shows the predicted aerodynamic forces from the NLH simulation of the 100% load with 2 harmonics for 1 blade passing. The orange line represents the predicted force history constructed by the ideal number of time steps, and the blue line represents the predicted force history constructed by 15 time steps. As it can be seen, the essential maxima and minima were captured and the slopes were captured quite well. Please note the aerodynamic forces are discussed in more detail in Section 3.2.
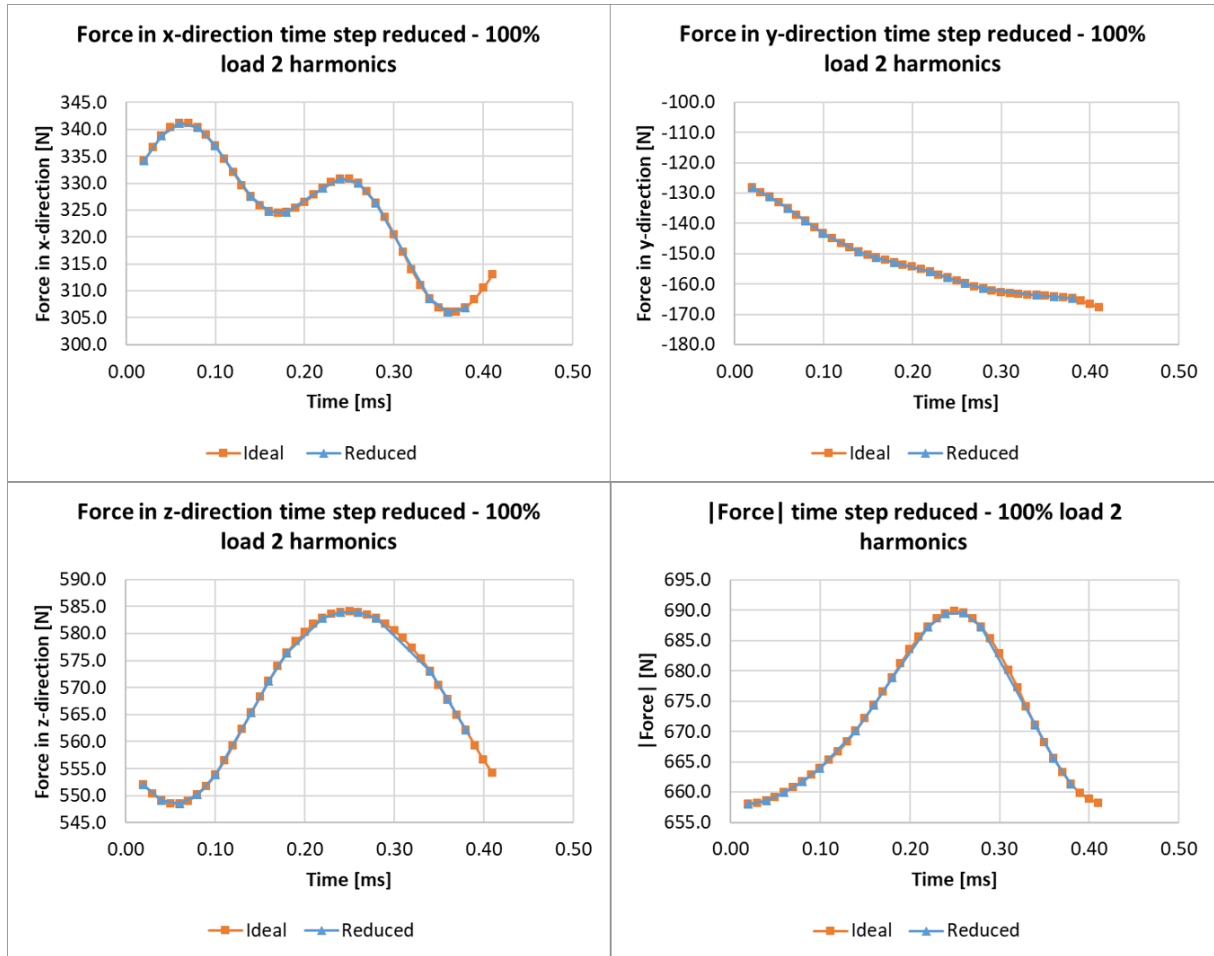
Figure 2.15: Reduced time steps - 100% load 2 harmonics

The boundary conditions at the root of the last stage rotor blade were specified as either frictionless or fixed in both the radial and theta directions. The latter represents the root serrations and the rotor disc attachment groove that fixes the rotor blade in place as the blades rotate at 3000 rpm. Figure 2.16 shows the locations of the frictionless and semi-fixed boundary conditions. Other combinations of boundary conditions were evaluated, but no significant change in the stress field was evident at the location of interest (Figure 2.13). This behaviour can be attributed to the Saint Venant's principle. Lastly, the centrifugal forces were accounted for by specifying that the blade rotates at 3000 rpm.

The unsteady static surface pressure distributions, predicted by an NLH simulation, were exported to a data file for every time step. The exported static surface pressure distributions were then imported using ANSYS's External Data module. The imported distributions were then mapped to the the wetted surface of the last stage rotor before the transient analysis was performed, see Figure 2.16. Therefore, the CFD mapping grid points could be properly orientated beforehand to ensure, for all practical purposes, that the CFD grid points match up with the last stage rotor blade's FE surface mesh. The mapping considered a profile preserving approach with a distance based average weighting. A static structural analysis was then performed with the mapped pressure distributions as the only applied load and the rotor fixed at its root. The computed reaction forces were compared with that of the predicted aerodynamic forces of the NLH

simulation. If the computed reaction forces did not match the predicted aerodynamic forces, the mapped static surface pressure distributions would then be scaled to match the aerodynamic forces.
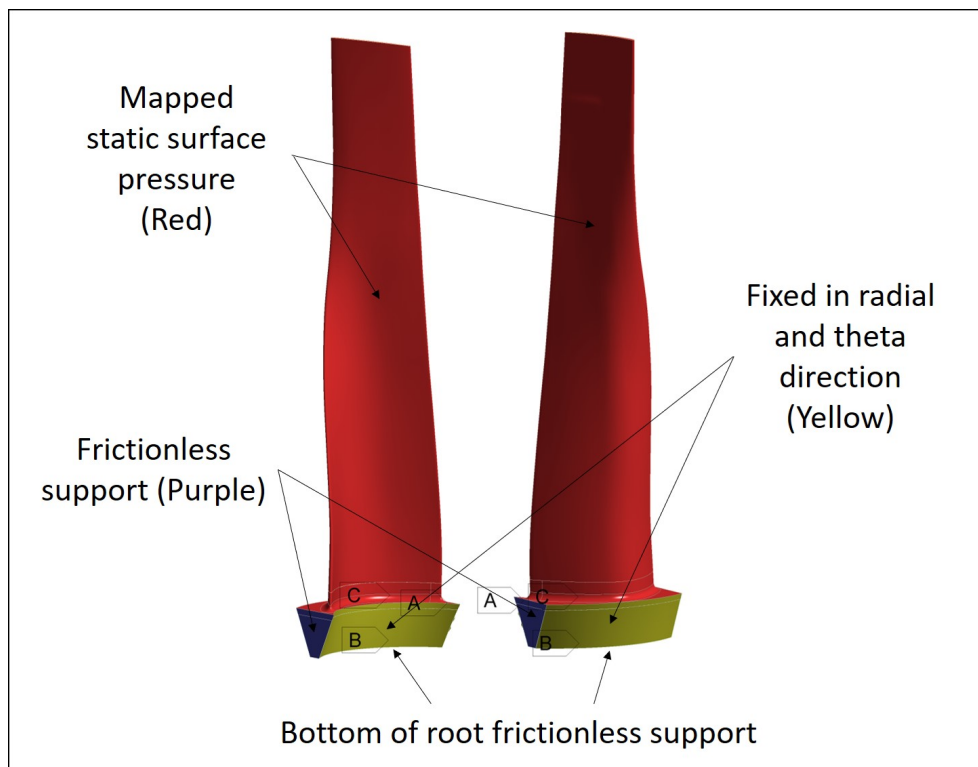

Figure 2.16: FE model boundary conditions

2.6 Fatigue model

The RUL was estimated at the node (location of interest) on the last stage rotor where the maximum Von Mises stress occurred, see Figure 2.13. The fatigue material properties and the fatigue analysis approach followed to estimate the RUL are described below.

2.6.1 Material properties

Insufficient fatigue material properties of the 12% Chromium steel were available and therefore the properties were generated using an alternative method. The Manson method was used to approximate the fatigue material properties. The fatigue strength coefficient was obtained by multiplying the ultimate tensile strength of 12% Chromium steel by 1.9. Subsequently giving the fatigue strength coefficient as 2584MPa. The fatigue strength exponent was set equal to -0.12 as specified by the Manson method (Jono and Inoue, 1992).

2.6.2 Analysis approach

The computed transient stress field of the last stage rotor blade was multi-axial, due to the centrifugal and unsteady aerodynamic forces. Therefore, a multi-axial analysis algorithm which incorporates both the shear and normal stress needed to be considered,

such as the stress-based Brown-Miller analysis algorithm. However, it was not possible to perform all the needed fatigue analyses in Quick Fatigue Tool using the stress-based Brown-Miller analysis algorithm. Consequently, the stress invariant parameter analysis algorithm, based on the von Mises stresses, was used.

The stress invariant parameter analysis algorithm was compared to the stress-based Brown-Miller analysis algorithm. It was found that the sensitivity of the estimated RUL to the number of harmonics used in an NLH simulation, were the same for both algorithms. Therefore, the stress invariant parameter algorithm, based on the von Mises stresses Equation 2.1, was found to be sufficient for the purpose of the sensitivity analysis. The 9×10^6 in the equation below gives the RUL, N_f in terms of hours as oppose to number of blade passing periods.

$$\sigma_{eff} = \sigma'_f((2N_f)/9 \times 10^6)^b \tag{2.1}$$

The Soderberg mean stress correction, Equation 2.2, was used to account for mean stresses, seeing that it produces very conservative results (Soderberg, 1939). The time varying stresses at the location of interest, were counted using the rainflow cycle counting method. Finally, Miner's Rule of linear damage accumulation was utilized to estimate the RUL.

$$\frac{\sigma_a}{\sigma_{eff}} + \frac{\sigma_m}{\sigma_y} = 1 \tag{2.2}$$

Chapter 3

Sensitivity Analysis

3.1 Introduction

The purpose of the sensitivity analysis is to establish the sensitivity of the estimated RUL to the number of harmonics used in an NLH simulation. In this sensitivity analysis 1, 2, and 3 harmonics were considered in the NLH simulations. The sensitivity analysis entails the estimation of the RUL for a five stage LP steam turbine's last stage rotor. The RUL was estimated for three loading conditions, namely 100%, 79%, and 44% load. All load conditions were simulated using 1, 2, and 3 harmonics as mentioned above, which adds up to 9 cases in total. The RUL was estimated by means of the numerical model discussed in Chapter 2.

3.2 CFD Analysis results

The NLH simulations were performed in order to determine the periodic aerodynamic forces exerted on the last stage rotor. Figure 2.5 shows the directions of the aerodynamic forces. The three aerodynamic force components (x, y, and z) and the norm thereof for 1, 2, and 3 harmonics for each of the three load cases for one blade passing, are shown in Figure 3.1, Figure 3.2, and Figure 3.3, respectively. The converged solution for all 9 cases, specifically for the 2 and 3 harmonics cases, had a discrepancy in the mass balance between the inlet and outlets of up to 2.5%.

In order to establish the sensitivity of the estimated RUL to the number of harmonics used in a NLH simulation, it is necessary to ensure that the change in the computed aerodynamic forces are only a function of the number of harmonics. Thus, all other aspects of CFD that can affect the computed aerodynamic forces must be eliminated. This was achieved for example by using the same mesh, the same turbulence model, and the same solver settings etc. in all 9 NLH simulations. To ensure the predicted aerodynamic forces remain a function of the number of harmonics, the effect of the mass imbalance on the predicted aerodynamic forces, had to be eliminated.

According to Jachens (1966) a linear relationship exists between the mass flow rate of the steam entering a steam turbine and the power generated by that steam turbine. This linear relationship is given by the "Willan's line". The generated power is a function of the rotational speed and torque, and the torque is a function of the aerodynamic force

in the tangential direction and radial distance. For the simulated LP steam turbine, the rotational speed and radial distance remained unchanged, therefore the only unknown in the prediction of the LP steam turbine's power, is the tangential aerodynamic force. The tangential aerodynamic force exerted on rotor blades changes between the 100%, 79%, and 44% loading conditions. Therefore, based on the "Willan's line" principle and the above reasoning it can be said that an increase in the mass flow rate results in a directly proportional linear increase in the tangential aerodynamic forces exerted on the last stage rotor blade.
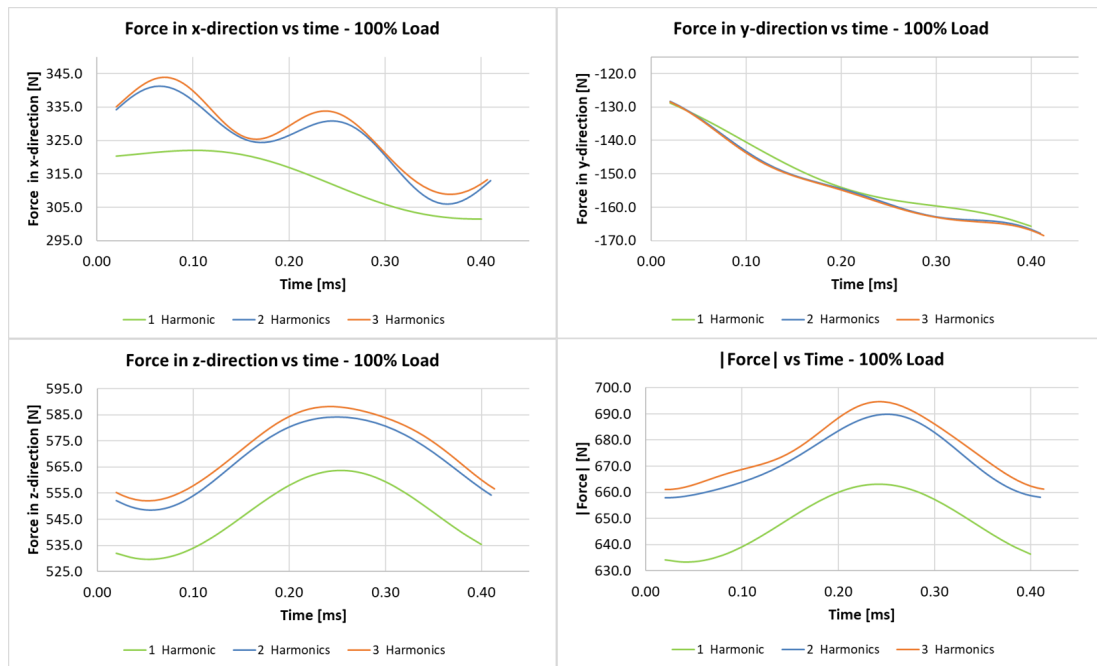

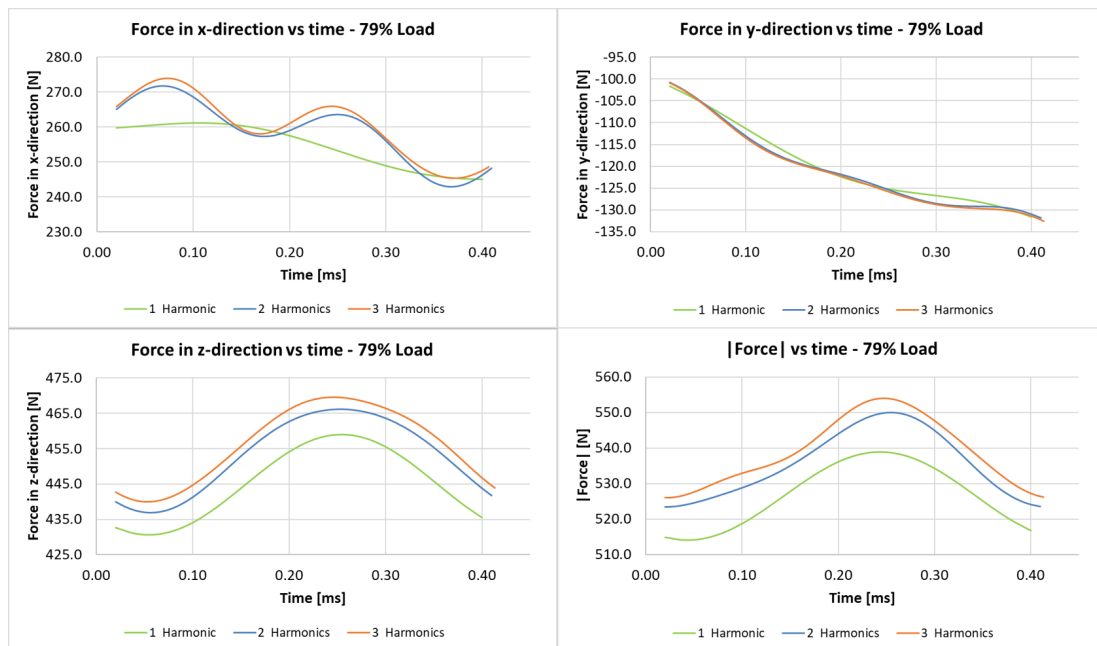Figure 3.1: CFD predicted aerodynamic forces - 100% load

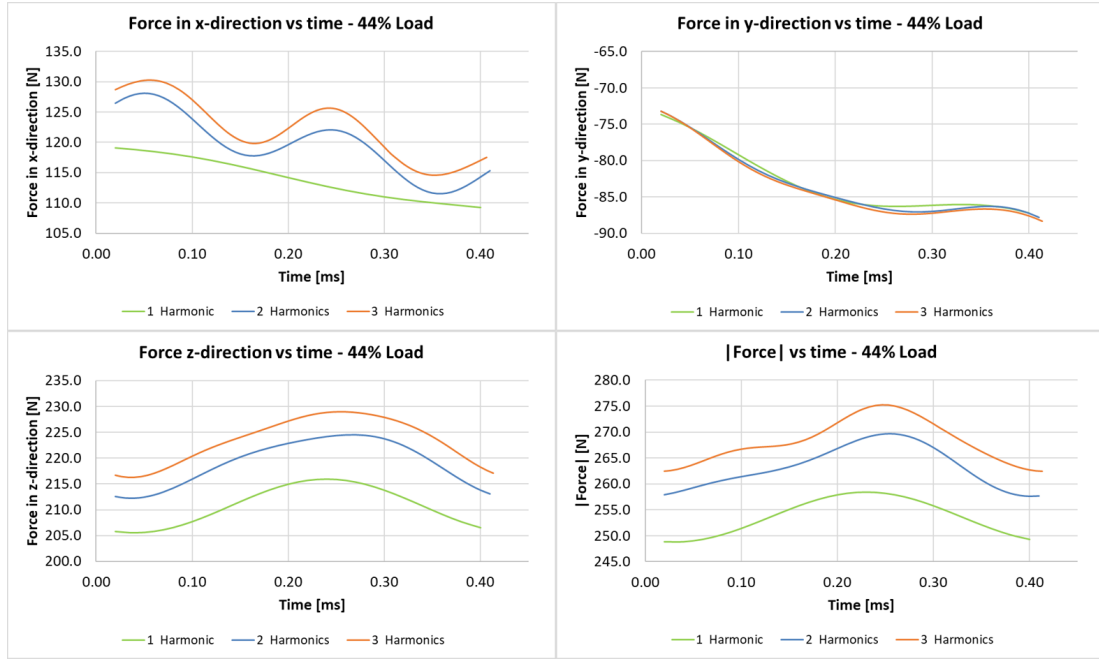Figure 3.2: CFD predicted aerodynamic forces - 79% load

Figure 3.3: CFD predicted aerodynamic forces - 44% load

Based on this reasoning, the effect of the mass imbalance could be eliminated. The elimination was achieved by normalizing the computed aerodynamic forces. Even though the above reasoning is based on the tangential aerodynamic force component, it was thought that normalizing all the force components based on this reasoning would be adequate. The normalization was done by multiplying the computed aerodynamic forces with a mass ratio based on the mass flow entering the row of the last stage rotor. For a given load and number of harmonics, the mass ratio is defined as the mass flow entering the row of the last stage rotor divided by the mass flow entering the row of the last stage of the 1 harmonic case for the given load condition. The reason why the mass ratios were relative to the mass flow rate of the 1 harmonic for the given load condition, was because the sensitivity between 1, 2, and 3 harmonics, for a given load, was the purpose of the sensitivity analysis.

The 3 normalized force components (x, y, and z) and the norm thereof for 1, 2, and 3 harmonics for each of the three load cases for one blade passing, are shown in Figure 3.4, Figure 3.5, and Figure 3.6, respectively. Comparing the overall form and distributional patterns of the normalized forces for the 3 loading conditions, it is evident that the normalized forces of the 100% and 79% loads are very similar to one another. The overall form and distributional patterns of the 44% load do show differences compared to that of the 100% and 79% load cases.

Furthermore, for all 9 cases it is clearly evident that both the force in the z-direction and the force magnitude |Force| are cyclic, where this is not so clearly seen for the forces in the x-direction and y-direction. Seeing that the problem being solved is periodic, it is expected that the forces in the x-direction and y-direction should also be cyclic. The reason for this phenomenon can be ascribed to the trailing edge shock wave which has impinged on the suction surface, that passes the leading edge and moves towards the pressure surface of the last stage rotor. This happens as the rotor blade nears the end

of a blade passing period and enters into a new blade passing period. The time period in which this all happens is so small that the current time step size is not sufficient to show how the forces in the x-direction and y-direction increase to the force values at the beginning of their blade passing periods. For this reason, the blade passing periods of the forces in the x-direction and y-direction do not match up at the beginning and end of their blade passing periods.
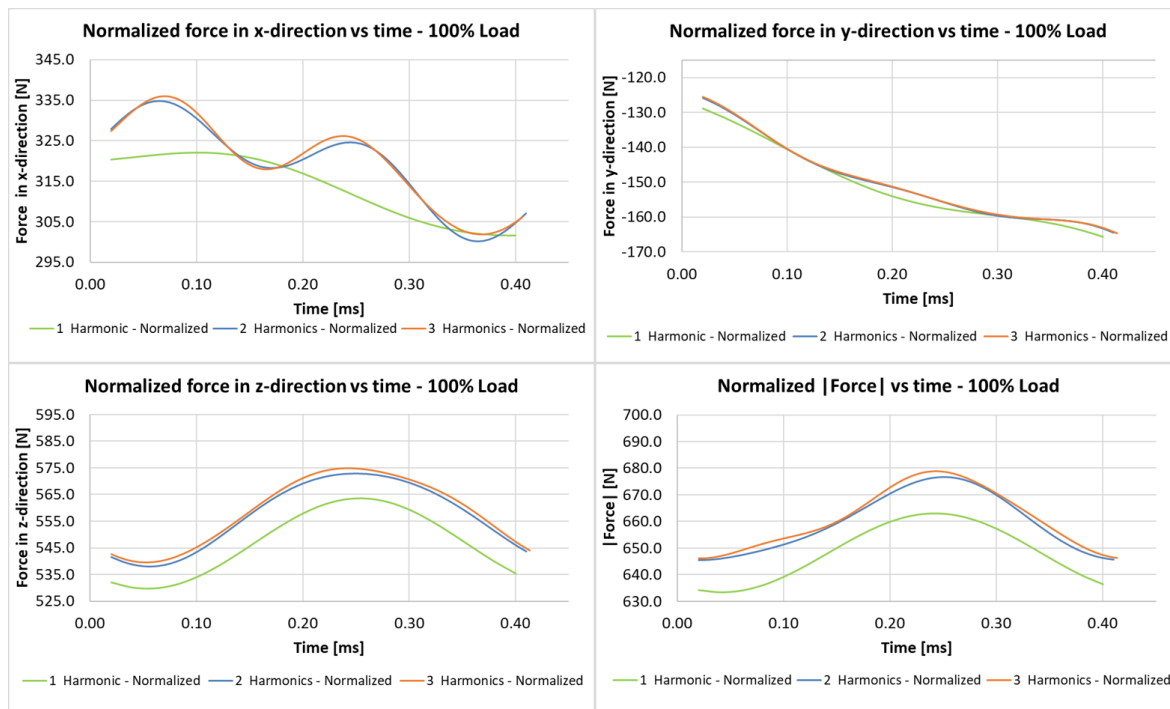

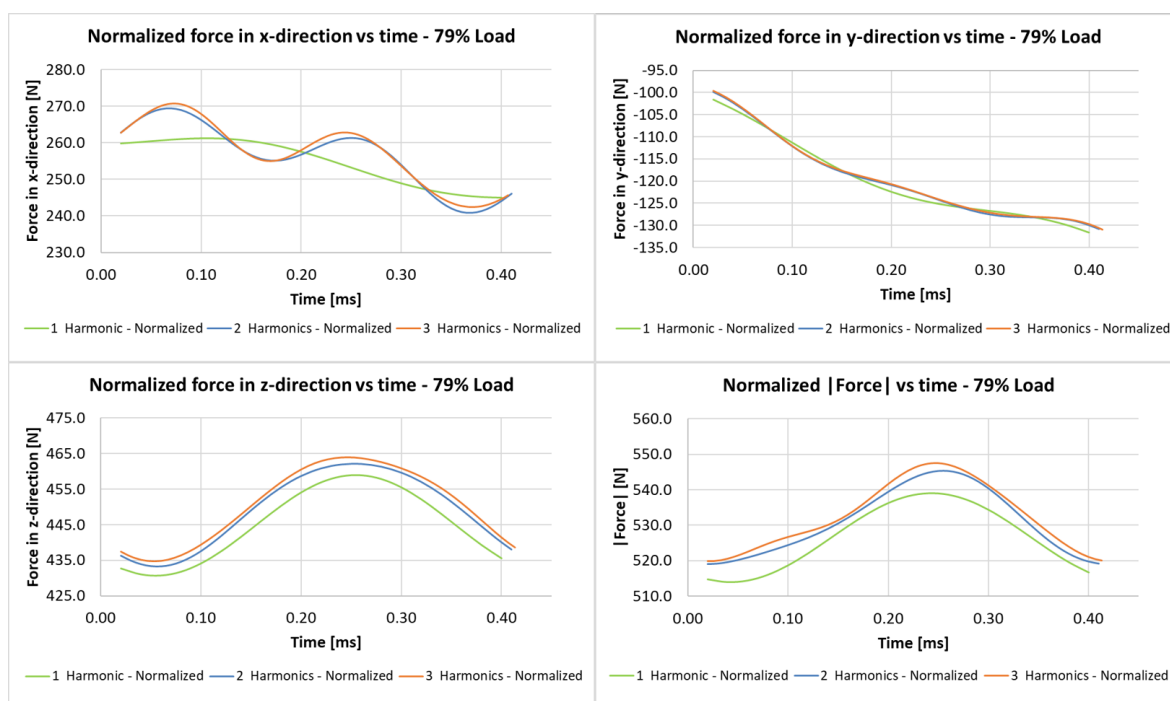Figure 3.4: Normalized CFD predicted forces - 100% load

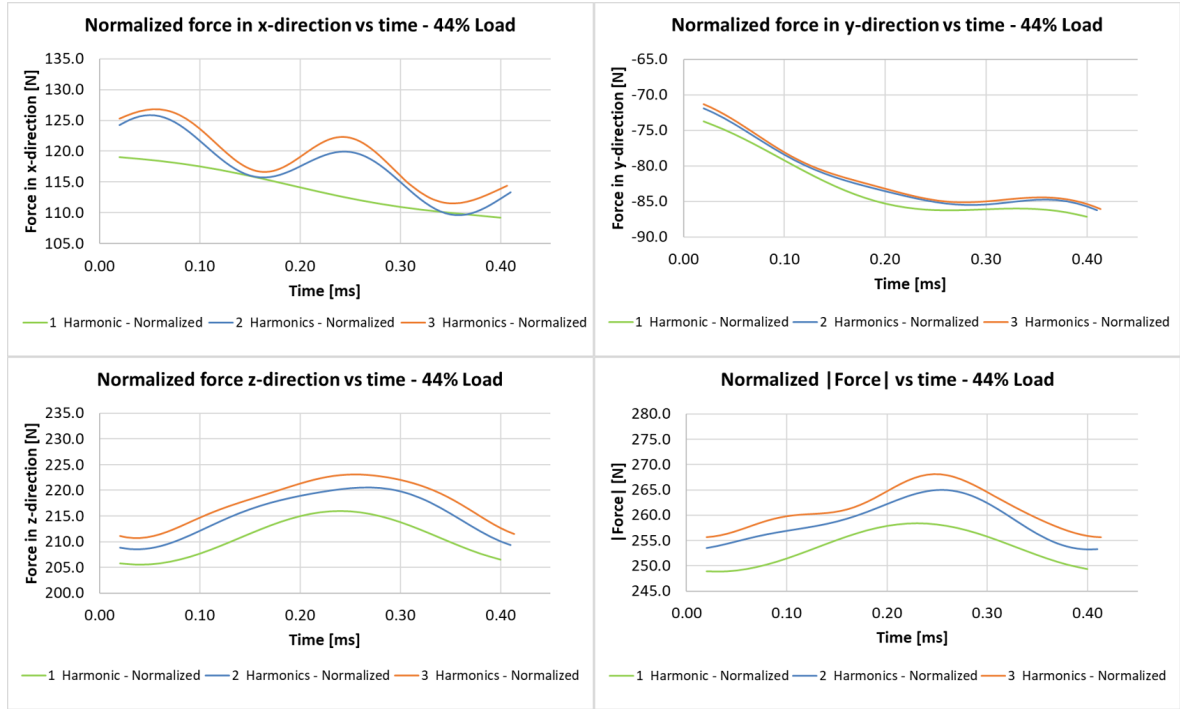Figure 3.5: Normalized CFD predicted forces - 79% load

Figure 3.6: Normalized CFD predicted forces - 44% load

3.2.1 Effect of harmonics on predicted aerodynamic forces

To illustrate the effect of additional harmonics on the predicted aerodynamic forces, let us consider the normalized aerodynamic forces predicted for the 1, 2, and 3 harmonics of the 100% load case. Figure 3.7 to Figure 3.10 show the normalized aerodynamic forces (left), and the components of the normalized aerodynamic forces that bring about the change in the normalized aerodynamic forces as the number of harmonics used in a NLH simulations increases (right).

The force components for the 2 harmonics case were obtained by subtracting the normalized forces of the 1 harmonic from the normalized forces of the 2 harmonics. The force components due to 3 harmonics were obtained in the same manner, by subtracting the normalized forces of the 2 harmonics from the normalized forces of the 3 harmonics. Please note that these force components do not show the effects of an added harmonic, but rather the combined effect of using either 2 or 3 harmonics in an NLH simulation. The reason is that the NLH method accounts for the nonlinear interaction between the unsteady disturbances and the time-averaged flow (He and Ning, 1998). Therefore, the overall effect on the predicted aerodynamic forces, due to for example the second harmonic, is not the same when predicting the aerodynamic forces using 2 and 3 harmonics.

Consider Figure 3.7 to Figure 3.10. Utilizing 2 harmonics in the NLH simulation compared to 1 harmonic, increases the overall magnitude of the forces in the x- and z-directions as well as the magnitude of the force |Force|. Including the 3 harmonics as opposed to 2 harmonics, also increases the overall magnitude of these forces, but to a much lesser extent. The force in the y-direction decreases as more harmonics are included. The decrease resulting from using 3 harmonics as opposed to 2 harmonics, is much smaller compared to the overall decrease resulting from using 2 harmonics as op-

43

posed to 1 harmonic. Thus, it is clearly evident that contribution of the third harmonic is much less than that of the first and second harmonic. Recalling that the predicted aerodynamic forces are based on the static surface pressure, the above findings are in agreement with the findings of Asghar et al. (2018).
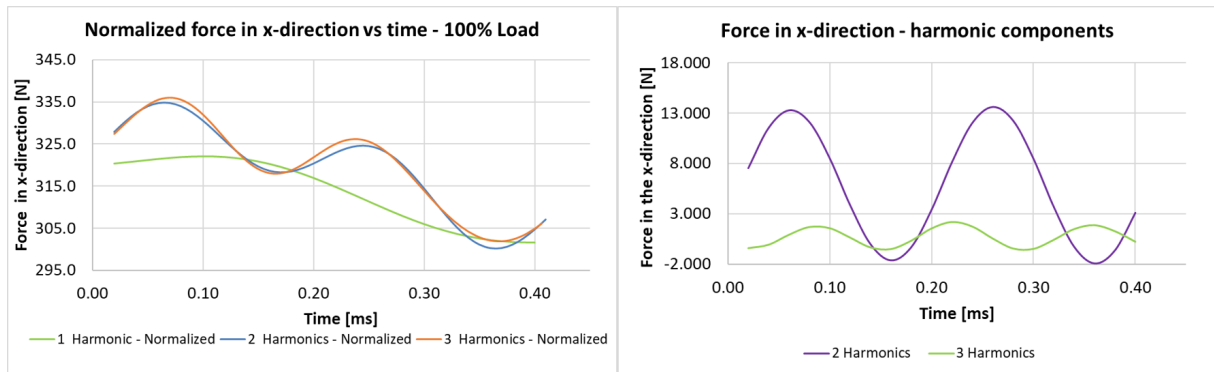

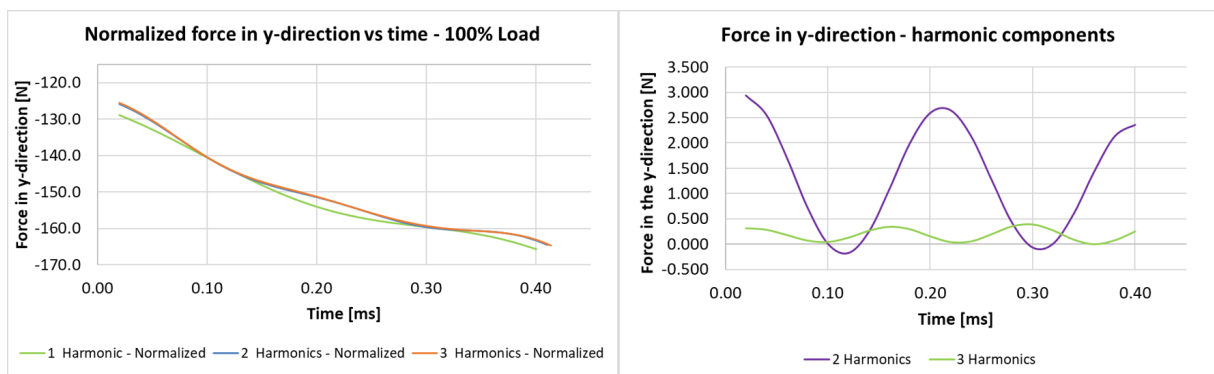Figure 3.7: Normalized force in x-direction and harmonic components - 100% load

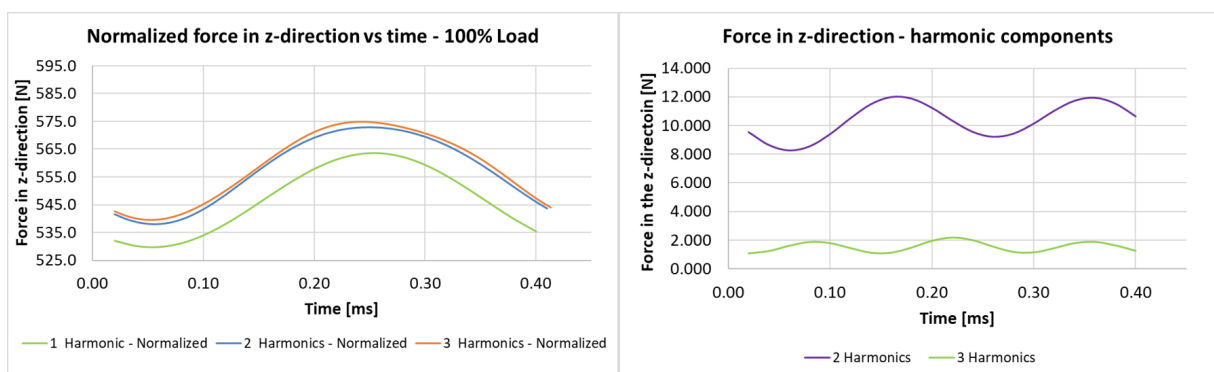Figure 3.8: Normalized force in y-direction and harmonic components - 100% load

Figure 3.9: Normalized force in z-direction and harmonic components - 100% load
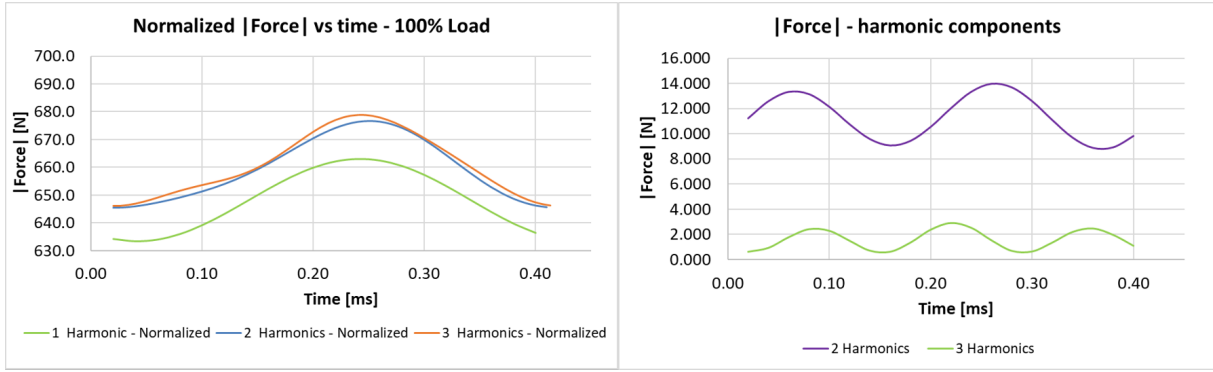
Figure 3.10: Normalized |Force| and harmonic components - 100% load

To demonstrate the effect of the frequency content of the additional harmonics on the predicted normalized aerodynamic forces, please consider Figure 3.10. It can be seen that the |Force| of the 2 harmonics is not just an offset of the |Force| of the 1 harmonic. Figure 3.11 (a) shows the |Force| of the 2 harmonics and an offset of the |Force| of the 1 harmonic. From Figure 3.11 (a) it can clearly be seen that the |Force| of the 2 harmonics oscillates around the offset of the |Force| of the 1 harmonic, at specific frequency. The oscillations occur at the frequency of the second harmonic, clearly evident in the force component of the 2 harmonics, shown on the right hand-side of Figure 3.10.

The same can be said regarding the |Force| calculations based on 2 and 3 harmonics, respectively. The |Force| of the 3 harmonics is also not just an offset of the |Force| of the 2 harmonics. Figure 3.11 (b) shows the |Force| of the 3 harmonics and an offset of the |Force| of the 2 harmonics. From Figure 3.11 (b) it can clearly be seen that the |Force| of the 3 harmonics oscillates around the offset of the |Force| of the 2 harmonics, at specific frequency. The oscillations occur at the frequency of the third harmonic, clearly evident in the force component of the 3 harmonics, shown on the right-hand side of Figure 3.10.

Investigating the effect of the second and third harmonics on the predicted forces in the x-, y- and z- direction, in the same manner as above, will result in the same conclusion as for |Force|. The effect of additional harmonics on the predicted aerodynamic forces for the 79% and 44% load cases are in principle the same as discussed above for the 100% load case.
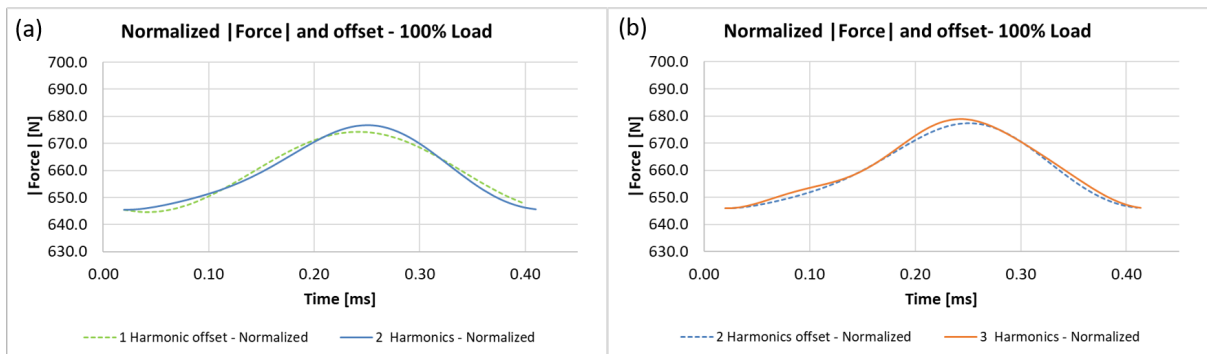

Figure 3.11: |Force| and offsets - 100% load

3.3 FE Analysis results

3.3.1 Location of interest

Figure 3.12 shows the location of interest, for which the sensitivity of the estimated RUL was established. The sensitivity analysis was performed on the last stage rotor blade, at the location where the maximum von Mises stress occurs. The maximum von Mises stress occurs in the hub fillet region at the trailing edge of the rotor blade, see Figure 3.12.
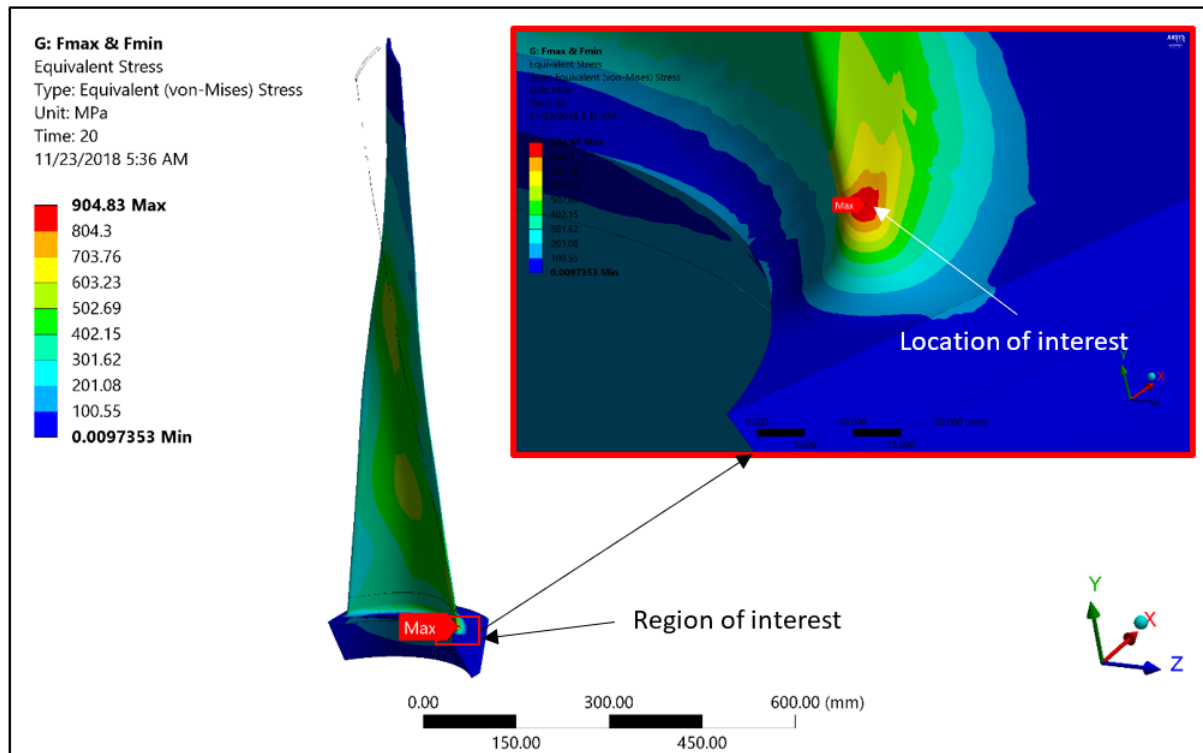

Figure 3.12: Location on the rotor blade for which the RUL was estimated

3.3.2 Transient FE results

Figure 3.13, Figure 3.14, and Figure 3.15 show the von Mises stress histories for 1, 2, and 3 harmonics for the 100% load condition, for the location of interest. The stress histories for 1, 2, and 3 harmonics for the 79% and 44% load conditions, look very similar to that of the 100% load, but just at lower von Mises stresses. Unfortunately, due to the limited computational resource available, all 9 transient FE simulations could not be run far enough to obtain a fully converged solution. It was noted that for all 9 cases the von Mises stress histories showed an asymptotic like convergence, see orange lines in Figure 3.13, Figure 3.14, and Figure 3.15. It was also evident that the amplitudes of the blade passing periods were of equal magnitude, for the greater part of the non-converged von Mises stress histories. Thus, it was hypothesised that averaging the stress histories in some manner, would give a reasonable approximation to the converged blade passing period.
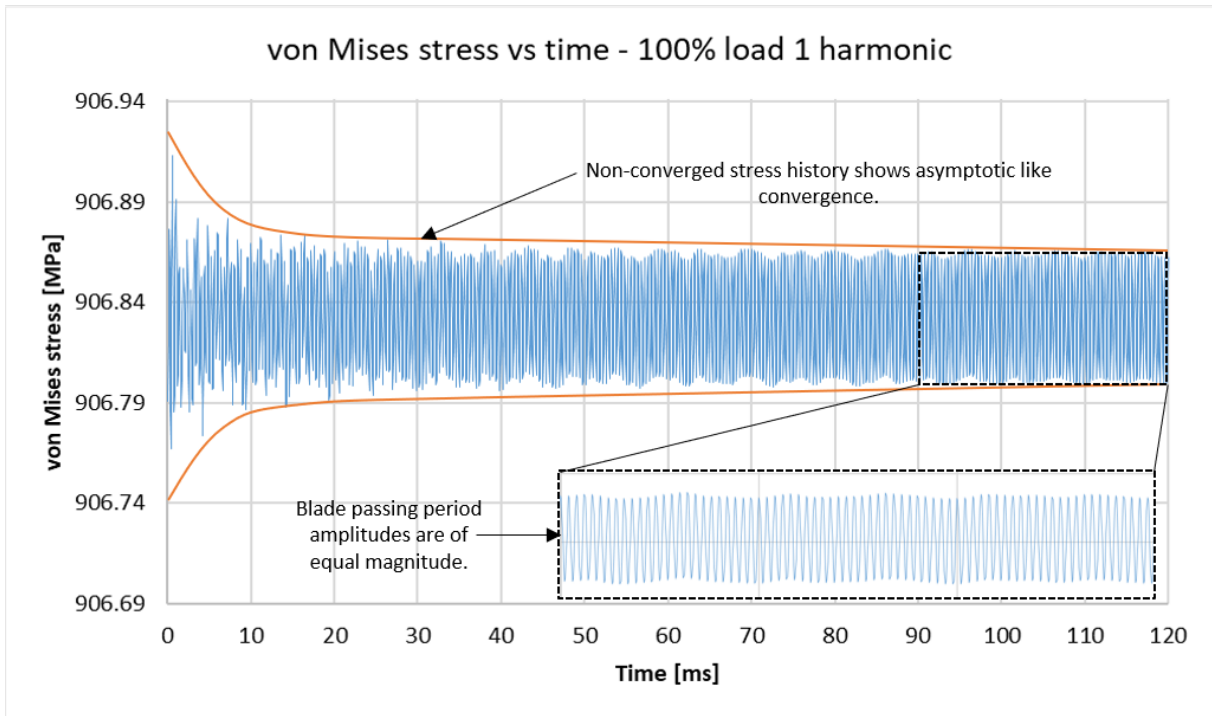
Figure 3.13: von Mises stress history with asymptotic like convergence behaviour - 100% load 1 harmonic
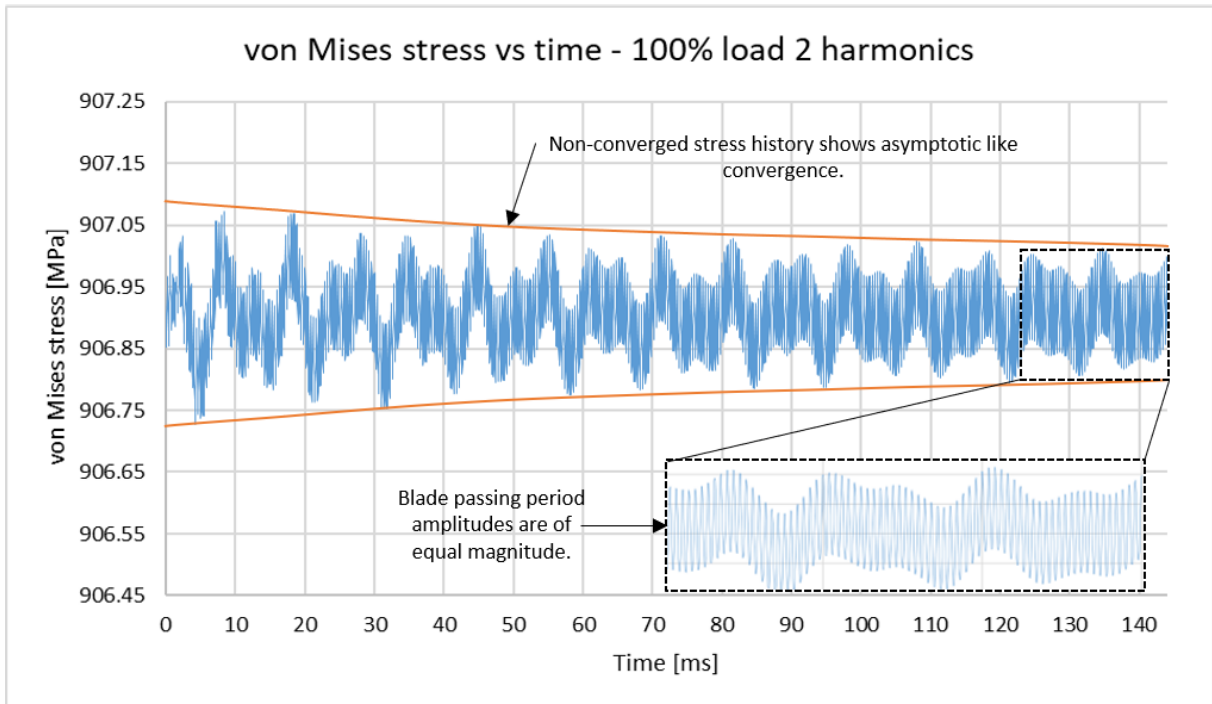
Figure 3.14: von Mises stress history with asymptotic like convergence behaviour - 100% load 2 harmonics
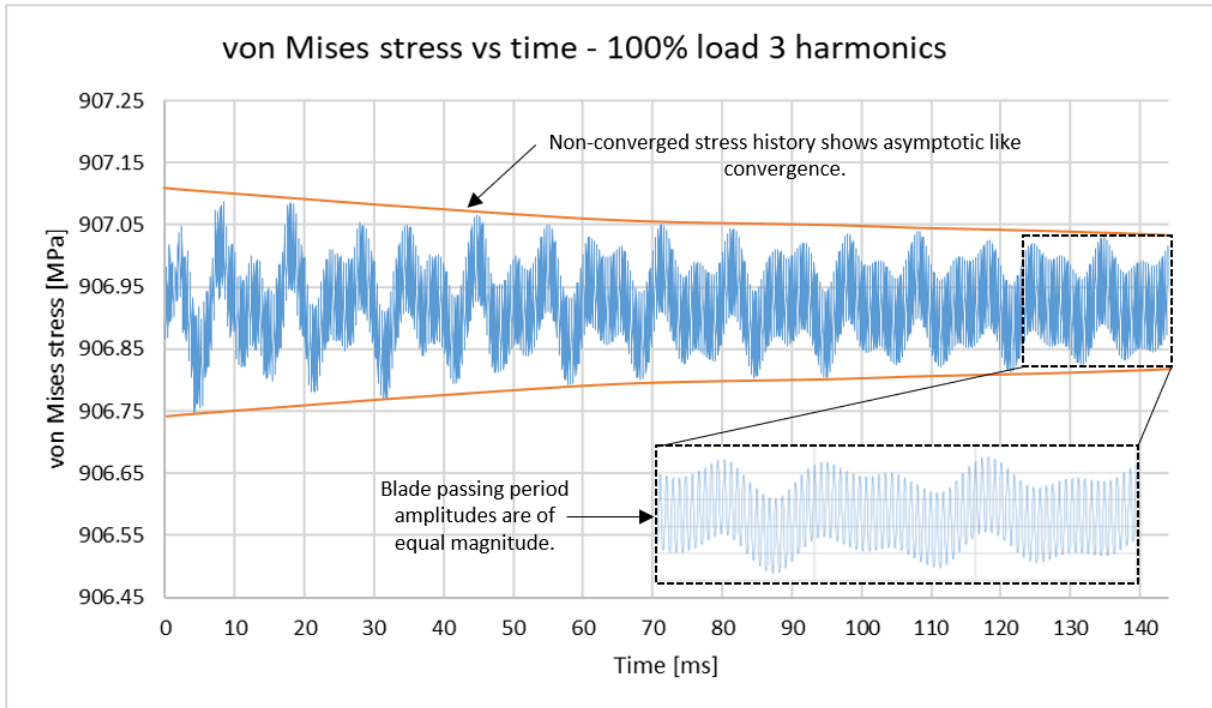
Figure 3.15: von Mises stress history with asymptotic like convergence behaviour - 100% load 3 harmonics

The purpose of the averaging process was to obtain a blade passing period that approximates the converged blade passing period. In order to explain the averaging process please consider Figure 3.16. Figure 3.16 shows the von Mises stress history for 3 blade passing periods each consisting of 10 time steps, for the 1 harmonic case of the 100% load condition. In order to obtain an approximation of the converged blade passing period, the von Mises stresses of the first-time step for the 3 blade passing periods were averaged. This gives an approximation to the first-time step of the converged blade passing period. This process was repeated for the remaining 9 time steps, consequently producing ans approximation to the converged blade passing period.

Figure 3.16: Averaging process example

48

In order to determine whether the hypothesis is true, the averaging process described above was applied using two approaches, see Figure 3.17. In the first approach the non-converged stress histories are averaged over 50, 100, 150, 200, 250, and 300 blade passing periods. The second approach entails the averaging of the non-converged stress histories over 6 non-overlapping intervals, each consisting of 50 blade passing periods. The hypothesis will be true i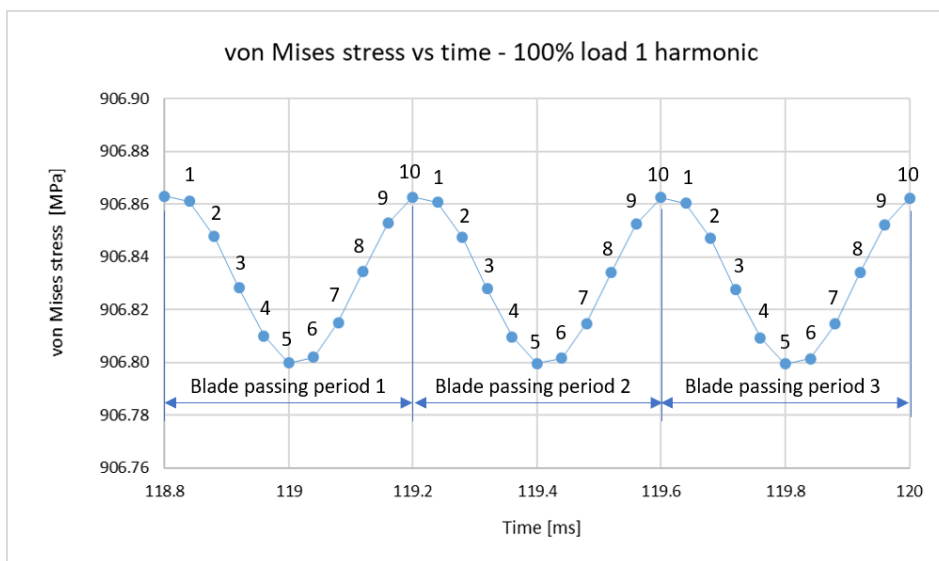f the two approaches yield averaged blade passing periods, that are found to be identical when compared to one another, within an acceptable tolerance.
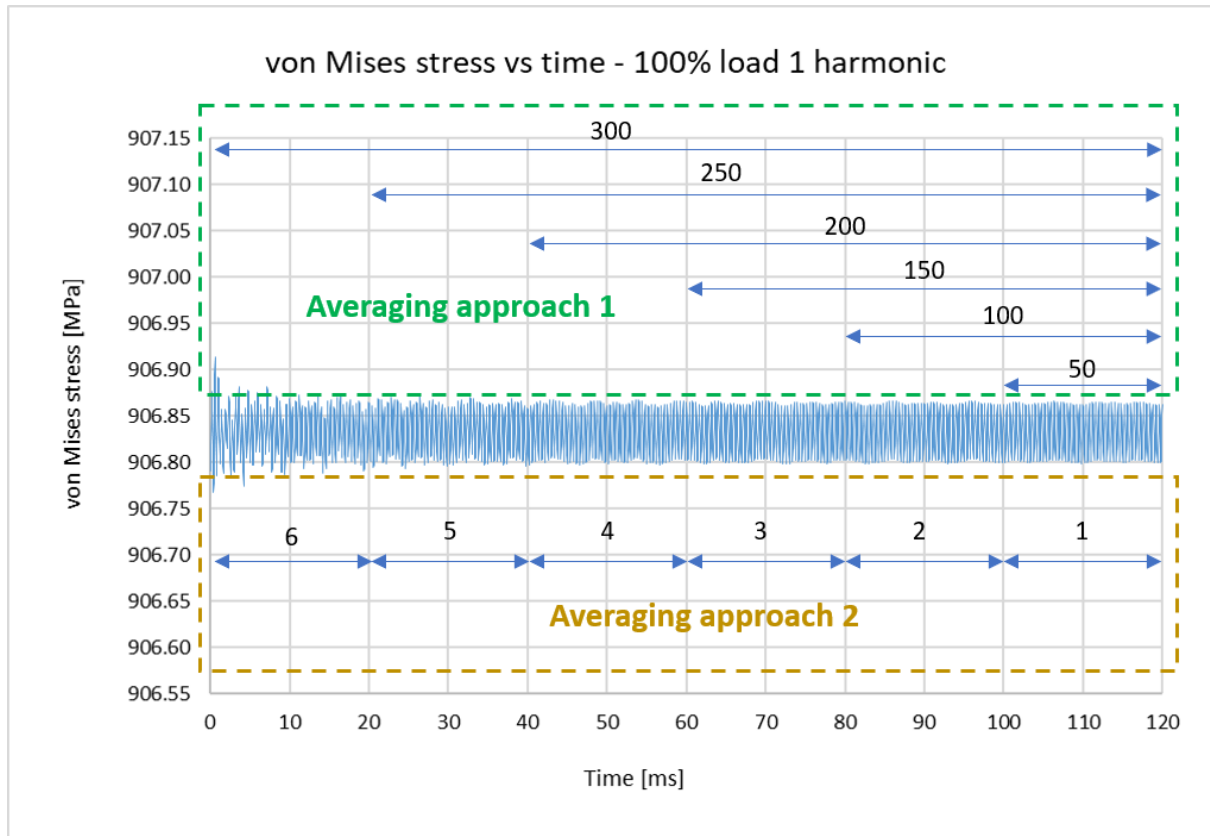
Figure 3.17: Averaging approach 1 and 2

Figure 3.18 to Figure 3.26, show the von Mises stress approximations to the converged blade passing periods of the 9 cases, obtained by applying approach 1 and 2. It is evident for approach 1, that for all 9 cases the approximations of the converged blade passing periods are essentially the same, as the number of averaged blade passing periods increase. For approach 2, it is evident that for all 9 cases the approximations of the converged blade passing periods differ a bit more, compared to that of approach 1. For the 3 load conditions considered, the 44% load case showed the largest differences in its approximation of the converged blade passing periods, for both approaches 1 and 2. The generally larger differences in the approximations obtained using approach 2 as compared to approach 1, are due to approach 1 averaging across an increasing number of blade passing periods, and so averaging out the differences evident in approach 2.

Overall the approximated converged blade passing periods for all 9 cases, using approach 1 and 2, showed little to no change. This indicates that the hypothesis of averaging of the non-converged stress histories to obtain a reasonable approximation of the converged blade passing period, was true.

Figure 3.18: Approximation of converged blade passing period for averaging approach 1 (Left) and approach 2 (Right) - 100% load 1 harmonic

Figure 3.19: Approximation of converged blade passing period for averaging approach 1 (Left) and approach 2 (Right) - 100% load 2 harmonics
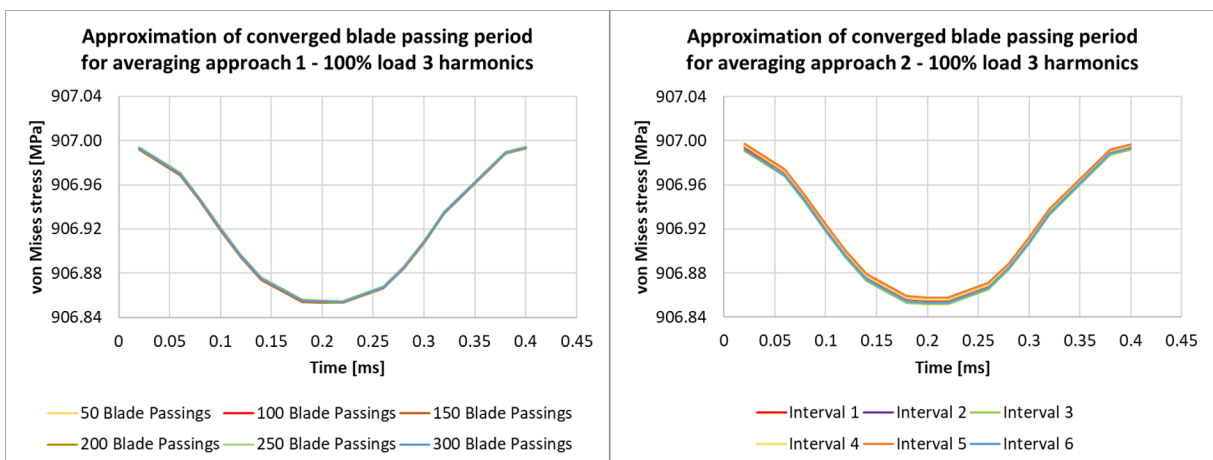
Figure 3.20: Approximation of converged blade passing period for averaging approach 1 (Left) and approach 2 (Right) - 100% load 3 harmonics
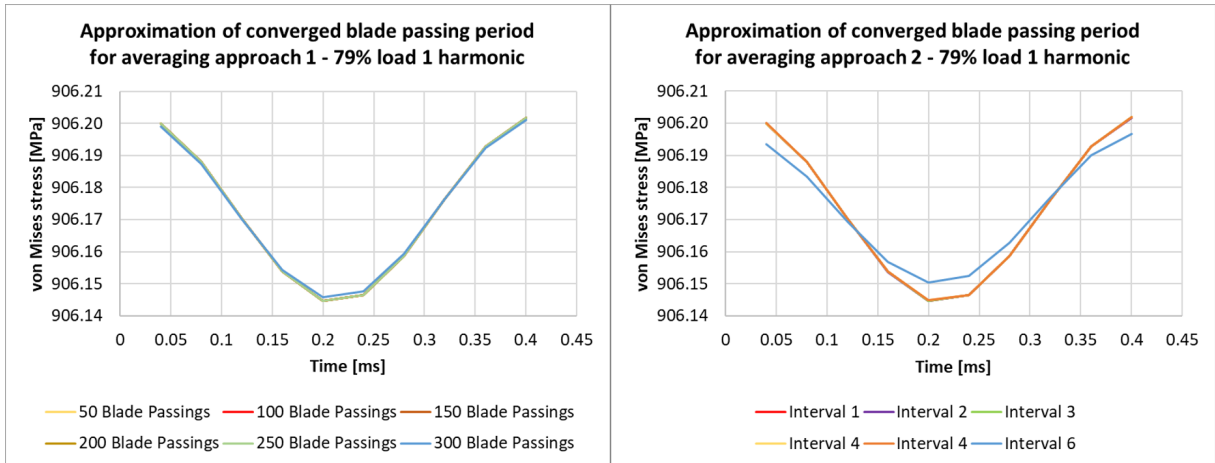
Figure 3.21: Approximation of converged blade passing period for averaging approach 1 (Left) and approach 2 (Right) - 79% load 1 harmonic
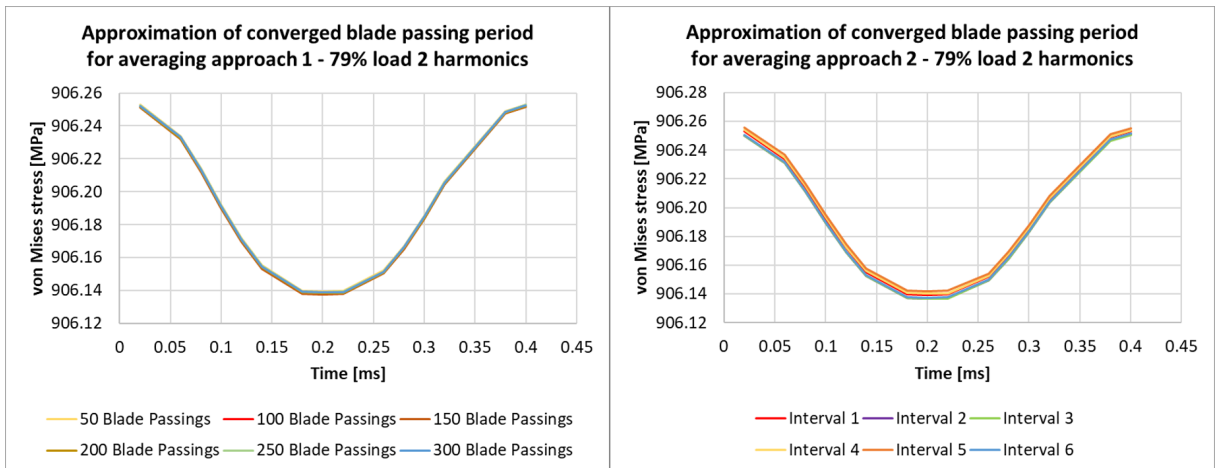
Figure 3.22: Approximation of converged blade passing period for averaging approach 1 (Left) and approach 2 (Right) - 79% load 2 harmonics
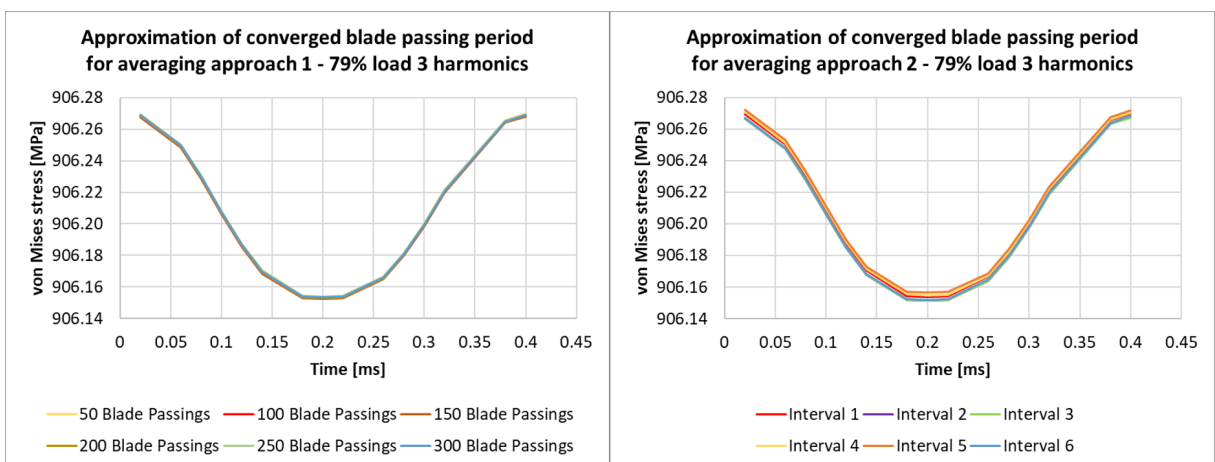
Figure 3.23: Approximation of converged blade passing period for averaging approach 1 (Left) and approach 2 (Right) - 79% load 3 harmonics
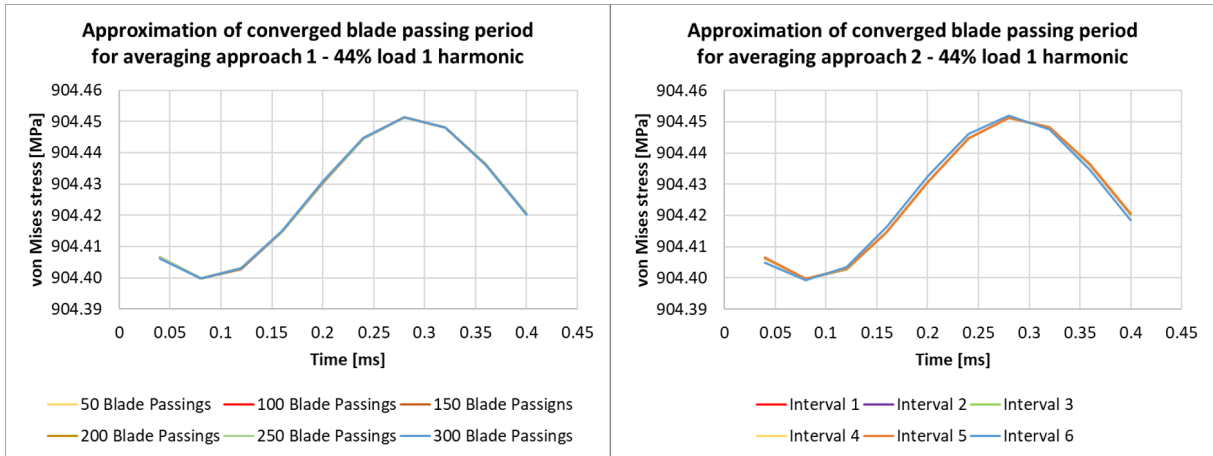
Figure 3.24: Approximation of converged blade passing period for averaging approach 1 (Left) and approach 2 (Right) - 44% load 1 harmonic
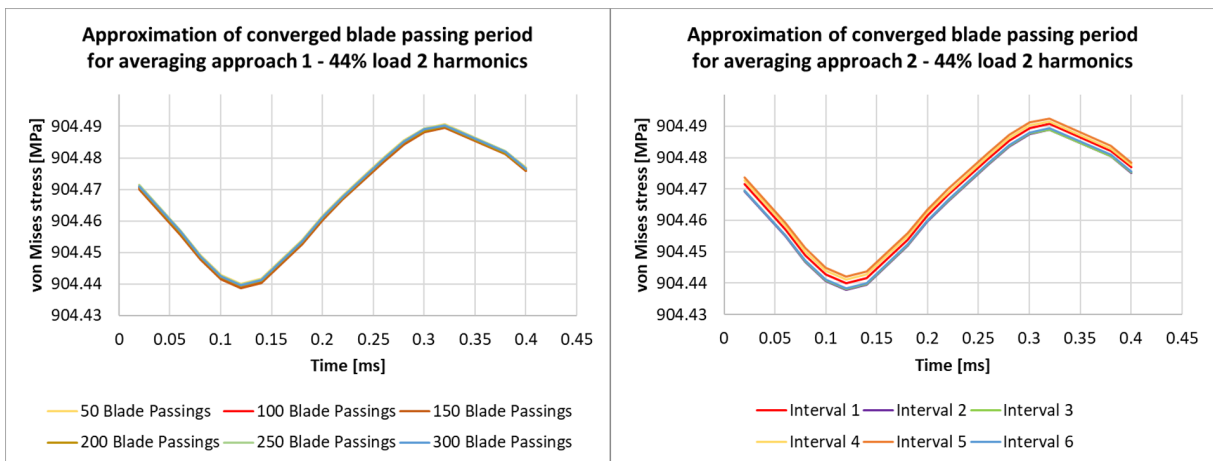
Figure 3.25: Approximation of converged blade passing period for averaging approach 1 (Left) and approach 2 (Right) - 44% load 2 harmonics
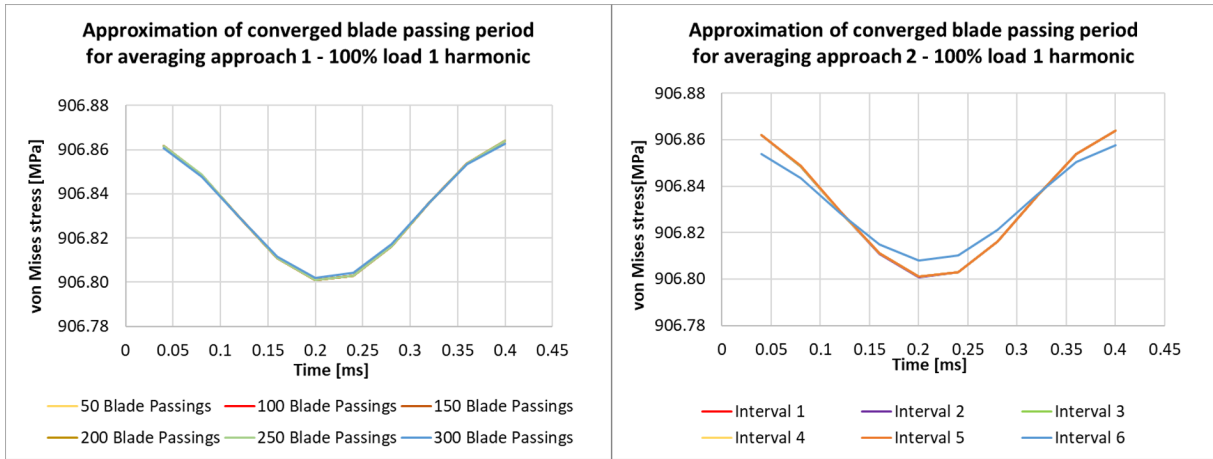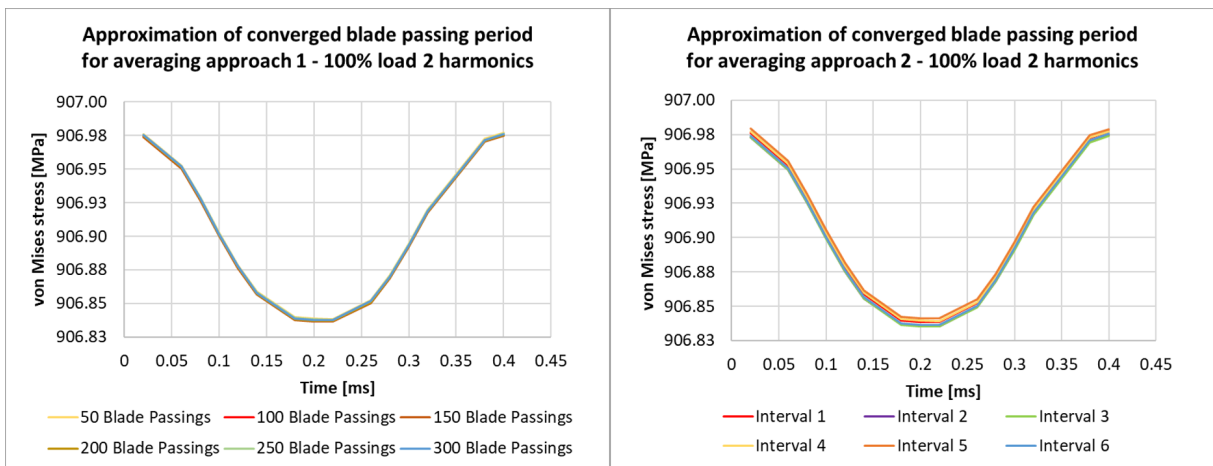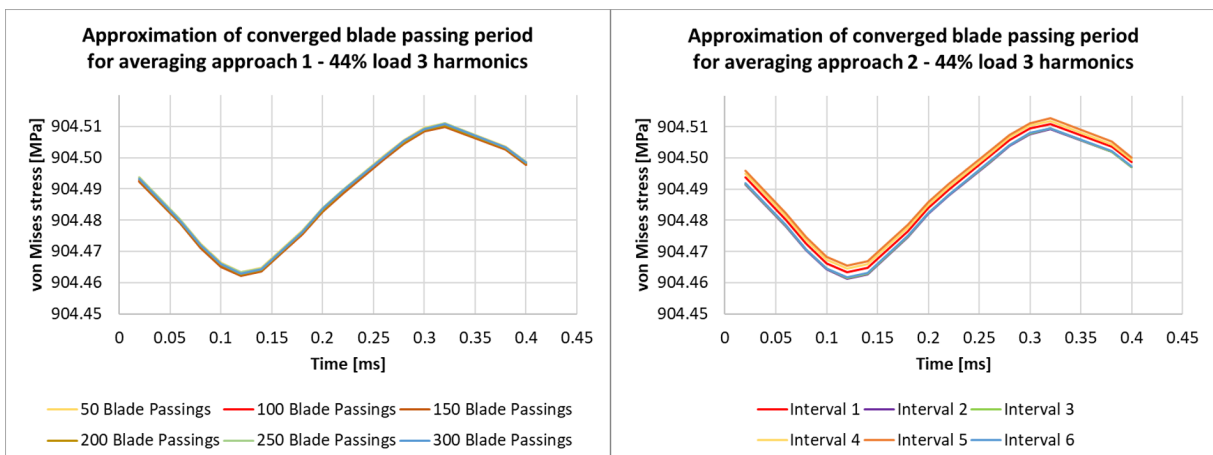

Figure 3.26: Approximation of converged blade passing period for averaging approach 1 (Left) and approach 2 (Right) - 44% load 3 harmonics

Figure 3.27, Figure 3.28, and Figure 3.29 show the approximated blade passing periods obtained by applying approach 1 over 250 blade passing periods, when considering the 1, 2, and 3 harmonics of the 100%, 79%, and 44% loads, respectively. It is evident for all 3 load conditions that the von Mises stresses increase as the number of harmonics increase. It was noted for the 100% and 79% load case, that the amplitudes of the von Mises stress for 2 and 3 harmonics are approximately double that of the 1 harmonic. In the case of the 44% load, the amplitudes of von Mises stresses histories for 1, 2, and 3 harmonics are however more equal in magnitude. Furthermore, comparing the stress histories of the three load conditions, reveals that the stress histories of the 44% load are not in phase with the stress histories of the 100% and 79% loads.
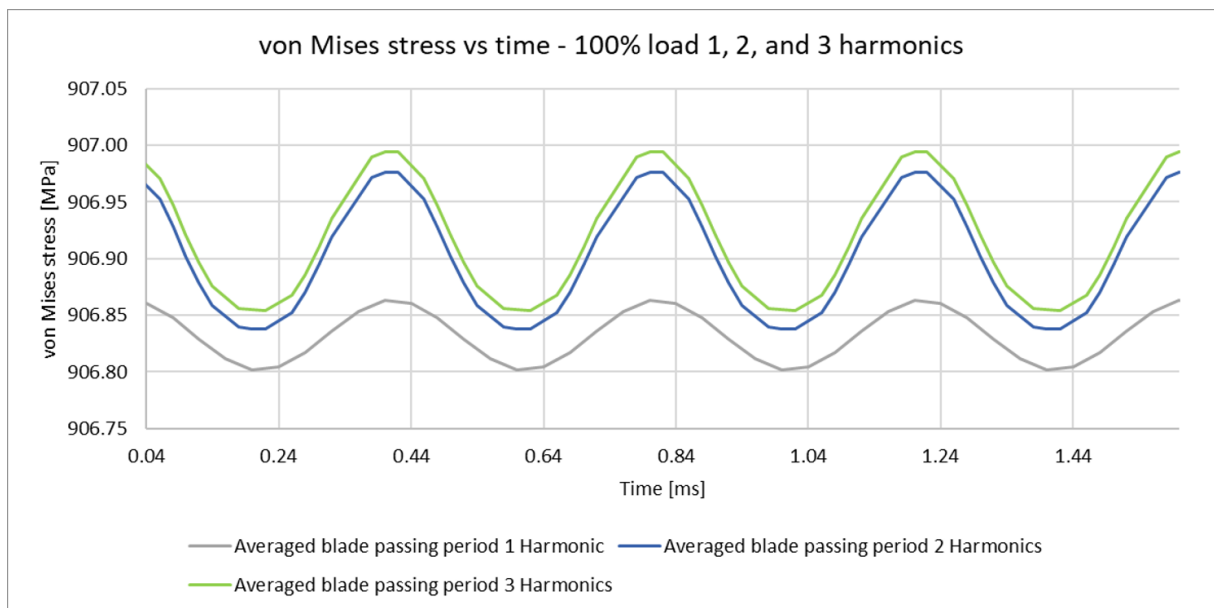
Figure 3.27: Approximation of converged blade passing periods for 100% load
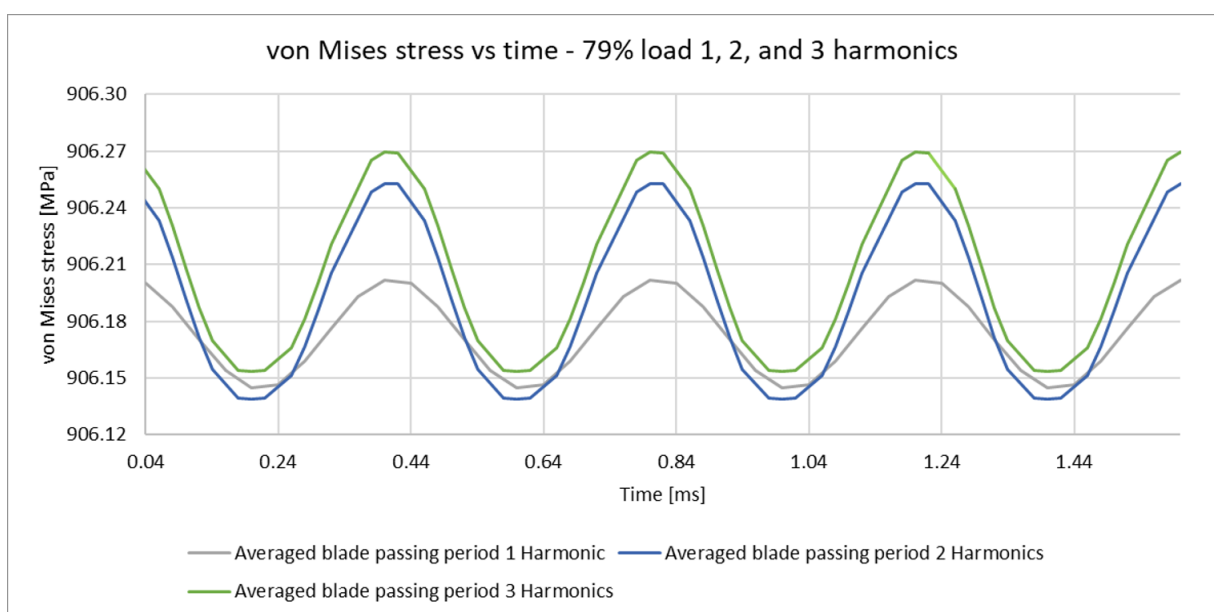
Figure 3.28: Approximation of converged blade passing periods for 79% load
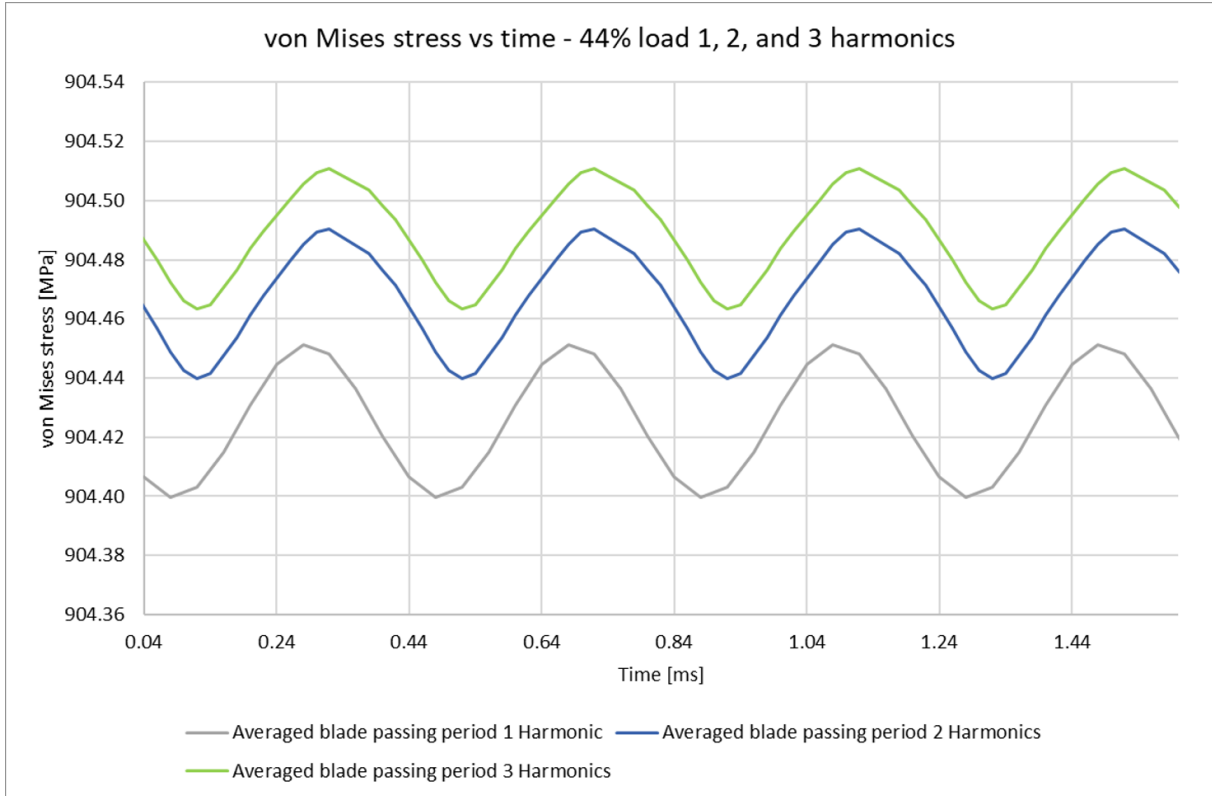
Figure 3.29: Approximation of converged blade passing periods for 44% load

3.4 Fatigue analysis results

The RUL was estimated for the approximated converged stress history obtained using approach 2. The reason being that using the results of approach 2 will give a more conservative answer to the question regarding the sensitivity of the estimated RUL to the number of harmonics used in an NLH simulation.

The tables below show the estimated RUL for the three loads for 1, 2, and 3 harmonics. The tables also show the percentage difference in the estimated RUL for the different intervals. The percentage differences were calculated relative to the estimated RUL of interval 1. It was noted that the RUL estimations tabulated below are extremely large and unrealistic. Further on in this section possible causes were identified and it was shown that it is still possible to draw meaningful conclusion from these RUL estimations.

Table 3.1: Estimated RUL for approach 2 - 100% load

Interval	Estimated RUL [Hours]			Percentage Difference		
	1 Harmonic	2 Harmonics	3 Harmonics	1 Harmonic	2 Harmonics	3 Harmonics
1	1.03312E+26	1.50057E+23	1.36943E+23	0.00000%	0.00000%	0.00000%
2	1.03313E+26	1.53771E+23	1.40295E+23	0.00068%	2.47537%	2.44788%
3	1.03312E+26	1.51920E+23	1.39457E+23	0.00000%	1.24122%	1.83589%
4	1.01953E+26	1.46464E+23	1.34499E+23	-1.31541%	-2.39418%	-1.78437%
5	1.03312E+26	1.46445E+23	1.33681E+23	0.00000%	-2.40739%	-2.38135%
6	7.23301E+26	1.53762E+23	1.39447E+23	600.11154%	2.46913%	1.82900%

Table 3.2: Estimated RUL approach 2 - 79% load

Interval	Estimated RUL [Hours]			Percentage Difference		
	1 Harmonic	2 Harmonics	3 Harmonics	1 Harmonic	2 Harmonics	3 Harmonics
1	2.41875E+26	7.82357E+23	6.80639E+23	0.00000%	0.00000%	0.00000%
2	2.41875E+26	8.05847E+23	6.95680E+23	0.00000%	3.00249%	2.20989%
3	2.38373E+26	7.94079E+23	6.90671E+23	-1.44790%	1.49839%	1.47386%
4	2.41874E+26	7.65295E+23	6.66036E+23	-0.00067%	-2.18074%	-2.14542%
5	2.41874E+26	7.65213E+23	6.61194E+23	-0.00067%	-2.19128%	-2.85692%
6	1.33898E+27	7.99899E+23	6.90638E+23	453.58485%	2.24218%	1.46908%

Table 3.3: Estimated RUL approach 2 - 44% load

Interval	Estimated RUL [Hours]			Percentage Difference		
	1 Harmonic	2 Harmonics	3 Harmonics	1 Harmonic	2 Harmonics	3 Harmonics
1	6.42523E+26	5.49031E+27	9.84480E+27	0.00000%	0.00000%	0.00000%
2	6.53017E+26	5.15797E+27	9.41471E+27	1.63322%	-6.05329%	-4.36872%
3	6.42523E+26	5.26633E+27	9.62755E+27	0.00000%	-4.07962%	-2.20683%
4	6.42523E+26	5.72533E+27	1.02977E+28	0.00000%	4.28061%	4.60056%
5	6.42523E+26	5.72499E+27	1.02971E+28	0.00000%	4.27438%	4.59431%
6	5.30307E+26	5.15783E+27	9.41446E+27	-17.46494%	-6.05578%	-4.37126%

In section 3.3.2 it was mentioned that for approach 2 the approximations of the converged blade passing periods differed a bit more compared to that of approach 1. These differences were in most cases very small, however the effect thereof on the estimated RUL are evident in the percentage differences tabulated in Table 3.1 to Table 3.3. In order to obtain a representative estimated RUL for a given load and number of harmonics, the RUL estimations were averaged over the first 5 intervals.

There are two reasons why the RUL estimations were averaged over only the first 5 intervals. Firstly, a clear discrepancy exists between the percentage differences of interval 6 and the first 5 intervals of the 1 harmonic cases for the 100% and 79% loads. The reason for this discrepancy is, because for the 1 harmonic cases interval 6 starts at 0ms and ends at 20ms, therefore encompassing the initial transient effects of when the aerodynamic forces are just applied to the last stage rotor, see Figure 3.13. Whilst interval 6 for the 2 and 3 harmonics cases of the 100% and 79% load do not include the initial transient effects, seeing that it starts at 24ms and ends at 44ms, see Figure 3.14 and Figure 3.15. The reason for this is because the simulated time of the non-converged histories of the 1 harmonic cases were for 120ms, whilst the 2 and 3 harmonics cases were 144ms. Due to time constraints it was not possible to re-simulated the 1 harmonic cases for 144ms.

Secondly, in order to compare the RUL estimations of 1, 2, and 3 harmonics for the three load conditions, the RUL estimations must be averaged over the same set of intervals. Seeing that interval 6 cannot be used in the averaging process, as explained in the above paragraph, the averaging process was performed over the first 5 intervals. Table 3.4 shows the averaged values of the estimated RUL of the three loads for 1, 2, and 3 harmonics.

Table 3.4: The estimated RUL for the 3 load conditions averaged over 5 intervals

Load	Estimated RUL [Hours]		
	1 Harmonic	2 Harmonics	3 Harmonics
100%	1.03041E+26	1.49731E+23	1.36975E+23
79%	2.41174E+26	7.82558E+23	6.78844E+23
44%	6.44622E+26	5.47298E+27	9.89638E+27

As mentioned earlier, it was noted that the RUL estimations tabulated in Table 3.1, Table 3.2, and Table 3.2 are extremely large and unrealistic and this is still the case for the averaged RUL estimations tabulated in Table 3.4. It would be expected that the estimated RUL would be of much lower order. Firstly, it should be remembered that the RUL of a turbine blade is affected by various mechanisms, of which HCF is one of them. Thus, it can be expected that the actual estimated RUL will be lower if all the aspects that effect the RUL of a turbine were accounted for. Secondly, temperature was also not account for in the RUL process, as mentioned in Section 2.3.

Thirdly, stated in the Scope of research, is that the sensitivity is to be evaluated in the HCF regime in the sense that the predicted stress histories will be below the yield strength of the material, but not necessarily of such nature that HCF failure will occur.

Fourthly, as mentioned in Section 2.5.1 the root had to be simplified. This resulted in the HCF location to move to the hub fillet region. Even though HCF damage mostly occurs in the fir-tree root, the simplification was found to be acceptable seeing that the location was not of interest for the sensitivity analysis. However, due to this simplification the location of interest could be in a location that does not experience extreme HCF conditions, thus resulting in the extremely large RUL estimations shown in Table 3.4.

Hariprasad et al. (2017) studied the failure of last stage rotor blades of a low pressure steam turbine. The rotor blades had three-tooth fir-tree type roots. Part of the study considered a static analysis of the rotor blade rotating at 3000rpm. The static analysis revealed that the maximum von Mises stress occurred in the serrations of the root, at the same location where blade failure was found to occur, due to cracking. The maximum von Mises stress was below the blade's proof stress of 1130MPa. It was evident from the authors' work that the maximum von Mises stress in the hub fillet region was approximately 200MPa lower than the maximum von Mises stress evident in the serrations of the root, where blade failure was found to occur.

Zhao et al. (2018) analysed the failure of a fourth stage rotor blade of a low pressure steam turbine. The fourth stage rotor blade had four-tooth fir-tree roots. Zhao et al. (2018) also performed a static analysis of the blade, the same as Hariprasad et al. (2017). However, Zhao et al. (2018) did not just consider the rotational speed component, but also included the aerodynamic forces induced by the steam flow. The maximum von Mises stress was found to occur in the serrations of the root, below the yield strength of the material. It was also evident from the authors' work that the maximum von Mises stress in the hub region was approximately 160MPa lower than the maximum von Mises stress in the serrations of the root.

Furthermore, from the work of Rzadkowski et al. (2016) and Sheng et al. (2017) it was also evident, for the last stage rotor blade of a LP steam turbine, that the maximum stress in the hub fillet region occurred at a lower stress when compared to the maximum stress found in the serrations of the fir-tree root. Thus, from the above four mentioned cases, it can be seen that the maximum von Mises stress found in the hub fillet region is noticeably lower that the maximum von Mises stress found in the serrations of the root of a fir-tree type LP steam turbine blade.

Therefore, firstly considering that the fir-tree root of the simulated last stage rotor blade was simplified, and secondly that the maximum von Mises stress in the hub fillet region can be approximately 160MPa-200MPa lower than the maximum von Mises stress in the serrations of the root due to for example centrifugal forces, can result in substantially different estimations of the RUL if the maximum von Mises stress in the serration was the location of interest for the sensitivity analysis.

Taking the above into consideration and the fact that the mean stress can have a substantial impact on the RUL, see Section 1.2.6, it can be demonstrated that useful conclusions can still be made from the extremely large RUL estimations. Let us consider the estimated RUL for the 9 cases, for the situation where the RUL decreases due to a larger mean stress resulting from larger centrifugal forces. Please note that for this demonstration the centrifugal force component of the mean stress for the stress histories reported in Section 3.3.2 were just increased, and the RUL was then estimated for the resulting stress history. This was done seeing that due to time constraints additional FEM simulations could not be performed. The centrifugal forces stress component was increased incrementally from 895MPa to 1017.5MPa, where the 895MPa is the actual centrifugal forces stress component of the last stage rotor, resulting from the last stage rotor blade rotating at 3000rpm.

To assist in this demonstration, the estimated RUL for 1 and 2 harmonics were compared to the estimated RUL for 3 harmonics, for a given load. The comparison was quantified by calculating the percentage difference between the estimated RUL of 1 and 3 harmonics and the percentage difference between the estimated RUL of 2 and 3 harmonics. From here on the former will be referred to as the percentage difference for 1 harmonic and the latter as the percentage difference for 2 harmonics. The percentage difference was always calculated relative the estimated RUL of the 3 harmonics.

The reason for this relative percentage difference calculation is, because in general a more accurate CFD solution is obtained as more harmonics are used in an NLH simulation. Therefore, in principle the RUL estimated for the 3 load condition using 3 harmonics should represent the most accurate RUL estimation. Furthermore, for the purpose of this sensitivity analysis the RUL estimations based on the 3 harmonics, can be considered as the "actual" or "real" RUL of the last stage rotor. Thus, calculating the percentage differences relative to the estimated RUL for the 3 harmonics, would be ideal as it provides an indication of how accurate the RUL was estimated.

Table 3.5, Table 3.6, and Table 3.7 show the estimated RUL for the three loads for 1, 2, and 3 harmonics, resulting from the increase of the centrifugal force component of the mean stresses. For a given load, number of harmonics, and centrifugal force compo-

nent, the estimated RUL was obtained by estimating the RUL for interval 1 to 5 and then taking the averaged thereof. Furthermore, for a given load condition and centrifugal force mean stress component, the tables also show the percentage differences of 1 harmonic and 2 harmonics. Lastly, for a given load condition and centrifugal force mean stress component, the tables show a ratio calculated by dividing the percentage difference of 1 harmonic by percentage difference of 2 harmonics.

From Table 3.5, Table 3.6, and Table 3.7 it is evident for all three load conditions, that as the centrifugal force component increases the estimated RUL decreases, yielding in a more realistic RUL estimation. However, it is important to note that the order of magnitude of the calculated ratios for each of the three load cases remains the same, as the centrifugal force component increases. Indicating that as one approaches more realistic RUL estimations, the difference in the order of magnitude between the percentage differences of the 1 and 2 harmonics remain the same for a given load condition. Therefore, one will find that the conclusions to follow will be the same for the unrealistic and realistic RUL estimations, thus demonstrating that it is possible to still draw meaningful conclusions w.r.t the sensitivity of the estimated RUL to the number of harmonics used in an NLH simulation.

Table 3.5: Estimated RUL for increased centrifugal forces - 100% load

Centrifugal force stress component [MPa]	Estimated RUL [Hours]			Percentage Difference		
	1 Harmonic	2 Harmonics	3 Harmonics	1 Harmonic	2 Harmonics	Ratio
895	1.03041E+26	1.49731E+23	1.36975E+23	75125.94%	9.31%	8.06673E+03
950	2.17305E+23	3.08970E+20	2.82149E+20	76917.95%	9.51%	8.09147E+03
990	1.37562E+20	1.92995E+17	1.75714E+17	78187.26%	9.83%	7.94996E+03
1017	4.14828E+08	3.37890E+05	2.70850E+05	153057.67%	24.75%	6.18373E+03
1017.5	1.34780E+07	7.36200E+03	5.26959E+03	255669.44%	39.71%	6.43888E+03

Table 3.6: Estimated RUL for increased centrifugal forces - 79% load

Centrifugal force stress component [MPa]	Estimated RUL [Hours]			Percentage Difference		
	1 Harmonic	2 Harmonics	3 Harmonics	1 Harmonic	2 Harmonics	Ratio
895	2.41174E+26	7.82558E+23	6.78844E+23	35427.1671%	15.2781%	2.3188E+03
950	5.28004E+23	1.67792E+21	1.45150E+21	36276.3939%	15.5990%	2.3256E+03
990	3.74068E+20	1.18385E+18	1.02141E+18	36522.6198%	15.9032%	2.2966E+03
1017	3.87687E+10	1.10420E+08	8.90062E+07	43457.3699%	24.0584%	1.8063E+03
1017.5	9.23246E+09	2.60390E+07	2.04479E+07	45051.2496%	27.3436%	1.6476E+03

Table 3.7: Estimated RUL for increased centrifugal forces - 44% load

Centrifugal force stress component [MPa]	Estimated RUL [Hours]			Percentage Difference		
	1 Harmonic	2 Harmonics	3 Harmonics	1 Harmonic	2 Harmonics	Ratio
895	6.44622E+26	5.47298E+27	9.89638E+27	-93.48629%	-44.69710%	2.09155E+00
950	1.54003E+24	1.35568E+25	2.43824E+25	-93.68384%	-44.39919%	2.11004E+00
990	1.44585E+21	1.26575E+22	2.26877E+22	-93.62718%	-44.20991%	2.11779E+00
1017	2.46725E+13	2.00566E+14	3.43386E+14	-92.81495%	-41.59178%	2.23157E+00
1017.5	2.41658E+13	1.87271E+14	3.19241E+14	-92.43024%	-41.33889%	2.23592E+00

Based on the above findings, the sensitivity of the estimated RUL to the number of harmonics used in an NLH simulation, was studied by normalizing the estimated RUL for the three load conditions for 1, 2, and 3 harmonics. The RUL estimations of the 1017.5MPa centrifugal force mean stress component cases tabulated in Table 3.5, Table 3.6, and Table 3.7, were considered in the normalization process. Table 3.8 shows the normalized values, which were obtained by dividing the estimated RUL of 1 and 2 harmonics by the estimated RUL of the 3 harmonics, for a given load condition. For the 100% and 79% load, it is evident that the estimated RUL decreases as the number of harmonics used in the NLH simulations increase. However, for the 44% load the opposite is evident. Table 3.9 and Table 3.10 show the percentage differences of 1 harmonic and the percentage differences of 2 harmonics respectively, for the normalized RUL estimations.

Table 3.8: Normalize estimated RUL for the 3 load conditions - Increased centrifugal forces

Load	Normalized Estimated RUL		
	1 Harmonic	2 Harmonics	3 Harmonics
100%	2557.69	1.40	1.00
79%	451.51	1.27	1.00
44%	0.08	0.59	1.00

Table 3.9: Percentage differences of 1 harmonic - Increased centrifugal force

Load	Percentage Difference	Uncertainty band
100%	255669.44%	20353.42%
		-17391.61%
79%	45051.25%	2267.19%
		-2244.61%
44%	-92.43%	0.45%
		-0.30%

Table 3.10: Percentage differences of 2 harmonics - Increased centrifugal force

Load	Percentage Difference	Uncertainty band
100%	39.71%	20.09%
		-17.07%
79%	27.34%	12.00%
		-9.94%
44%	-41.34%	5.32%
		-5.10%

As mentioned earlier there are very small differences between the approximated converged blade passing periods, obtained using approach 2. This shows that there is a band of uncertainty in the estimated RUL, and consequently in the evaluation of the sensitivity of the estimated RUL to the number of harmonics. In order to establish the sensitivity of the estimated RUL to the number of harmonics, requires the quantification of the uncertainty bands. An uncertainty analysis was performed and the upper and lower limits of the uncertainty bands are tabulated in Table 3.9 and Table 3.10.

From the percentage differences tabulated in Table 3.9 and Table 3.10 it is evident, for all 3 load conditions, that as the number of harmonics used in an NLH is increased from 1 to 2 harmonics, the estimated RUL approaches the estimated RUL obtained using 3 harmonics. For the 100% load and 79% loads, it can be seen that the order of magnitude difference between the percentage differences of 1 and 2 harmonics are four and three, respectively. Whilst no difference in the order of magnitude is evident when comparing the percentage differences of 1 and 2 harmonics for the 44% load case.

Further comparison of the percentage differences, reveals that all 3 load conditions have the same order of magnitude for the percentage differences of 2 harmonics. However, the 100% and 79% loads differ 1 order of magnitude for the percentage differences of 1 harmonic, whilst the 44% load's are the same order of magnitude as its percentage difference of 2 harmonics. Furthermore, above findings remain the same even when considering the uncertainty bands.

Based on the above established sensitivity of the estimated RUL to the number of harmonics, it is clear that relative small changes in the predicted aerodynamics forces (see Section 3.2) can have a substantial impact on the estimated RUL. This can explain, as mentioned in Section 1.1, why utilities using empirical methods to determine the forces experienced by turbine blades, desire more accurate methods.

Furthermore, based on the established sensitivity of the estimated RUL to the number of harmonics, the following recommendations are made, from a conservative point of view. Firstly, in general if the RUL is to be estimated with reasonable accuracy, just using 1 harmonic in an NLH simulation will not be sufficient and 2 harmonics should be used. Secondly, if the RUL has to be estimated with high accuracy, 3 harmonics should be used.

From the above results it is evident that there exists a rather distinctive relationship between the estimated RUL and number of harmonics for the 100% and 79% load condition, which is very different to that of the 44% load condition. Comparing the results of

the 44% load to that of the 100% and 79% loads for the entire sensitivity analysis, gives an indication as to why the 44% load does not show the same distinctive relationship. From the onset of the RUL estimation process, it was evident that the overall form and distributional patterns of the predicted aerodynamic forces of the 44% load differed to that of the 100% and 79% loads.

Furthermore, differences were also evident from the transient structural analyses results. Firstly, for the 100% and 79% load cases, the amplitudes of the von Mises stresses for 2 and 3 harmonics were approximately double that of the 1 harmonic. Whilst the amplitudes of the von Mises stresses for 2 and 3 harmonics, of the 44% load, were roughly the same as that of the 1 harmonic. Secondly, the stress histories of the 44% load were not in phase with that of the 100% and 79% loads.

Considering all the differences mentioned above, it is evident that the first difference between the 44% load and, the 100% and 79% loads was noted in the predicted aerodynamic force. This suggest that the reason why the 44% load does not have the same distinctive relationship as that of the 100% and 79% loads, is connected to the 44% load condition in some way. Seeing that the 44% load is a low load (or flow) condition compared to the 100% and 79% loads, it was reasoned that the main reason why the 44% load does not have the same distinctive relationship, is due to the 44% load condition being a low load (or flow) condition.

Chapter 4

Conclusion and Recommendation

4.1 Conclusion

In this work a sensitivity analysis was conducted, with the purpose of establishing the sensitivity of the estimated remaining useful life (RUL) to the number of harmonics used in a nonlinear harmonic (NLH) CFD simulation. NLH simulations were performed on the one half of a dual low pressure (LP) steam turbine, consisting of 5 stages and 3 flow extractions. The LP steam turbine was modelled for 100%, 79%, and 44% load conditions. Each load condition was simulated for 1, 2, and 3 harmonics, adding up to a total of 9 NLH simulations or 9 cases.

The predicted aerodynamic forces were utilized in a transient structural FE analysis, to calculate the resulting stress history of the last stage rotor, for each of the 9 cases. The stress history at the location (or node) on the last stage rotor where the maximum von Mises stress occurred, was used to estimate the RUL. Unfortunately, due to limited computational resources, none of the stress histories of all 9 cases were found to be fully converged.

However, the non-converged stress histories all showed an asymptotic like convergence. Also, the amplitude of each blade passing period was found to be equal in magnitude for most of the stress history. Thus, it was hypothesised that averaging the non-converged stress histories of the 9 cases would result in a reasonable approximation to the converged blade passing periods for the 9 cases. A blade passing averaging process was implemented for two approaches, in order to determine if the hypothesis was true. The hypothesis was found to be true, as both approaches indicated that averaging the blade passing periods of the non-converged stress histories could yield in an approximated converged blade passing period, for each of the 9 cases.

The approximation to the converged blade passing periods, obtained using approach 2, were then given as an input to a fatigue model to estimate the RUL for all 9 cases. It was noted that the order of magnitude of the RUL estimations were very large. However, it was shown that whether the RUL estimations were realistic or unrealistic, that the same conclusions could be made with regards to the sensitivity of the estimated RUL to the number of harmonics used in an NLH simulation. Subsequently, for the 100% and 79% loads, the estimated RUL were found to decrease as the number of harmonics used in a NLH simulation increased. The opposite was found to be true for the 44% load.

The sensitivity of the estimated RUL to the number of harmonics, were further investigated by performing addition calculations for each load condition. The percentage difference between the estimated RUL of 1 and 3 harmonics and the percentage difference between the estimated RUL of 2 and 3 harmonics, were calculated. The former will be referred to as the percentage difference of 1 harmonic and the latter as the percentage difference of 2 harmonics. Both percentage differences were calculated relative to the estimated RUL for 3 harmonics.

Comparing the percentage differences for all 3 load conditions, showed that as the number of harmonics used in an NLH is increased from 1 to 2 harmonics, the estimated RUL approached the estimated RUL obtained using 3 harmonics. For the 100% load and 79% load, it was seen that the order of magnitude difference between the percentage differences of 1 and 2 harmonics were four and three, respectively. Whilst no difference in the order of magnitude was evident when comparing the percentage differences of 1 and 2 harmonics for the 44% load case.

Further comparison of the percentage differences, revealed that all 3 load conditions had the same order of magnitude for the percentage differences of 2 harmonics. However, the 100% and 79% loads differed 1 order of magnitude for the percentage differences of 1 harmonic, whilst the 44% load's was the same order of magnitude as it's percentage difference of 2 harmonics.

Based on the above established sensitivity of the estimated RUL to the number of harmonics, it was clear that relatively small changes in the predicted aerodynamics forces could have a substantial impacted on the estimated RUL. This could explain why utilities using empirical methods to determine the forces experienced by turbine blades, desire more accurate methods.

Furthermore, based on the established sensitivity of the estimated RUL to the number of harmonics, the following recommendations were made, from a conservative point of view. Firstly, in general if the RUL was to be estimated with reasonable accuracy, just using 1 harmonic in an NLH simulation would not be sufficient and 2 harmonics should be used. Secondly, if the RUL had to be estimated with high accuracy, 3 harmonics should be used.

It was evident that there exists a rather distinctive relationship between the estimated RUL and number of harmonics, for the 100% and 79% load condition, which is very different to that of the 44% load. The results of the 44% load were compared to that of the 100% and 79% loads for the entire sensitivity analysis, in an effort to determine why the 44% load did not show the same distinctive relationship.

Various differences were evident, but the first difference between the 44% load and, the 100% and 79% loads was noted in the predicted aerodynamic forces. This suggested that the reason why the 44% load did not have the same distinctive relationship, was connected to the 44% load condition in some way. Seeing that the 44% load was a low load (or flow) condition compared to the 100% and 79% loads, it was reasoned that the main reason why the 44% load did not have the same distinctive relationship, was due to the 44% load condition being a low load (or flow) condition.

4.2 Recommendations

The following recommendations are made for future work:

- Utilizing the NLH method, estimate the RUL for 1, 2, and 3 harmonics for load conditions lower than 44%. So as to determine whether the trends found in the estimated RUL of the 44% load, are a function of low load (or flow) conditions.

- Evaluate whether the same sensitivity of the estimated RUL to the number of harmonics, remains the same when the effect of temperature is included in the RUL estimation process.

- The results of the sensitivity analysis suggests that there may be a load condition below which the trends found for the 100% and 79% load will no longer be evident. Conduct a study to determine this load condition.

- The resulting stress histories, used to demonstrate that useful conclusions can be drawn from the unrealistic RUL estimations, see Section 3.4, were obtained by just increasing the centrifugal force stress components. Therefore, not account for the effect the increased centrifugal forces will have on the resulting stress histories due to the blade stiffness that increases. Conduct a study to evaluate if the conclusions drawn from this demonstration will remain the same.

- Conduct a similar sensitivity analysis as the one presented in this dissertation, for the case where the location of interest is located such that the estimated RUL is realistic, and compare the findings with the findings of this study w.r.t the sensitivity of the estimated RUL to the number of harmonics used in an NLH simulation.

Bibliography

Alwan, R. A., AbdulRazzaq, A. and Al-Taie, A. K. H. (2007), 'Design of a constant stress steam turbine rotor blade', *Journal of Engineering and Sustainable Development* **11**(3), 76–94.

Andreini, A., Bonini, A., Da Soghe, R., Facchini, B., Ciani, A. and Innocenti, L. (2012), Conjugate heat transfer calculations on gt rotor blade for industrial applications: Part II—improvement of external flow modeling, *in* 'ASME Turbo Expo 2012: Turbine Technical Conference and Exposition', American Society of Mechanical Engineers, pp. 681–692.

Asghar, M., Liu, Y., Cui, J. and Lu, L. (2018), 'Investigation of unsteady flow interactions in a transonic high pressure turbine using nonlinear harmonic method', *Energies* **11**(2), 342.

Booysen, C. (2014), Fatigue life prediction of steam turbine blades during start-up operation using probabilistic concepts, Master's thesis, University of Pretoria.

Branco, R., Antunes, F. V. and Costa, J. D. (2015), 'A review on 3D-FE adaptive remeshing techniques for crack growth modelling', *Engineering Fracture Mechanics* **141**, 170–195.

Brits, J. C. P., Heyns, P. S. and Inglis, H. M. (2016), 'An experimental and stochastic approach to estimate the fatigue crack life of a turbomachinery blade using finite element modelling', pp. 1–86.

Butler, R. J., Byerley, A. R., VanTreuren, K. and Baughn, J. W. (2001), 'The effect of turbulence intensity and length scale on low-pressure turbine blade aerodynamics', *International Journal of Heat and Fluid Flow* **22**(2), 123–133.

Chiang, H.-W. D. and Kielb, R. E. (1993), 'An analysis system for blade forced response', *Journal of Turbomachinery* **115**(4), 762–770.

Choi, J., Teng, S., Han, J.-c. and Ladeinde, F. (2004), 'Effect of free-stream turbulence on turbine blade heat transfer and pressure coefficients in low reynolds number flows', *International Journal of Heat and Mass Transfer* **47**(14-16), 3441–3452.

Dewey, R., Rieger, N. and McCloskey, T. (1985), 'Survey of steam turbine blade failures', *EPRI Report CS* **3891**.

Drozdowski, R., Völker, L., Häfele, M. and Vogt, D. (2015), Experimental and numerical investigation of the nonlinear vibrational behavior of steam turbine last stage blades with friction bolt damping elements, *in* 'ASME Turbo Expo 2015: Turbine Technical Conference and Exposition', American Society of Mechanical Engineers.

Dunn, D., Roos, T. and Hildebrandt, T. (2011), 'Application of transition modelling in cfd for use with turbine blades', pp. 1–7.

Fan, S. and Lakshminarayana, B. (1995), Time accurate euler simulation of interaction of nozzle wake and secondary flow with rotor blade in an axial turbine stage using nonreflecting boundary conditions, *in* 'Volume 1: Turbomachinery', ASME, pp. 1–20.

FERP (2017), 'Martensitic steel (manet)'.
URL: *http://www-ferp.ucsd.edu/LIB/PROPS/PANOS/fs.html*

Frey, K. K. and Fleeter, S. (1998), Rotating blade row oscillating airfoil aerodynamics, *in* 'Unsteady Aerodynamics and Aeroelasticity of Turbomachines', Springer, pp. 67–82.

Gottlich, E., Woisetschlager, J., Pieringer, P., Hampel, B. and Heitmeir, F. (2006), 'Investigation of vortex shedding and wake-wake interaction in a transonic turbine stage using laser-doppler-velocimetry and particle-image-velocimetry', *Journal of Turbomachinery* **128**(1), 178.

Green, B. R., Mathison, R. M. and Dunn, M. G. (2013), 'Comparison of harmonic and time marching unsteady computational fluid dynamics solutions with measurements for a single-stage high-pressure turbine', *Journal of Turbomachinery* **136**(1), 11005.

Hariprasad, T., Sagar, M. V. and Kumari, D. M. (2017), 'Failure analysis of last stage low pressure steam', *International Journal for Research in Applied Science & Engineering Technology (IJRASET)* **5**(Xii), 1284–1294.

He, L. and Ning, W. (1998), 'Efficient approach for analysis of unsteady viscous flows in turbomachines', *AIAA journal* **36**(11), 2005–2012.

Hodson, H. P., Dawes, W. N. and Ody, C. C. B. (1996), 'Wake-turbine blade interaction studies', pp. 1–10.

Hou, J., Wescott, R. and Attia, M. (2014), 'Prediction of fatigue crack propagation lives of turbine discs with forging-induced initial cracks', *Engineering Fracture Mechanics* **131**, 406–418.

Hummel, F. (2002), 'Wake–wake interaction and its potential for clocking in a transonic high-pressure turbine', *Journal of Turbomachinery* **124**(1), 69.

Jachens, W. (1966), 'Steam turbines-their construction, selection and operation', *Proc. The South African Sugar Technologist's Association* pp. 113–131.

Jöcker, M. (2002), Numerical Investigation of the Aerodynamic Vibration Excitation of High-Pressure Turbine Rotors, PhD thesis, Energiteknik.

Jono, M. and Inoue, T. (1992), Mechanical behaviour of materials-vi; proceedings of the 6th international conference, kyoto, japan, july 29-aug. 2, 1991. vols. 1-4, *in* 'Mechanical Behaviour of Materials-VI, Volume 1', Vol. 1.

Kachel, C. E. and Denton, J. D. (2006), 'Experimental and numerical investigation of the unsteady surface pressure in a three-stage model of an axial high pressure turbine', *Journal of Turbomachinery* **128**(2), 261.

Krishnababu, S. K., Newton, P. J., Dawes, W. N., Lock, G. D., Hodson, H. P., Hannis, J. and Whitney, C. (2009), 'Aerothermal investigations of tip leakage flow in axial flow turbines—part I: Effect of tip geometry and tip clearance gap', *Journal of Turbomachinery* **131**(1), 011006.

Lakshminarayana, B., Chernobrovkin, A. and Ristic, D. (2000), 'Unsteady viscous flow causing rotor-stator interaction in turbines, part 1: Data, code pressure', *Journal of Propulsion and Power* **16**(5), 744–750.

Lampart, P., Rusanov, A., Yershov, S., Marcinkowski, S. and Gardzilewicz, A. (2005), 'Validation of a 3D rans solver with a state equation of thermally perfect and calorically imperfect gas on a multi-stage low-pressure steam turbine flow', *Journal of Fluids Engineering* **127**(1), 83.

Latcovich, J., Astrom, T., Frankhuizen, P., Fukushima, S., Hamberg, H. and Keller, S. (2005), 'Maintenance and overhaul of steam turbines', *International Association of Engineering Insurers, 38th Annual Conference* **42**(05).

Laumert, B. (2002), Numerical Investigation of Aerodynamic Blade Excitation Mechanisms in Transonic Turbine Stages, PhD thesis, Energiteknik.

Laumert, B., Martensson, H. and Fransson, T. H. (2002), 'Investigation of unsteady aerodynamic blade excitation mechanisms in a transonic turbine stage—part I: Phenomenological identification and classification', *Journal of Turbomachinery* **124**(3), 419.

Mayorca, M. A. (2011), Numerical Methods for Turbomachinery Aeromechanical Predictions, PhD thesis, Royal Institute of Technology.

Mazur, Z., Garcia-Illescas, R., Aguirre-Romano, J. and Perez-Rodriguez, N. (2008), 'Steam turbine blade failure analysis', *Engineering Failure Analysis* **15**(1-2), 129–141.

Mccloskey, T. H. (2002), 'Troubleshooting turbine steam path damage mechanisms', *Proceedings of the thirty-first turbomachinery symposium* pp. 105–144.

McCloskey, T. H., Dooley, R. B. and McNaughton, W. P. (1999), 'Turbine steam path damage: theory and practice', *Electric Power Research Institute, Palo Alto, CA* .

Mestanek, P. (2008), 'Low cycle fatigue analysis of a last stage steam turbine blade', *Applied and Computational Mechanics* **2**, 71–82.

Miller, R., Moss, R., Ainsworth, R. and Harvey, N. (2003*a*), 'Wake, shock, and potential field interactions in a 1.5 stage turbine—part I: Vane-rotor and rotor-vane interaction', *Journal of turbomachinery* **125**(1), 33–39.

Miller, R., Moss, R., Ainsworth, R. and Harvey, N. (2003*b*), 'Wake, shock, and potential field interactions in a 1.5 stage turbine—part II: Vane-vane interaction and discussion of results', *Journal of turbomachinery* **125**(1), 40–47.

Miller, R., Moss, R., Ainsworth, R. and Horwood, C. (2003), 'Time-resolved vane-rotor interaction in a high-pressure turbine stage', *Journal of Turbomachinery* **125**(1), 1.

Misek, T., Tetiva, A., Prchlik, L. and Duchek, K. (2007), Prediction of high cycle fatigue life of steam turbine blading based on unsteady CFD and FEM forced response calculation, *in* 'Volume 5: Turbo Expo 2007', ASME, pp. 509–518.

Mishra, M., Saari, J., Galar, D. and Leturiondo, U. (2014), *Hybrid models for rotating machinery diagnosis and prognosis: estimation of remaining useful life*, Luleå tekniska universitet.

Mohan, R. S., Sarkar, A. and Sekhar, a. S. (2014), 'Vibration analysis of a steam turbine blade', *Inter-noise 2014* pp. 1–10.

Montomoli, F., Carnevale, M., D'Ammaro, A., Massini, M. and Salvadori, S. (2015), Limitations in turbomachinery CFD, *in* 'SpringerBriefs in Applied Sciences and Technology', Vol. 127, pp. 21–32.

Moon, Y. J. and Koh, S. R. (2001), 'Counter-rotating streamwise vortex formation in the turbine cascade with endwall fence', *Computers and Fluids* **30**(4), 473–490.

Ning, W., Moffatt, S., Li, Y. and Wells, R. G. (2003), Blade forced response prediction for industrial gas turbines: Part 2 — verification and application, *in* 'Volume 4: Turbo Expo 2003', ASME, pp. 415–422.

Patel, R. S. and Palazotto, A. N. (2004*a*), 'Finite-element method-based model to study high-cycle fatigue in turbine blades', *Journal of Aerospace Engineering* **17**(2), 45–55.

Patel, R. S. and Palazotto, A. N. (2004*b*), 'Finite-element method-based model to study high-cycle fatigue in turbine blades', *Journal of Aerospace Engineering* **17**(2), 45–55.

Prabakaran, S. and Pradeep, G. (2015), 'A study on turbine blade fatigue protection', *2014 18th National Power Systems Conference, NPSC 2014* .

Rahman, M. H., Kim, S. I. and Hassan, I. (2013), 'Tip leakage flow and heat transfer on turbine blade tip and casing, part 1: Effect of tip clearance height and rotation speed', *International Journal for Computational Methods in Engineering Science and Mechanics* **14**(4), 290–303.

Rieger, N. F. (1988), *Rotordynamics 2*, Vol. 297 of *CISM International Centre for Mechanical Sciences*, Springer Vienna, Vienna.

RPMturbo (2016), 'Flutter analysis'.
URL: *http://www.rpmturbo.com/flutter/index.html*

Rzadkowski, R., Maurin, A., Kubitz, L. and Szczepanik, R. (2016), Forced vibration of mistuned bladed discs in last stage lp steam turbine, *in* 'Volume 7A: Structures and Dynamics', ASME.

Sheng, S., Flegler, J., Janos Becs, B. and Dankert, M. (2017), Component fatigue test facilities for full-scale lp steam turbine end stage blades, *in* 'Proceedings of the 1st Global Power and Propulsion Forum', pp. 1–8.

Soderberg, C. R. (1939), 'Factor of safety and working stress', *Trans Am Soc Mech Eng* **52**, 13–28.

Szwedowicz, J. (2008), 'High cyclic fatigue', *VKI Lecture Series* **5**, 1–54.

Szwedowicz, J., Secall-Wimmel, T. and Dünck-Kerst, P. (2008), 'Damping performance of axial turbine stages with loosely assembled friction bolts: The nonlinear dynamic assessment', *Journal of Engineering for Gas Turbines and Power* **130**(3), 032505.

Ubulom, I. A., Neely, A. J. and Shankar, K. K. (2017), 'Fluid-structure interactions for high-cycle fatigue life estimation', pp. 1–23.

Wang, W. Z., Xuan, F. Z., Zhu, K. L. and Tu, S. T. (2007), 'Failure analysis of the final stage blade in steam turbine', *Engineering Failure Analysis* **14**(4), 632–641.

Wissenschaften, D. D. T. (2003), 'Evolution of unsteady secondary flows in a multistage shrouded axial turbine', (15230).

Xu, Z.-l., Park, J.-p. and Ryu, S.-j. (2007), 'Failure analysis and retrofit design of low pressure 1st stage blades for a steam turbine', **14**, 694–701.

Zhao, W., Li, Y., Xue, M., Wang, P. and Jiang, J. (2018), 'Vibration analysis for failure detection in low pressure steam turbine blades in nuclear power plant', *Engineering Failure Analysis* **84**, 11–24.